EFFECT OF TEMPERATURE AND HUMIDITY CONDITIONING ON MOLD COMPOUND/COPPER INTERFACIAL FRACTURE AND THE ASSOCIATED COHESIVE ZONE MODELING PARAMETERS

A Thesis
Presented to
The Academic Faculty

by

Abhishek Kwatra

In Partial Fulfillment
of the Requirements for the Degree
Masters of Science in the
Woodruff School of Mechanical Engineering

Georgia Institute of Technology
December 2016

EFFECT OF TEMPERATURE AND HUMIDITY CONDITIONING ON MOLD COMPOUND/COPPER INTERFACIAL FRACTURE AND THE ASSOCIATED COHESIVE ZONE MODELING PARAMETERS

Approved by:

Dr. Suresh K. Sitaraman, Advisor
School of Mechanical Engineering
Georgia Institute of Technology

Dr. Samuel Graham
School of Mechanical Engineering
Georgia Institute of Technology

Dr. Karl Jacob
School of Materials Science Engineering
Georgia Institute of Technology

Date Approved: November 21, 2016

ACKNOWLEDGEMENTS

First and foremost I would like to thank my parents and my brother Amritansh for their invaluable support and encouragement to pursue my master's degree at Georgia Tech. I wouldn't be who I am today without you.

I would like thank my advisor, Dr. Suresh K. Sitaraman for his invaluable advice and guidance throughout my master's degree at *Georgia Tech.* I would also like to thank Dr. Samuel Graham and Dr. Karl Jacob for serving on my thesis committee and for their valuable research input.

I would like to acknowledge the Semiconductor Research Corporation (SRC). This work wouldn't have been possible without their support and funding. I would also like to thank industry liaisons from *NXP semiconductor* for providing samples for this research as well as their advice and direction in this project.

A special thanks to the members of the CaSPAR Lab, including Dave Samet, Trilochan Rambhatla and Scott McCann for going out of their way to help me and guide me through obstacles I faced throughout my time here. I would like to thank other members of the CaSPAR lab including Justin Chow, Casey Woodrum, Yaqin Song and Christine Taylor for making time spent in the lab fun and enjoyable.

Lastly I would like to thank my friends at *Georgia Tech*, especially Rohan and Oscar for their support during my time here.

TABLE OF CONTENTS

LIST OF TABLES

LIST OF FIGURES

LIST OF SYMBOLS AND ABBREVIATIONS

Abbreviations

VCCT – Virtual Crack Closure Technique

CTE – Coefficient of Thermal Expansion

SERR – Strain Energy Release Rate

CZM – Cohesive Zone Modeling

SOIC – Small outline integrated chip

2D – two dimensional

3D – three dimensional

LEFM – Linear Elastic Fracture Mechanics

SIF – Stress Intensity Factor

FEM – Finite Element Modelling

DCB – Double Cantilever Beam

FPB – Four Point Bend

EMC – Epoxy Molding Compound

CL – Crack Length

Symbols

G – strain energy release rate

G_c – critical strain energy release rate

G_{IC} – mode I critical strain energy release rate

G_{IIC} – mode II critical strain energy release rate

K – stress intensity factor

K_I – mode I stress intensity factor

K_{II} – mode II stress intensity factor

Π – potential energy

ψ – mode mixity

ΔE – change in energy

a – crack length

ε – bi-material constant

β – one of Dundurs parameters

E – Elastic Modulus

ν – Poisson's ratio

T_{ref} – reference temperature

D – damage incurred on cohesive zone elements

σ_{max} – maximum interfacial traction

δ_c – maximum interfacial separation

$P_{critical}$ – critical load of delamination

b – width of the EMC/Copper sample

SUMMARY

Microelectronic packages are continuing to become smaller and more complex. Interfacial delamination is a common failure mechanism present in microelectronic packages due to the mismatch in the coefficient of thermal expansion (CTE) between different materials. Epoxy Molding Compound/Copper is a common interface found in microelectronic packages that is susceptible to delamination issues due to CTE mismatch between the two layers. This work analyzes interfacial delamination at an EMC/Copper interface and how the interfacial fracture energy is affected by temperature and humidity conditioning. In particular, this work employs delamination experiments to determine how the temperature and humidity conditioning will influence cohesive zone models (CZM). Previous work has investigated delamination in on-chip and off-chip interfaces using traditional fracture mechanics techniques where the starter crack location and propagation path are known. Cohesive zone theory is a new technique that can model multiple cracks without the presence of a starter crack. A cohesive zone model represents the traction forces between two materials as a function of separation in displacement between the two layers. Traction separation parameters for mixed mode loading for an interface can be determined by experimental fracture studies of its delamination and crack propagation. Using these results cohesive zone parameters can be used to predict crack propagation and delamination for interfaces in microelectronic packages. The goal of this study is look at delamination in an EMC/Copper interface and how delamination is affected by temperature and humidity using a double cantilever beam test. Cohesive zone parameters are obtained for as-received, thermally aged and humidity conditioned

samples. These cohesive zone models can be used to predict delamination in an EMC/Copper interface and how these models are affected by factors such as time, temperature and humidity conditioning.

CHAPTER 1. INTRODUCTION AND MOTIVATION

Microelectronic packaging is a material-intensive application that utilizes semiconductors, ceramics, glasses, polymers, and metals [1]. Multilayered dissimilar material structures are commonly used in microelectronic packages nowadays to improve mechanical integrity, enhance fatigue life, reduce cross talk and capacitance and increase electrical performance. These interfaces are usually prone to debonding or delamination under high temperature load operations during fabrication such as solder reflow process or under the influence of harsh environment exposure during reliability qualification tests. For example, die attach delamination at the die attach/epoxy molding compound interface in system on integrated chip (SOIC) packages is a reliability problem. Delamination at this interface may cause thermal management and electrical issues and increase the chance of contamination related/failure as well as stitch bond failures. One major reason for die attach delamination is due to the mismatch in the coefficient of thermal expansion of the die attach and the epoxy molding compound. This is especially noticeable at the interface edge of the die attach, die and mold compound which is an area of high stress and possibly an initiation spot of die attach delamination [2]. Epoxy Molding Compound and copper leadframe is another common interface susceptible to delamination once again due to stress concentrations and CTE material mismatch [3]. For flip chip package reliability, interfaces such as underfill and die passivation or underfill and substrate solder mask have dominant failure modes due to CTE mismatch between the two materials and are areas of high concern [4]. Delamination is also prevalent in metallization and dielectric layers built on top of a base substrate in System on Package

solutions due to thermal gradients and CTE mismatch between the different materials [5]. Thermal interface material (TIM), a material with high conductivity that is applied between a heat-generating chip and a heat spreader is also prone to delamination. Due to CTE mismatch between the chip and TIM at reflow temperatures, the center of the TIM is under tension and therefore tends to delaminate from the interface [6].

All of these interfaces are further weakened in the presence of moisture and high temperature conditioning. Moisture ingress can influence interfacial adhesion in microelectronic packages by moisture absorption of polymeric materials, hygroscopic swelling of polymeric materials and changes in the mechanical properties of polymeric materials [2, 7, 8]. Thermal aging can generate compressive residual stresses and high warpage at various interfaces due to CTE mismatch between different materials. The growth of oxides on copper leadframe surfaces in copper/underfill interfaces can also play a part in the reducing its adhesion strength. The growth of oxide on the copper substrate exposed to high temperature conditioning potentially could be displacing the underfill at the adhesive bond hence reducing the interfacial strength of the copper/underfill bond. [9]. It is important to understand how temperature and moisture affect interfacial adhesion in microelectronic packages.

Although experiments are available for interfacial characterization of various interfaces after moisture and thermal conditioning, most of the current studies have focused on using a traditional fracture mechanics approach.

Cohesive zone theory is an alternative approach to interfacial delamination that considers both crack initiation and crack propagation without the presence of a starter

crack. This technique has experienced renewed interest since it has become more computationally affordable [3]. In addition, cohesive zone theory can model multiple cracks in a model and is a better alternative to fracture mechanics techniques in analyzing interfacial delamination in microelectronic packages.

CHAPTER 2. BACKGROUND AND LITERATURE REVIEW

The rapid miniaturization of microelectronic packages has put more emphasize on factors such as thermo-mechanical reliability and electrical performance. For this reason, delamination and debonding issues in dissimilar materials are more prevalent due to CTE mismatch and stress concentrations at material interfaces. Moisture absorption from the environment and the effect of high temperature from processes such as solder reflow can further weaken material interfaces. Important consideration should be given to mechanical reliability in microelectronic packages at high temperatures and humidity conditions to lower costs and improve design and process guidelines [10, 11].

2.1 Fracture Mechanics

Fracture Mechanics has been widely used in analyzing delamination and debonding issues in multilayered structures found in microelectronic packages. Numerous experimental and analytical studies have been conducted to investigate the delamination issues in bi-material interfaces such as copper/epoxy molding compound, copper/resin, die/die attach and glass/epoxy systems [12, 13]. Studies have been conducted to evaluate how residual stresses and mode mixity affect interfacial strength [12-15]. Fracture mechanics approaches assume some initial defect/crack in the material or the interface under consideration. Experiments are used to quantify a failure criteria. If the loading conditions exceed the failure criteria the package geometry under consideration will delaminate [3]. The two most common ways to characterize interfacial adhesion for a specimen with a crack is using a stress-intensity factor (SIF) or strain energy release rate (SERR) approach. It is hard to use a stress based approach to analyze

the interfacial strength of a bi-material specimen, due to how complex the closed form stress solution can get at an interfacial crack for certain geometries. SERR uses an energy based fracture mechanics approach to model cracks in package geometries and is nowadays more commonly used in modeling delamination in microelectronic packages.

2.1.1 Strain Energy Release Rate (SERR)

An energy approach to model fracture was proposed by Irwin in 1956. He proposed a term known as the strain energy release rate (SERR) or *G*. The SERR is the energy available for an increment of crack growth in a given geometry. Irwin's approach is an extension of the Griffith criterion which states that for fracture to occur the energy in the structure must be enough to overcome the surface energy of the material. Irwin defined SERR as the rate of change in potential energy, Π with respect to a given crack area, *A* as shown in Equation 2.1 [16]

$$G = -\frac{d\Pi}{dA} \tag{2.1}$$

The crack in a given geometry will propagate when *G* reaches a critical strain energy release rate G_c. G_c is a function of mode mixity, ψ and the crack will propagate in any geometry if $G > G_c$ for that particular geometry.

2.1.2 Virtual Crack Closure Technique

For simple geometries it is easier to obtain the closed form equation of SERR [16]. If the geometry is not homogeneous, complex or non-linear in behavior analytical expressions to calculate the critical SERR are more difficult to obtain. Finite element

modeling (FEM) is a useful technique that can be implemented to calculate SERR using different fracture mechanics techniques [17-20]. There are a variety of ways to characterize the SERR of a specimen including Virtual Crack Closure Technique (VCCT), J- integral method and Virtual Crack Extension (VCE) method [17-22]. For the purposes of this work a VCCT approach will be used to obtain the SERR by conducting interfacial fracture mechanics experiments.

Irwin states that if the crack extends by a small amount, Δa the energy absorbed in the process is equal to the work that is needed to close the crack to its original length, a. The crack closure technique, developed by Rybicki and Kanninen, is based on the assumption that the change in energy, ΔE that occurs when a crack propagates by Δa from a to $a+\Delta a$ is equal to the energy required to close the crack a distance of Δa [23, 24]. For a four noded two-dimensional plane stress or plane strain finite element model, the top and bottom nodes before the crack tip, a have identical coordinates but are left uncoupled. Figure 2.1shows a schematic of the geometry with a crack.

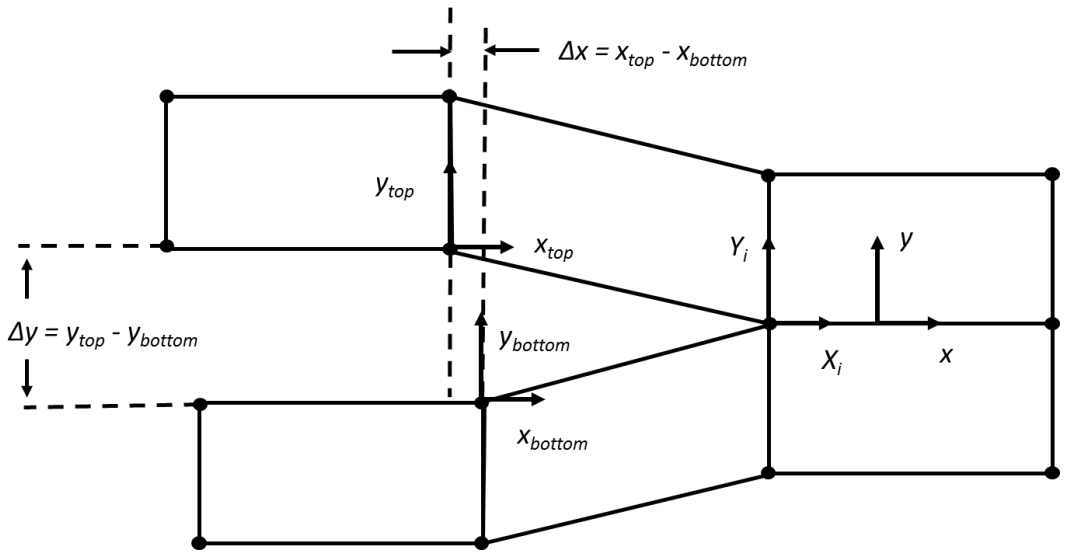

Figure 2.1 – Crack geometry used for VCCT [23]

After calculating the Mode I and Mode II components of the strain energy release rate, the total SERR is given by Equation 2.2 [23],

$$G = \frac{1}{2\Delta a} F_{Xi}\left(x_{top} - x_{bottom}\right) + \frac{1}{2\Delta a} F_{Yi}\left(y_{top} - y_{bottom}\right) \quad 2.2$$

In the above equations, F_{Yi} and F_{xi} are the horizontal and vertical forces at the crack tip. The horizontal displacement between the top and bottom surface Δa ahead of the crack tip is calculated by computing the difference between the horizontal nodal displacement at the top node, x_{top} and the horizontal nodal displacement at the bottom node, $x_{bottom.}$ Similarly, the vertical displacement between the top and bottom surface Δa ahead of the crack tip is calculated by computing the difference between the vertical nodal displacement at the top node, y_{top} and the horizontal nodal displacement at the bottom node, $y_{bottom.}$ The relative change in displacement between the top and bottom nodes ahead of the crack tip, in the x and y is given by Δx and Δy respectively. The total SERR is computed by adding its mode I and mode II components. It is important to note that VCCT is only valid while assuming that the material behavior is elastic and not plastic.

2.1.3 Fracture Mechanics for dissimilar material geometries

The above fracture mechanics techniques are usually meant to be applied to cracks in homogenous materials. It is more difficult to evaluate the interfacial strength of a crack geometry with different materials. Figure 2.2 shows a schematic of a bi-material crack geometry.

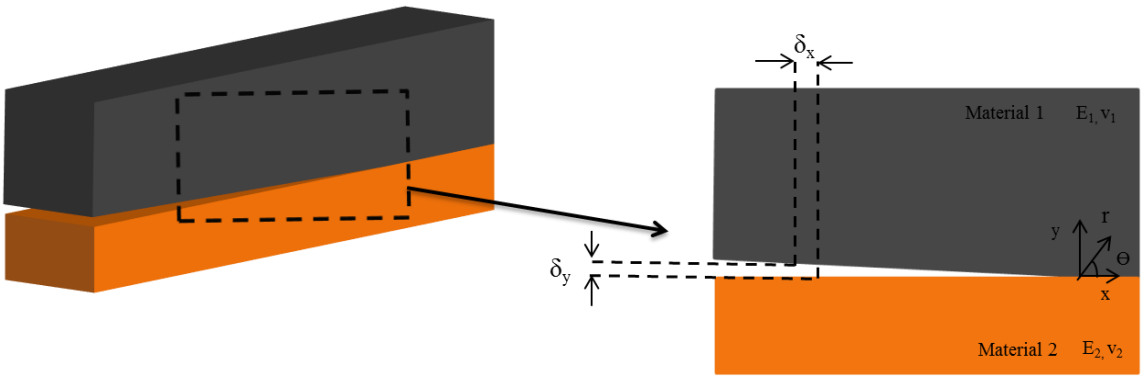

Figure 2.2 – Bi-material specimen with crack geometry

The stress field around a bi-material crack tip was first studied by Williams in 1959 [25]. Williams found out that the stress field around the crack is coupled and the singularity is is of the order r^{ξ} where $\xi = -1/2 + i\varepsilon$. In this equation, ε is the bi-material constant, given by,

$$\varepsilon = \frac{1}{2\pi} ln\left[\frac{1-\beta}{1+\beta}\right] \tag{2.3}$$

where β is one of "Dundur's parameters" given by Equation 2.4 as follows.

$$\beta = \frac{\mu_1(\vartheta_2 - 1) - \mu_2(\vartheta_1 - 1)}{\mu_1(\vartheta_2 + 1) + \mu_2(\vartheta_1 + 1)} \tag{2.4}$$

The greater the value of the bi-material constant, ε the more dissimilar the two materials used in the crack geometry. The stress intensity factors, K_I and K_{II} for a bi-material specimen are not similar to the stress intensity factors for a homogeneous material. Rice and Sih formulated a complex stress intensity factor, K for a bi-material specimen, given by [26],

$$\sigma_{yy} + i\sigma_{xy} = \frac{K}{\sqrt{2\pi r}} r^{i\varepsilon} \tag{2.5}$$

where $K = K_1 + iK_2$.

2.1.4 Mode Mixity for dissimilar material geometries

A variety of studies have been conducted to study mode mixity of a bi-material specimen. Matos et al. developed the crack-face displacement method that is widely used in most problems involving a crack geometry [27]with different materials [28]. Yau et al. proposed the M-integral method and VCCT has also been used to extract SIF factor based or SERR based mode mixity for bi-material geometries [29]. For the purpose of this work the crack-face displacement method, first developed by Matos et al. [28] will be used to determine the mode mixity of the bi-material crack geometry.

Hutchinson and Suo [27], formulated a relationship between the crack displacements ahead of the crack tip and the complex stress intensity factors for a bi-material crack geometry, given by,

$$\delta_y + i\delta_x = 8\frac{K_I + iK_{II}}{(1 + 2i\varepsilon)E^*\cosh(\pi\varepsilon)\sqrt{2\pi}}\sqrt{r}\left(\frac{r}{l}\right)^{i\varepsilon} \tag{2.6}$$

As shown in Figure 2.2 the relative displacements δ_y and δ_x a distance r ahead of the crack tip can be calculated using an FEM software. The parameter, l is the characteristic specimen dimension used to normalize the crack tip distance and is usually chosen to be the width/height of the specimen. Once crack tip displacements are obtained the mode mixity of the bi-material specimen can be calculated using the equation below.

$$\psi = tan^{-1}(\frac{\delta_x}{\delta_y}) - tan^{-1}(-2\varepsilon) - \varepsilon\, ln(\frac{r}{l}) \quad 2.7$$

The distance r ahead of the crack tip used to calculate the mode mixity, ψ can be determined using Equation 2.8

$$\frac{{\delta_y}^2 + {\delta_x}^2}{r} = 64\frac{G^*}{2\pi(1+4\varepsilon^2)E^*} \quad 2.8$$

where the value G^* is the SERR. G^* is obtained by using VCCT in a FEM software. E^* is calculated using Equation 2.9.

$$\frac{1}{E^*} = \frac{1}{2}(\frac{1}{E_1} + \frac{1}{E_2}) \quad 2.9$$

As mentioned earlier, the relative displacements δ_y and δ_x, a distance r ahead of the crack tip are also obtained from then FEM software. The value of r for which the above relationships in Equation 2.8 intersect or are equivalent is then used in Equation 2.7 to obtain the mode mixity, ψ of the bi-material interface.

G_c can also be obtained as a function of ψ. Hutchinson and Suo [27] formulated a model to obtain this relationship as shown below.

$$G_c = G_{IC}\{1 + \tan^2(\psi(1-\lambda))\} \quad 2.10$$

In the above relationship, G_{IC} is the mode I critical strain energy release rate of the bi-material interface and λ is a non- dimensional parameter that relates to the brittleness

of the structure. At $\lambda = 0$, delamination is dominated by Mode I behavior. At $\lambda = 1$, the bi-material geometry is "ideally brittle" and the crack initiates at $G = G_{IC}$

Figure 2.3 shows a typical G_c vs mode mixity ψ graph obtained for a material where $\lambda = 0.1$ and G_{IC} 10 =J/m^2.

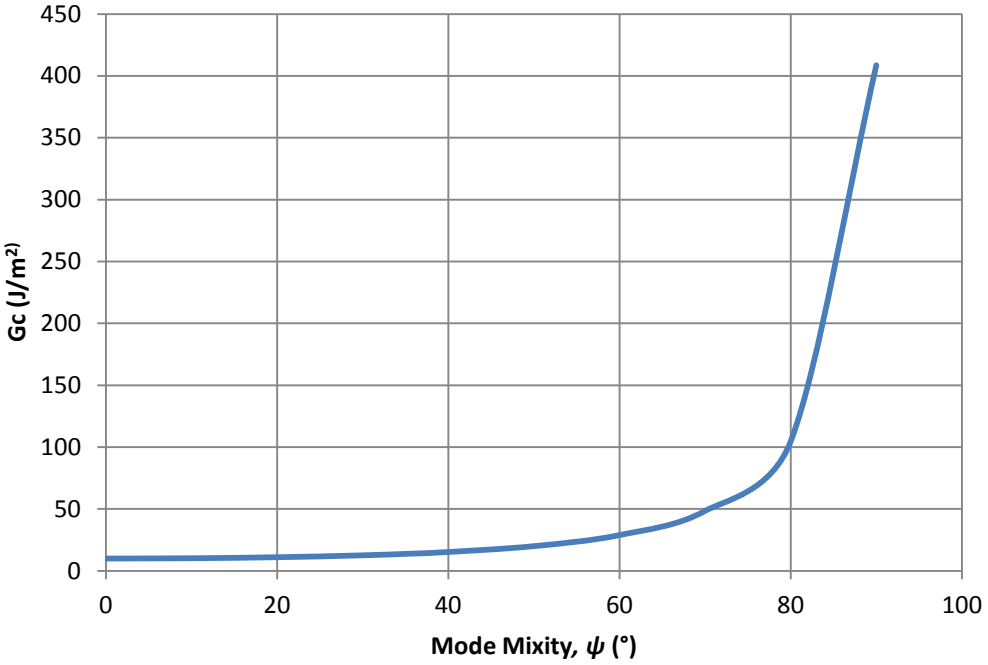

Figure 2.3 – G_c vs. mode mixity, ψ for a material with $\lambda = 0.9$ and G_{IC} =10 J/m^2

2.2 Cohesive Zone Models

Cohesive Zone Modeling (CZM) is an innovative way of simulating crack initiation and propagation at an interface. CZM doesn't require a starter crack and has been applied in a number of applications to simulate interfacial crack propagation including thin-film structures, adhesively bonded polymers, glass/elastomers, and on-chip interfaces [30-33].

CZM can be used in FEM software to model complexities such as inelasticity, large deformation and delamination and debonding in complex geometries.

2.2.1 CZM theory

The basic premise of the CZM technique is that it assumes that there is a certain macro-scale fracture process zone that exists ahead of the crack tip in the geometry that is another consideration. This zone can be described by CZM laws that model traction forces and physical separations at the crack tip region [34].

Interfacial separation in a CZ model occurs in a cohesive damage zone when the damage exceeds a certain pre-set value. There are a number of traction-separation laws available to characterize interfacial separation. These include, for example, bi-linear, trapezoidal, exponential and others as shown in Figure 2.4. For the purposes of this paper, a bilinear traction-separation law that was proposed by Alfano and Crisfield will be used [35].

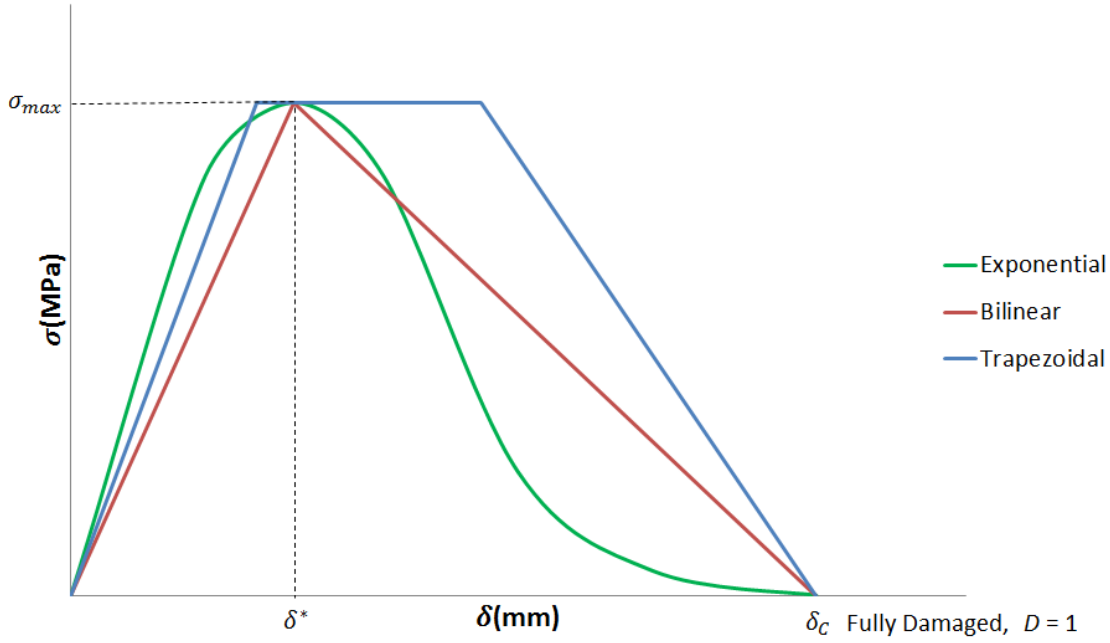

Figure 2.4 – Traction separation laws for cohesive zone elements

2.2.2 CZ Bi-linear Traction Separation Law

The bilinear law represents the interfacial traction, σ vs. the interfacial separation, δ. As the CZ elements undergo interfacial delamination, they show elastic loading for, $\delta < \delta^*$. For this elastic loading region, the interface is assumed not to experience any damage, and unloading will return the elements to their original configuration. The damage accumulated at the interface can be represented by a damage parameter, D. When, $\delta > \delta^*$, D starts to increase, and when $\delta \geq \delta_c$, D reaches a maximum value of 1. D can be represented by Equation 2.11.

$$D = \begin{cases} 0 & \text{if } \delta \leq \delta^* \\ \left(\frac{\delta - \delta^*}{\delta}\right)\left(\frac{\delta_c}{\delta_c - \delta^*}\right) & \text{if } \delta^* < \delta < \delta_c \\ 1 & \text{if } \delta \geq \delta_c \end{cases} \qquad 2.11$$

The path of the load-unload curve for the different damage criteria mentioned up is shown in Figure 2.5 as follows:

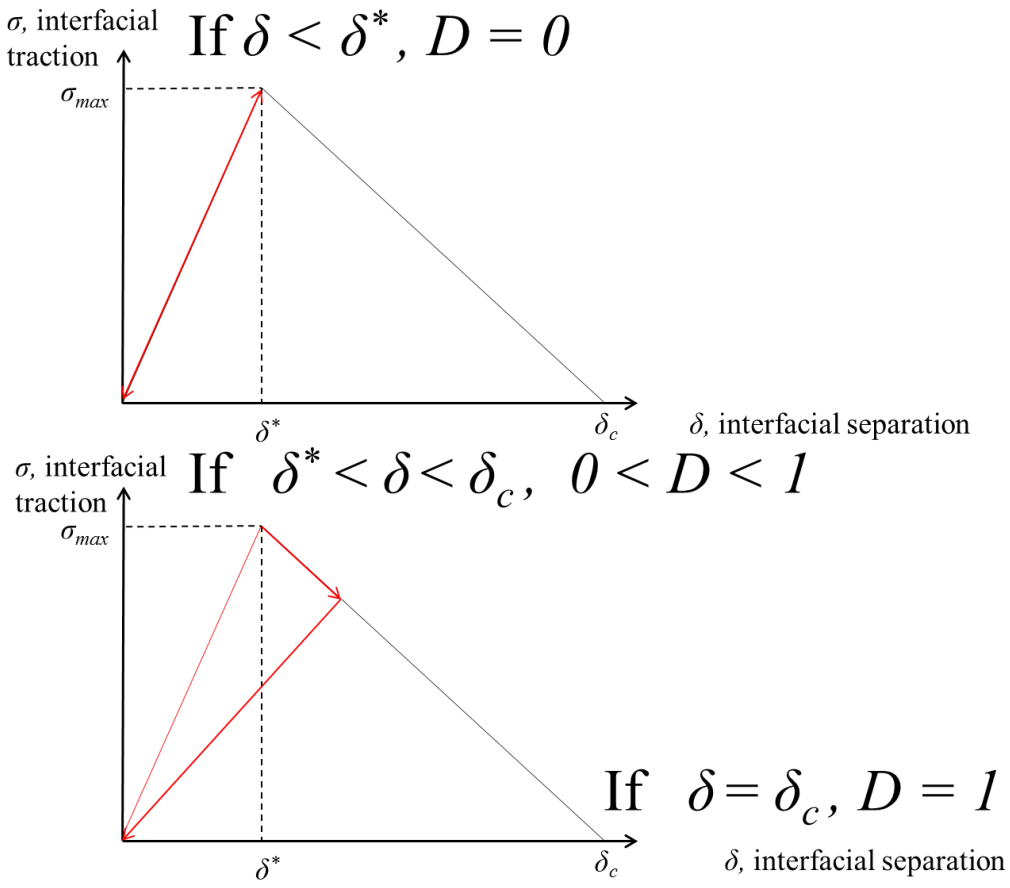

Figure 2.5 – Damage criteria for bi-linear traction separation law

If $\delta < \delta^*$ then no damage will accumulate at the elements in the crack tip region and load unload path will be the same. If $\delta^* < \delta < \delta_c$ then some elements will be partially damaged and the unload path will have a higher compliance than the load path. The value of D will never decrease, regardless of the current state of loading. When $D = 1$, the interfacial stiffness of CZ elements is zero, and the interface is assumed to be fully separated.

The interfacial traction can be represented as a function of δ and D as follows.

$$\sigma = \frac{\sigma_{max}}{\delta^*}(1 - D)\delta \qquad 2.12$$

The area under the traction-separation curve is G_c, and for a bi-linear curve, it can be computed as:

$$G_C = 0.5\delta_c\sigma_{max} \qquad 2.13$$

2.2.3 Implementing CZ laws using FEM software

A few data reduction techniques are available to implement CZ laws, including the property method, the direct method and the inverse method [34]. The inverse method will be implemented in this study to obtain CZ laws for the bi-material geometry. The inverse method involves changing certain CZ parameters in FEM software to obtain simulated load vs. displacement curves for a various loading conditions and a given geometry. These results will then be compared and matched with experimental load vs. displacement data obtained by conducting interfacial fracture mechanics experiments. The bilinear laws for CZM consist of Mode I and Mode II parameters. These parameters include the maximum traction, $\sigma_{max,}$ the maximum interfacial separation, $\delta_{c,}$ and the ratio $\alpha = \delta^* / \delta_c$ for both Mode I and Mode II, resulting in a total of six parameters. It is important to note that the mesh used around the crack tip region in the FEM software has an impact on the model. Alfano and Crisfield [35] mention that increasing the σ_{max} to a higher values might require the mesh around the crack tip region to be refined as well.

Not doing so will lead to discretization errors in the simulated load vs. displacement data and oscillatory behavior during delamination as shown in Figure 2.6.

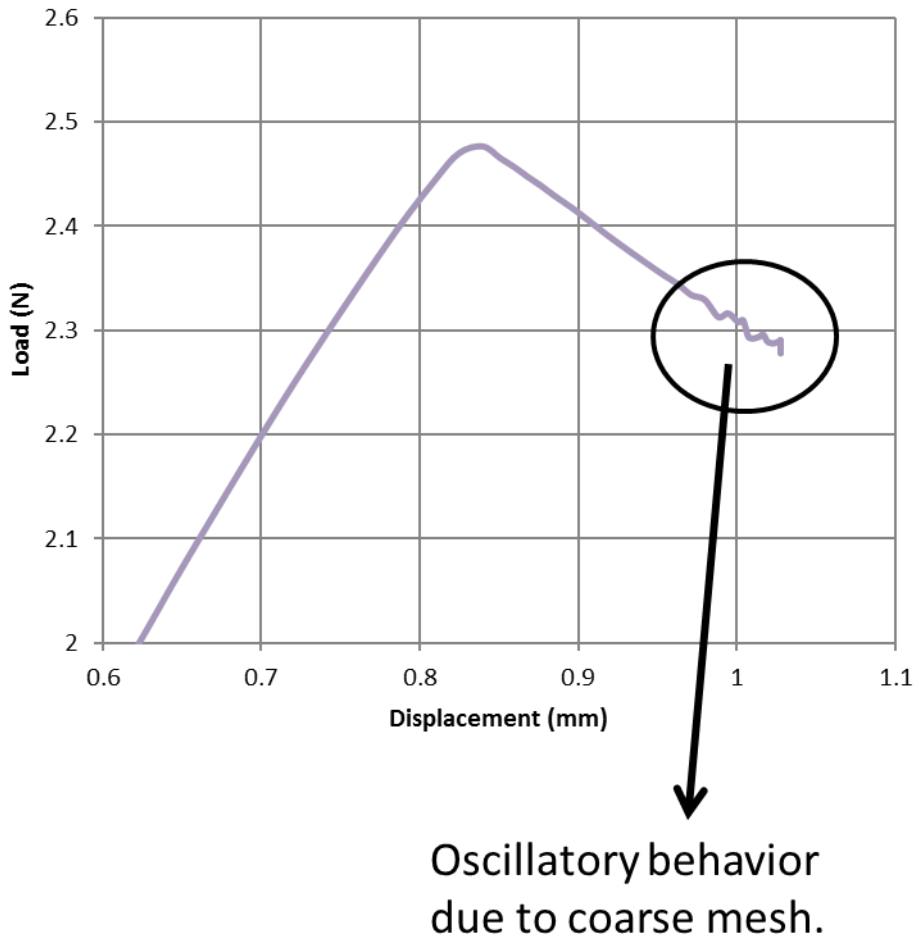

Figure 2.6 – Discretization error and oscillatory behavior in DCB CZ simulation due to coarse mesh around crack tip.

For σ_{max} values which are too high for a given mesh density and result in discretization errors and oscillatory behavior, sufficiently increasing the mesh density around the crack tip will reduce the discretization errors and smooth out the curve. In this study, as different values of σ_{max} are fitted, the mesh density is altered as required for higher maximum traction values to avoid these discretization errors.

2.3 Moisture Absorption Studies on Dissimilar Material Layers in Microelectronic Packages

Several studies have been done to understand how polymer interfaces, specifically underfill respond to moisture absorption. In general, moisture exposure on underfill/epoxy molding compound has shown to reduce the interfacial adhesion of the interface being investigated. Ferguson and Qu [9]investigated the effect of interfacial adhesion on an epoxy underfill with a copper substrate while keeping the temperature exposure constant at 85 °C. Interfacial fracture tests were conducted on samples exposed to temperature/humidity conditions including dry, 85 °C only, 85 °C/50% R.H., 85 °C/65% R.H. and 85 °C/85% R.H. There is no change in the mass of the specimen from moisture uptake after 168hrs of exposure hence verifying that the underfill was fully saturated and steady state conditions existed. The samples were tested at these conditions for 168hrs.

Interface cracks were created between the substrate and the underfill. The interfacial fracture strength was computed using the SERR, the energy at which the bi-material specimen will begin to delaminate. Using the underfill elastic modulus obtained at various humidity conditioning levels, the interfacial fracture toughness of the underfill/copper sample was evaluated. Table 2.1 shows the G_c values obtained at various humidity conditioning levels.

Table 2.1 – Effect of moisture exposure on the critical energy release rate of the copper/underfill sample [9]

Humdiity Conditioning Level	G_c (J/m^2)
Control	8.97
85°C only	8.18
85°C / 50 R.H.	5.26
85°C / 65 R.H.	4.57
85°C / 85 R.H.	3.76

As can be seen from Table 2.1, temperature exposure itself didn't have much affect on the SERR value of the copper/underfill sample. Once moisture conditioning was introduced, there was a significant reduction in G_c and this value kept dropping as the humidity conditioning level was increased. Using a flexural three point bend test, Ferguson and Qu [9] also evaluated the change in elastic modulus of the underfill due to moisture presence. The elastic modulus of the underfill was only tested because copper is a metal and hence unaffected by moisture uptake. The elastic modulus of the underfill didn't change much after moisture preconditioning at 85 °C/50% R.H and 85 °C/65% R.H. However at 85 °C/85% R.H there was a 8.76% in the elastic modulus value of the underfull. Furthermore, exposure at 85 °C/95% R.H led to a 17.6 % drop in the elastic modulus of the underfill. Ferguson and Qu [9] showed that this change in elastic modulus didn't affect the ψ of the underfill/copper substrate significantly and therefore was assumed to be held constant for their study.

Another study by Shirangi et al. [36] investigated the effect of moisture absorption and desorption on an epoxy molding compound/copper interface. An end-notched flexure (ENF) test was used to characterize the interfacial fracture toughness of a EMC/copper sample. A VCCT approach was implemented using FEA software to measure the interfacial fracture toughness of the EMC/Copper sample.

Shirangi et al. [36] calculated the interfacial fracture toughness after putting the EMC/Copper sample through humidity conditioning at 85 °C and 85% R.H for a period of 2 weeks. This was numerically determined as the time it took for the EMC to reach virtual saturation. The samples were then removed from the humidity chamber and the ENF test was conducted at room temperature. The effect of desorption was also investigated. The samples were dried for 24hrs at 125 °C and the ENF test was conducted at room temperature. In addition, EMC/Copper samples were conditioned at 85 °C and 85% R.H for longer durations (up to 4 weeks) and dried for 24hrs at 125 °C before the ENF test was done at room temperature.

The results showed that after exposure at 85 °C and 85% R.H for 2 weeks there is an appreciable drop in the G_c value of the EMC/Copper sample from 58.7 J/m^2 in the dry state to 26.3 J/m^2 after moisture conditioning. Upon subsequent drying at 125 °C for 24hrs, the G_c value of the EMC/Copper sample obtained was 44.9 J/m^2 suggesting that some of the EMC/Copper adhesion loss was recovered. However on baking the sample at 125 °C for 24hrs after placing it in the humidity chamber for up to 4 weeks the interfacial adhesion obtained was 28.8 J/m^2 .

In another study, Shirangi et al. [36] also investigated how humidity conditioning as a function of time affected the fracture toughness of the EMC/Copper sample. An ENF test was used to determine the fracture toughness of the EMC/Copper geometry after conditioning the sample at 85 °C and 85% R.H for up to 8 weeks. EMC/Copper samples were removed at 1 week (168hrs) intervals and the interfacial fracture toughness was calculated at room temperature. The results showed that a major reduction in the G_c value of the EMC/Copper sample was seen right after 168 hrs. There was no appreciable

change in the G_c value after humidity conditioning the EMC/Copper sample for longer durations [36-39].

It is clear that the reduction in the interfacial strength of the underfill/copper substrate occurs primarily because of the presence of moisture. Moisture exposure might be causing a reduction in adhesion strength through the displacement of the underfill, hence reducing Van der Waals forces at the interface. In addition, moisture exposure might also be resulting in chemical degradation of the adhesive bonds at the underfill/copper interface. Since the elastic modulus of the underfill wasn't significantly affected after moisture exposure, any plasticization of the underfill didn't impact the interfacial fracture toughness of the bi-material specimen [9].

The second study revealed that the duration of moisture exposure has an effect on the interfacial strength of the EMC/Copper sample. Moisture absorption after two weeks of exposure at 85 °C and 85% R.H was primarily caused by the presence of water molecules at the interface. On exposing the EMC/Copper sample to longer durations of humidity conditioning, there seems to be permanent damage in the adhesion bonds of the EMC/Copper that cannot be reversed. In addition, in an EMC/Copper sample most of the adhesion loss due to moisture absorption occurs within the 1st week of exposure and levels out from that point on. This suggests that the EMC has a high moisture diffusion rate and most of the absorption occurs within 1 week of exposure [36].

2.4 Thermal Aging Studies on Dissimilar Material Layers in Microelectronic Packages

Many studies have been done to study the effect of isothermal aging in an EMC/Copper specimen, especially at temperatures of 85 °C and 175 °C. These two temperatures are really important because they represent the temperatures applied during packaging processes such as solder reflow. Isothermal conditioning at 85 °C is relevant in order to be able to isolate the effect of moisture conditioning conducted at 85 °C and 85 % R.H. 175 °C is usually the temperature of the transfer mold process during fabrication of the EMC/Copper specimen. Several studies have shown that isothermal aging at temperatures as low as 85 °C shows no significant change in the interfacial strength of an EMC/Copper specimen. As shown in Table 2.1, Ferguson and Qu [9] showed that exposing an underfill/copper sample to 85 °C for 168hrs didn't significantly affect the G_c value. This was also confirmed by Shirangi et al. [38] who didn't seen a change in the interfacial adhesion of the EMC/Copper sample after thermally aging it at 85 °C for 2 weeks (336 hours). However, if the aging temperature is raised to 175 °C, a significant drop in G_c value was observed. The G_c value of the EMC/Copper sample drops by 45.4 % after exposing the EMC/Copper sample to 175 °C for a period of 2 weeks.

The adhesion loss at 175 °C could be due to the degradation of the EMC polymer at high temperatures which lead to a reduction in the Van Der Waals forces at the interface. In addition, oxide deposition on the copper leadframe could be a reason for the drop in G_c value for the interface in question [39]. Ferguson and Qu [9] conduct X-ray Photoelectron Spectroscopy studies to investigate the surface of the Cu leadframe after fracture testing.

The shake up satellite observed in the Cu scan indicates the presence of cupric oxide, CuO on the Cu Leadframe. The oxide formation could potentially be displacing the

underfill at the adhesive bond hence contributing to the loss in adhesion [9]. The effective stress relaxation and creep strain generated at the interface due to thermal aging could also be a cause for the interfacial drop in G_c.

CHAPTER 3. OBJECTIVES AND SCOPE OF THIS RESEARCH

As outlined in the previous chapters, the effect of humidity conditioning and thermal aging on interfacial delamination have been studied in existing literature using fracture mechanics-based approaches. However, to the best of the author's knowledge, there are no studies in open literature that investigate the effect of humidity conditioning and thermal aging on cohesive zone modeling and cohesive zone parameters, particularly for epoxy mold compound (EMC)/copper interface.

The objectives of this thesis are to determine modified cohesive zone parameters through experiments and simulations for EMC/copper interface that is subjected to moisture conditioning or thermal aging, and to study how these modified cohesive zone parameters compare against the cohesive zone parameters for pristine CMC/copper interface. The following sections outline the approach taken in this research to address the objectives:

1. The critical SERR (G_c) of EMC/Copper pristine interface is first determined by conducting interfacial fracture experiments. These experiments include double cantilever beam test and four-point bend test.
2. From the load versus displacement experimental data of the interfacial fracture experiments, G_c can be calculated through FEM and analytical calculations. The variation of G_c as a function of mode mixity is then determined.
3. Using load vs. displacement experimental data as well as G_c variation as a function of mode mixity, the cohesive zone parameters are then determined for as-received or pristine EMC/copper interface.

4. EMC/Copper specimens will then be subjected to different humidity conditioning and thermal aging profiles, and the interfacial fracture mechanics experiments are then repeated at room temperature.
5. As discussed in Step #2 and #3, modified CZ parameters are then determined for humidity- and temperature-conditioned EMC/Copper samples.
6. The modified CZ parameters for conditioned samples are compared against the CZ parameters for as-received pristine samples, and a discussion is provided as to effect of humidity and temperature conditioning on CZ parameters.

CHAPTER 4. EXPERIMENTAL PROCEDURE AND RESULTS FOR AS-RECEIVED EMC/COPPER SAMPLE

The strength of the EMC/Copper interface is calculated using the critical strain energy release rate (G_c). A double cantilever beam (DCB) and a four point bend (FPB) test are used to determine the strength of the EMC/Copper interface for different loading conditions. It is important to calculate G_c for different combination of peel and shear stresses, as G_c is a function of mode mixity (ψ). Using the DCB and FPB test results, a relationship between G_c and Mode Mixity (ψ) is determined for the EMC/Copper interface. These results and the experimental load vs. displacement data are used to determine the CZ parameters for as-received EMC/Copper sample

4.1 EMC/Copper Specimen

NXP Semiconductor provided us with the EMC/Copper sample to conduct experimental tests. The EMC/Copper sample is fabricated by cooling molten EMC on copper from the cure temperature of 175 °C to room temperature (25 °C) in 4 hours. The EMC is poured into a transfer mold that is clamped onto the copper leadframe. As the EMC cures and solidifies from the cure temperature of 175 ºC it experiences cure shrinkage. Cure shrinkage is shrinkage experienced in the EMC that is unrelated to CTE. A study showed that the cure shrinkage of the EMC was around 1 % [40]. The 1 % volumetric shrinkage can be accounted by increasing the reference temperature as show in Equation 4.1.

$$T'_{ref} = T_{ref} + \frac{0.1\%}{3\alpha} \quad 4.1$$

where α is the CTE of the EMC at T_{ref} = 175 ºC From Equation 4.1 the new reference temperature obtained for the EMC is 185.42 ºC, which is used in this analysis.

Figure 4.1shows the bi-material strip that consists of a *Sumitomo Sumikon*® EME-G630AY mold compound on top and a CDA194 copper alloy as the leadframe on the bottom. The material properties for the EMC and the copper are shown in Table 4.1and Table 4.2 respectively.

Table 4.1 - Material properties of EMC compound

Property	Value
E (GPa)	25 at 25 °C; 0.7 at 260 °C
ν	0.30
α (ppm/°C)	9 at 25°C; 32 at 260 °C
T_{ref} (°C)	185.42

Table 4.2- Material Properties of Cu leadframe

Property	Value
E (GPa)	121
ν	0.33
α (ppm/°C)	17.6

T_{ref} (°C)	175

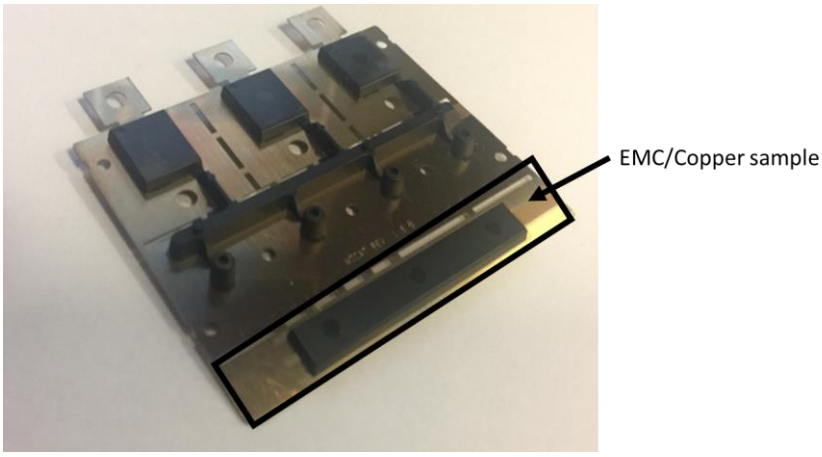

Figure 4.1 – EMC/Cu leadframe bi-material sample

4.2 DCB Experimental Testing

In order to conduct DCB testing, a pre-crack is first created in the EMC/Copper sample. A schematic of the test set up is shown in Figure 4.2.

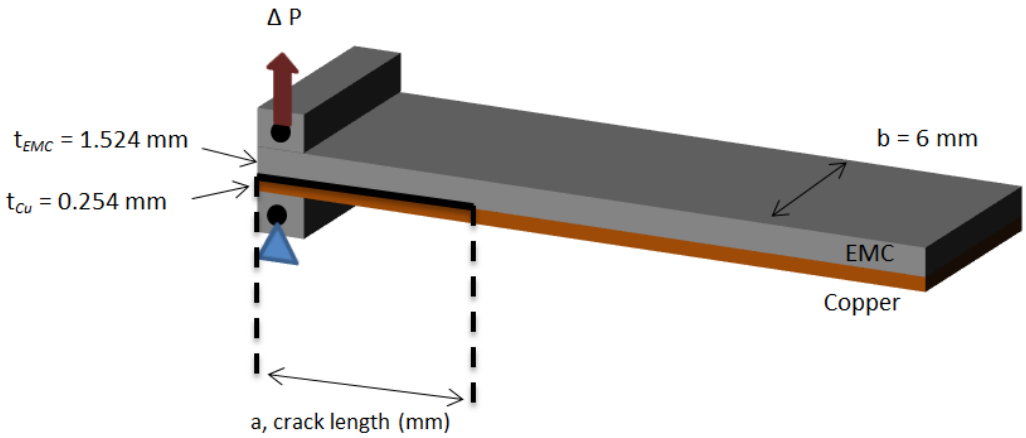

Figure 4.2 – Schematic of DCB set up of EMC/Copper sample

The pre-crack is created by clamping down the end of the specimen and pushing down on the copper from the EMC at the other end [3]. After the pre-crack is created, aluminum loading fixtures are affixed on the specimen using epoxy resin. The sample is then placed in a *Delamination Testing System*™ (DTS) to determine the load vs. displacement, the critical load for crack propagation, and the unloading curve. For this test, a displacement-controlled loading is applied at 5 µm/sec. Figure 4.3 shows pictures of the DCB test in progress on the DTS machine and the crack growth of the EMC/Copper sample.

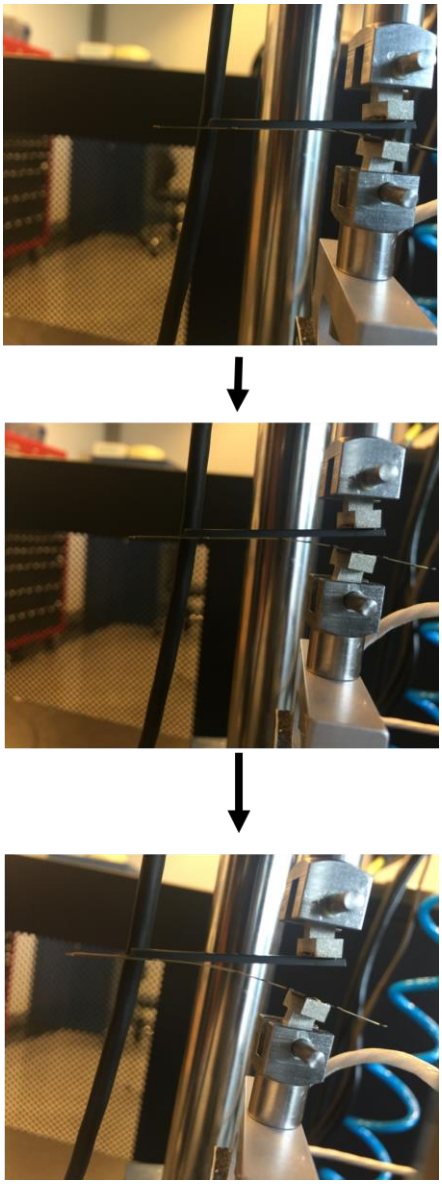

Figure 4.3 –Pictures of the DCB test in progress

Figure 4.4 shows a typical load vs. displacement curve where the sample is loaded until delamination propagates, then unloaded and re-loaded to further propagate the crack, and these loading and unloading steps are repeated several times.

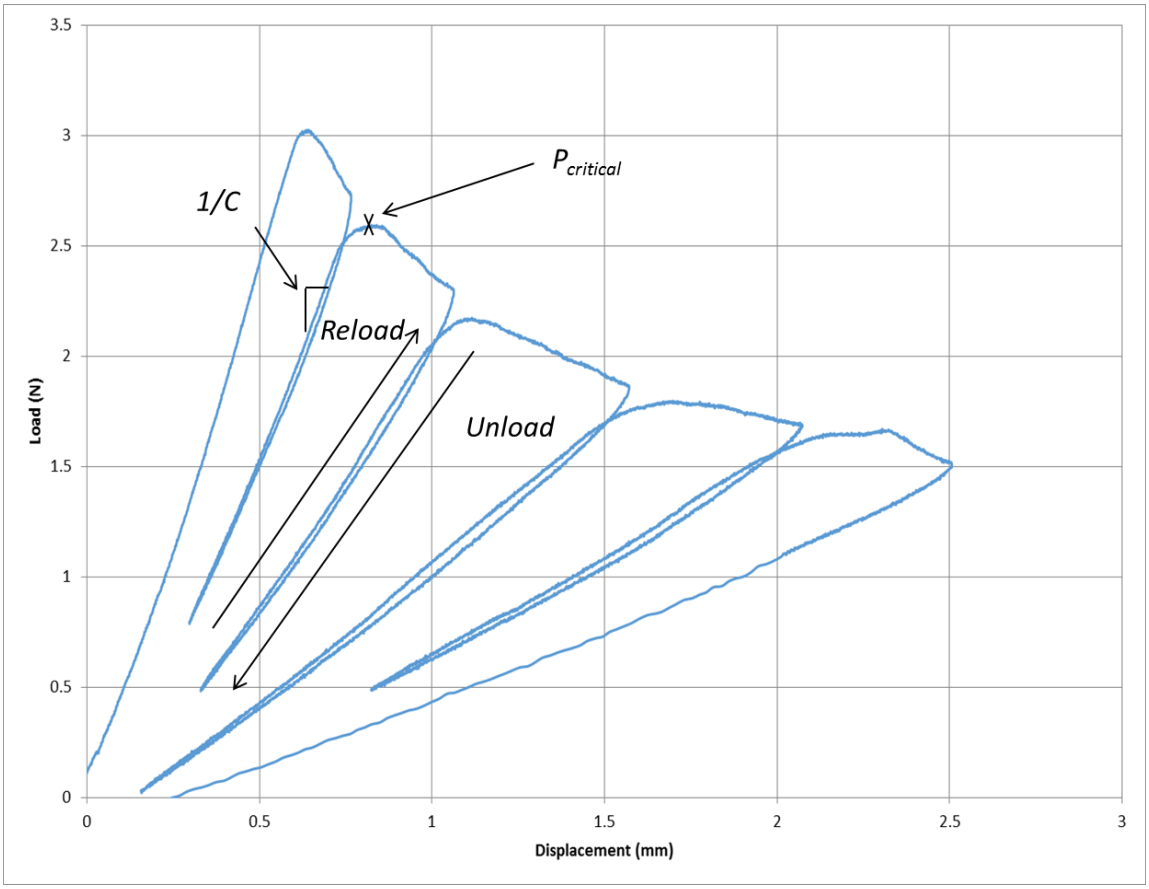

Figure 4.4 - Typical load vs. displacement curve for a DCB experiment

As shown in Figure 4.4, at first the load increases linearly until some critical point, $P_{critical}$.Once the delamination starts to propagate, the load drops. The sample is then unloaded and a linear unloading path is observed. As can be seen in the graph for the next loading path, the compliance of the sample, *C* has increased from before. This increase in the compliance *C* is due to the increase in the crack length of the sample.

4.3 DCB Numerical Simulations

To obtain the interfacial crack length from a DCB experiment, a Finite-Element Model (FEM) of the EMC/Copper is generated. The model is constructed in ANSYS™ Version 14.0. For the purposes of this geometry a 2-D plain strain assumption is used to

construct the model. Figure 4.5 shows a schematic of the mesh and loading conditions applied to the EMC/Copper geometry. A force is applied on the top left corner node. The force applied is divided by the width of the sample, *b* since this model assumes plain strain. A denser mesh is used around the crack region compared to the rest of the geometry. The bottom left pin in the model is fixed in the *x* and *y* directions. EMC and copper element nodes are not merged in the regions to the left of the crack tip to mimic the crack in the specimen. The solid green line represents the region where the EMC and copper elements are not merged and is equal to the crack length of the sample. Regions ahead of the crack tip are merged together. The material properties used for the EMC and Copper are obtained from Table 4.1 and Table 4.2.

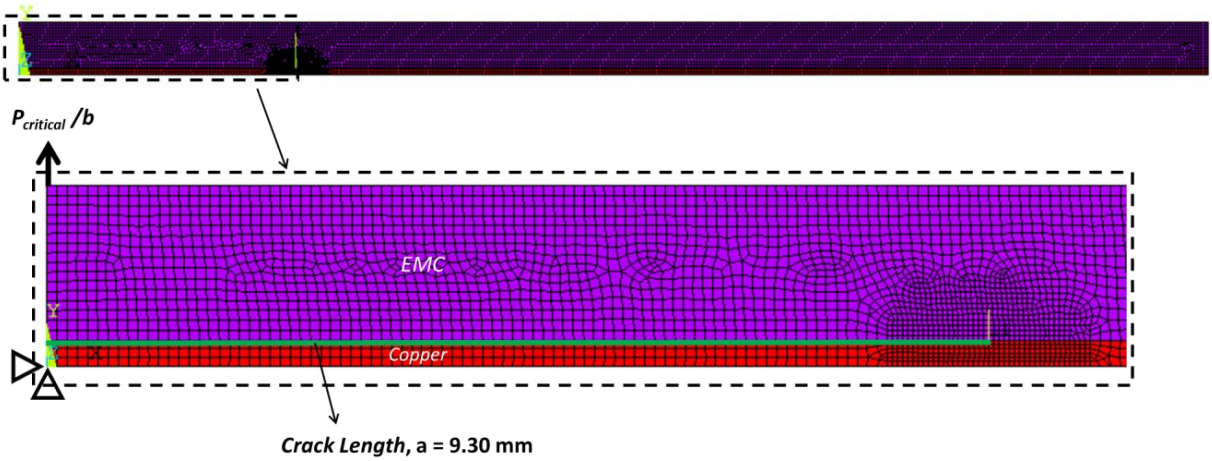

Figure 4.5 – 2-D plane strain model of DCB test

4.3.1 Compliance vs. Crack Length Relationship

The 2-D plane strain DCB model is used to generate a compliance vs. crack length relationship for the EMC/Copper specimen. To construct this compliance vs. crack

length relationship, it is assumed that the EMC/Copper specimen behaves like a classic beam and so the materials under consideration are elastic and isotropic.

To generate the compliance vs. crack length relationship, FEM simulations are performed at crack lengths ranging from 8 to 27 mm. These crack lengths are representative crack lengths in most experiments. At each crack length, the increase in vertical displacement of the top left node in the 2-D plan strain DCB model is computed as the load is increased from 0 to 10 N. Using the load vs. displacement curve, the compliance, the inverse of the slope of load vs. displacement data, can be computed for that crack length. Thus, by running such simulations over a wide range of crack lengths and keeping the crack length constant for a given simulation, compliance values for various crack lengths can be obtained. Figure 4.6 shows the compliance vs. crack length relationship generated through such simulations. The data from the simulations can be fitted with a polynomial curve, and as seen, a cubic polynomial fits the compliance vs. crack length curve. A cubic polynomial fit is in agreement with the order of deflection for classic Euler beams. The additional terms ahead of the cubic term in the fitted equation take into consideration non ideal aspects of the geometry, such as large deflections and use of different materials.

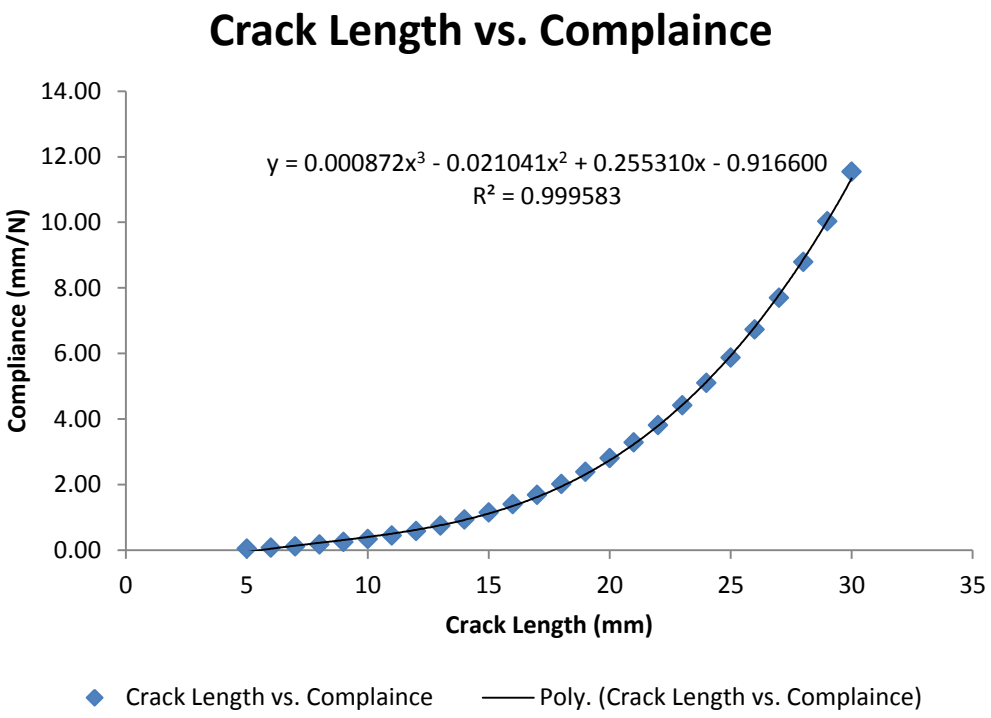

Figure 4.6 - Compliance vs. crack length relationship for DCB test

Using the compliance obtained from load/unload curves after conducting DCB experiments, the fitted cubic equation from Figure 4.6 can be used to determine the crack length of the EMC/Copper sample for a given compliance value.

4.3.2 Calculating G_c for the DCB experiment

Using the relationship in Figure 4.6, the crack length is computed from the experimental compliance, *C* obtained through the DCB experiment. The experimental compliance may be obtained as the inverse of the slope of the unloading curve [3] and thus, the crack length can be obtained. When the sample is then loaded, $P_{critical}$ value can be obtained for that crack length. The 2-D plane strain model is re-run with the crack length obtained, and a force, $P_{critical}/b$ is applied to the upper loading pin. For this loading

condition, the SERR obtained will be equal to G_c. Here, VCCT [23] is used to determine G_c.

*4.3.3 As-Received EMC/Copper DCB Test Results *

DCB experiments are conducted for 10 as-received, unconditioned EMC/Copper samples. Table 4.3 shows the average G_c values obtained for each sample. The average G_c value obtained for as-received EMC/Copper samples from DCB testing is 45.1 J/m^2.

Table 4.3 - **G_c values for as-received EMC/copper DCB samples**

As Received EMC/Copper Specimen	**Average G_c (J/m^2) (VCCT)**
Sample 1	47.8
Sample 2	44.5
Sample 3	47.3
Sample 4	41.4
Sample 5	45.6
Sample 6	43.3
Sample 7	46.2
Sample 8	42.7
Sample 9	46.9
Sample 10	43.7
Average	**45.1±3.73**

4.4 DCB Mode Mixity Calculation

The mode mixity, ψ of the DCB geometry is calculated using the crack displacement method as described in Section 2.1.4. For this specific geometry, an as-received sample with a crack length of 10.8 mm and $P_{critical}$ value of 2.29 N is used to obtain the mode mixity, ψ of the EMC/Copper specimen. Nodal displacements, δ_y and δ_x are calculated for varying values of r ahead of the crack tip for this given geometry. G^* in this case is equal to G_c of the EMC/Copper DCB geometry, which is obtained through VCCT. Both sides of Equation 2.8 are plotted together on Figure 4.7 for two different values of r.

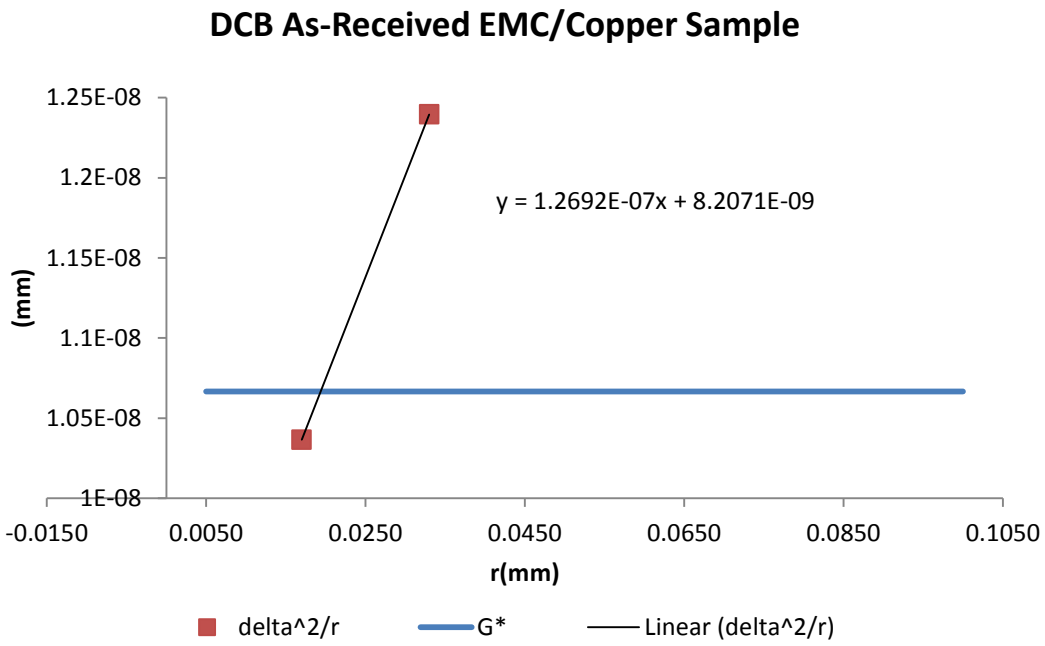

Figure 4.7 - Finding r to calculate ψ for an as-received DCB EMC/copper sample

A linear interpolation equation can be formulated between the two r values and used to calculate the intersection point of the two graphs as shown in Figure 4.7. The intersection point occurs at r = 0.0194 mm. Putting this value of r in Equation 2.7 gives a mode mixity, ψ of 29.2° for the DCB geometry. Mode mixity is also calculated for longer

crack length DCB experiments. Figure 4.8 shows the graph used to find r for a DCB EMC/Copper specimen with a crack length of 19.4 mm and a $P_{critical}$ value of 1.21 N.

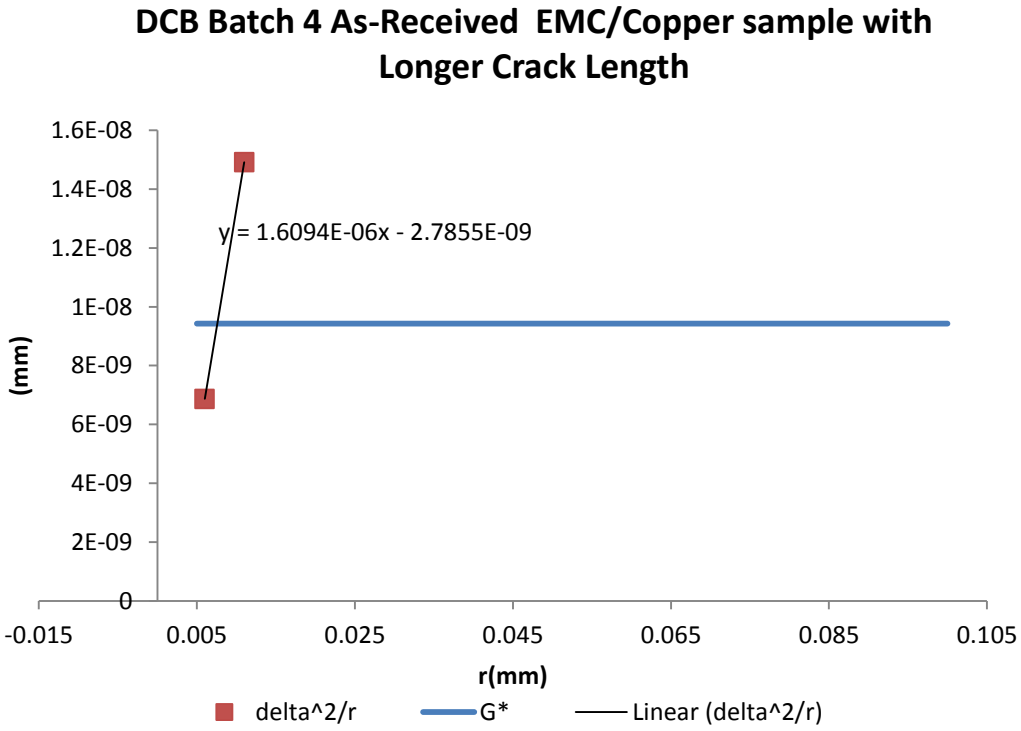

Figure 4.8 - Finding r to calculate ψ for an as received DCB EMC/copper sample with a longer crack length

The intersection of the two graphs in Figure 4.9 gives an r value of 0.00759 mm. Inputting this value in Equation 2.7 gives a mode mixity, ψ of 29.6° for the as received DCB specimen. Both the mode mixities obtained at different crack lengths yield similar values, confirming that mode mixity doesn't change with crack length. The average mode mixity obtained for the as-received EMC/Copper DCB geometry is 29.4°.

4.5 DCB Analytical Solution

There are not many analytical SERR solutions available for a DCB geometry with different materials. Xiao et al. presents an analytical solution to obtain G_c for an

asymmetric DCB geometry with different materials, but this formulation is only valid for cracks with lengths much longer than the beam thickness [41]. Sundararaman and Davidson present an analytical solution for a DCB geometry with different materials, however this solution is complex and harder to implement [42]. Soboyejo et. al presents a simpler analytical solution for a DCB geometry to calculate G_c. Soboyejo et. al's calculations assume that the thickness of the two materials is the same, so the mode mixity of the geometry is much closer to mode I than the set up used in this study [43]. The following equations are used to calculate G_c analytically for the DCB geometry.

$$G = \frac{6P^2a^2(1+\frac{1}{\beta_E{\beta^3}_T})}{E_{EMC}b^2{t_{EMC}}^3} \tag{4.2}$$

$$\beta_T = \frac{t_{Cu}}{t_{EMC}} \tag{4.3}$$

$$\beta_E = \frac{E_{Cu}}{E_{EMC}} \tag{4.4}$$

Inputting the crack length and the $P_{critical}$ values for each of the 10 as-received samples and taking the average gives a G_c of 46.4 J/m^2. As can be seen, the G_c value obtained through FEM is in good agreement with the analytical formulation used for the EMC/Copper DCB geometry.

4.6 Discussion of As-Received EMC/Copper DCB Simulation Results

Figure 4.9 shows the peel stress, σ_Y generated in a DCB simulation for an as-received EMC/Copper sample with a crack length of 9.30 mm and a $P_{critical}$ value of 2.59 N.

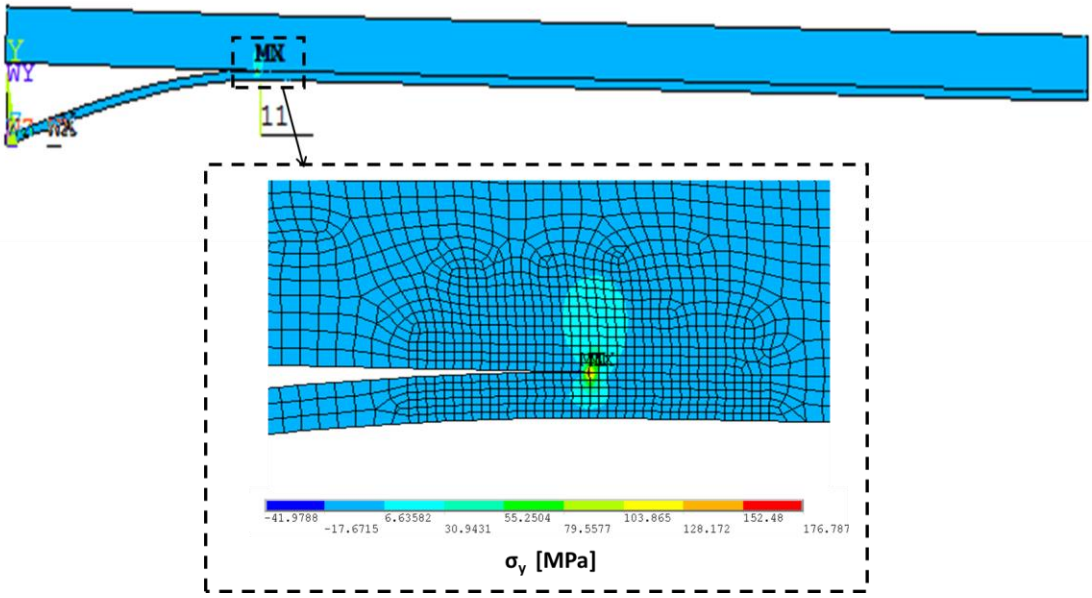

Figure 4.9 – Peel stress (σ_Y) for an as-received EMC/copper sample with a crack length = 9.30mm and $P_{critical}$ = 2.59N

As can be seen from shape of the elastic-plastic stress zone around the crack tip there is high asymmetry in the EMC/Copper geometry. This is further confirmation that the mode mixity of the DCB EMC/Copper geometry is not purely Mode I loading.

Figure 4.10 shows the von Mises stress contours generated for an as-received DCB EMC/Copper geometry with the same crack length and $P_{critical}$ values as mentioned above.

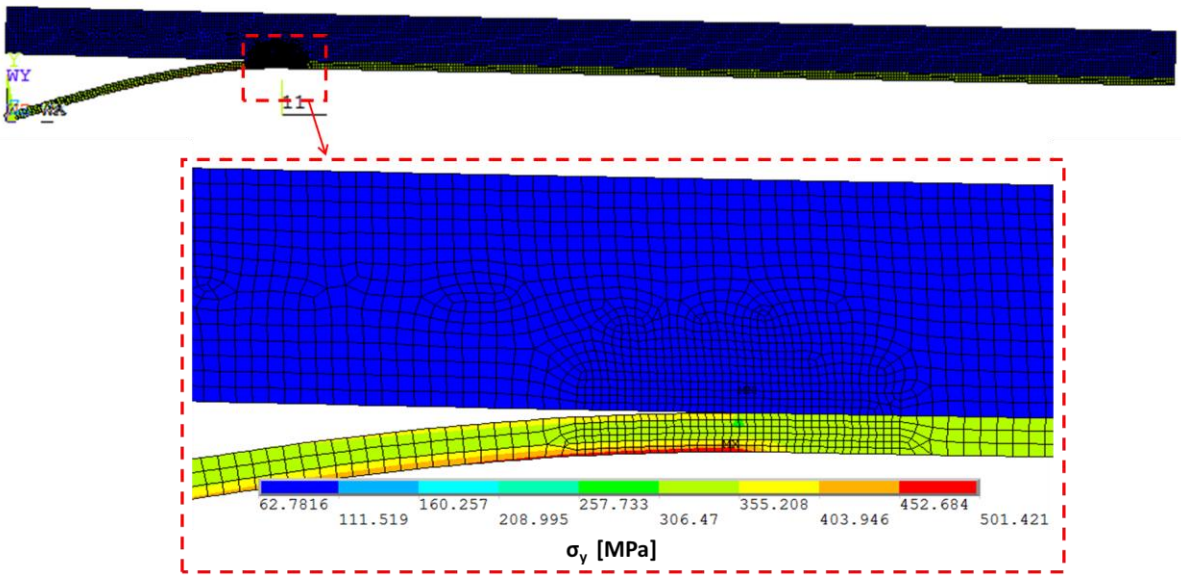

Figure 4.10 –von Mises stress (σ_{eqv}) generated for an as-received DCB EMC/copper sample

The maximum stress in the EMC/Copper sample occurs at the bottom edge of the Cu strip and is around 501 MPa. This value is greater than the yield stress of the copper leadframe which is around 334 MPa. However, since the stresses around the interface are below the copper leadframe yield stress value, it is safe to assume that there is very little plasticity in the DCB geometry and using a linear elastic model is sufficient for this study.

4.7 FPB Experimental Testing

FPB is a mixed-mode fracture mechanics test that is commonly used to test the interfacial strength of bi-material specimen found in microelectronic packages. FPB delamination is independent of the crack length of the geometry [24, 38]. The moment created between the inner loading pins during delamination results in a constant load at which steady state delamination occurs. The FPB schematic for the EMC/Copper sample is shown in Figure 4.11.

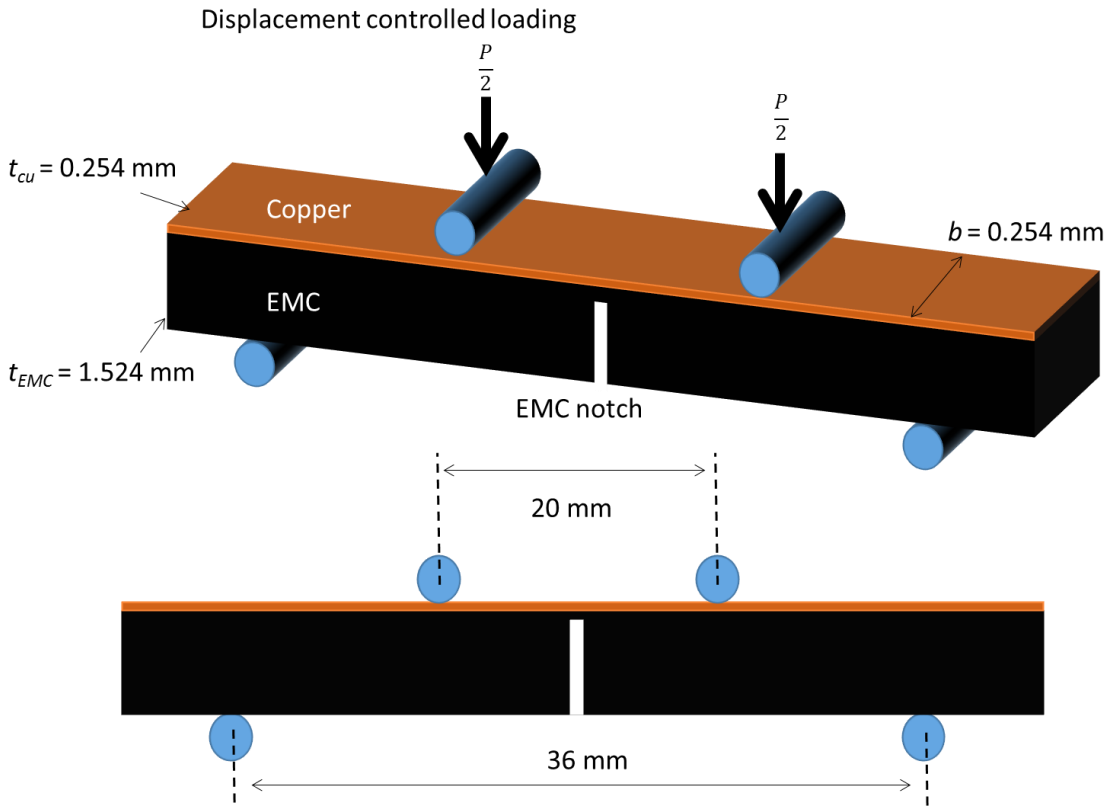

Figure 4.11 - Schematic of FPB test set up for EMC/copper sample

A notch is created at the center of EMC such at 100 µm is leftover after the cut. This is done using a *DISCO*™ automated dicing machine. The EMC/Copper sample is placed with the copper leadframe facing up, on two pins 36 mm apart in length. A displacement controlled loading is applied by two other pins from the top that are 20mm apart. The load is applied until at some $P_{critical}$ load the crack will propagate rapidly from the EMC notch to the copper leadframe. From this point a constant moment arm is maintained between the inner loading pins and steady state delamination occurs at a $P_{critical}$ value. Figure 4.12 shows a picture of the FPB experiment in progress. The tests are performed on a *Test Resources*™ tensile tester. A deflectometer from *Epsilon*

Technologies™ is used to keep accurate track of the displacement of the sample. The load applied on the sample is measured by the *Test Resources*™ machine.

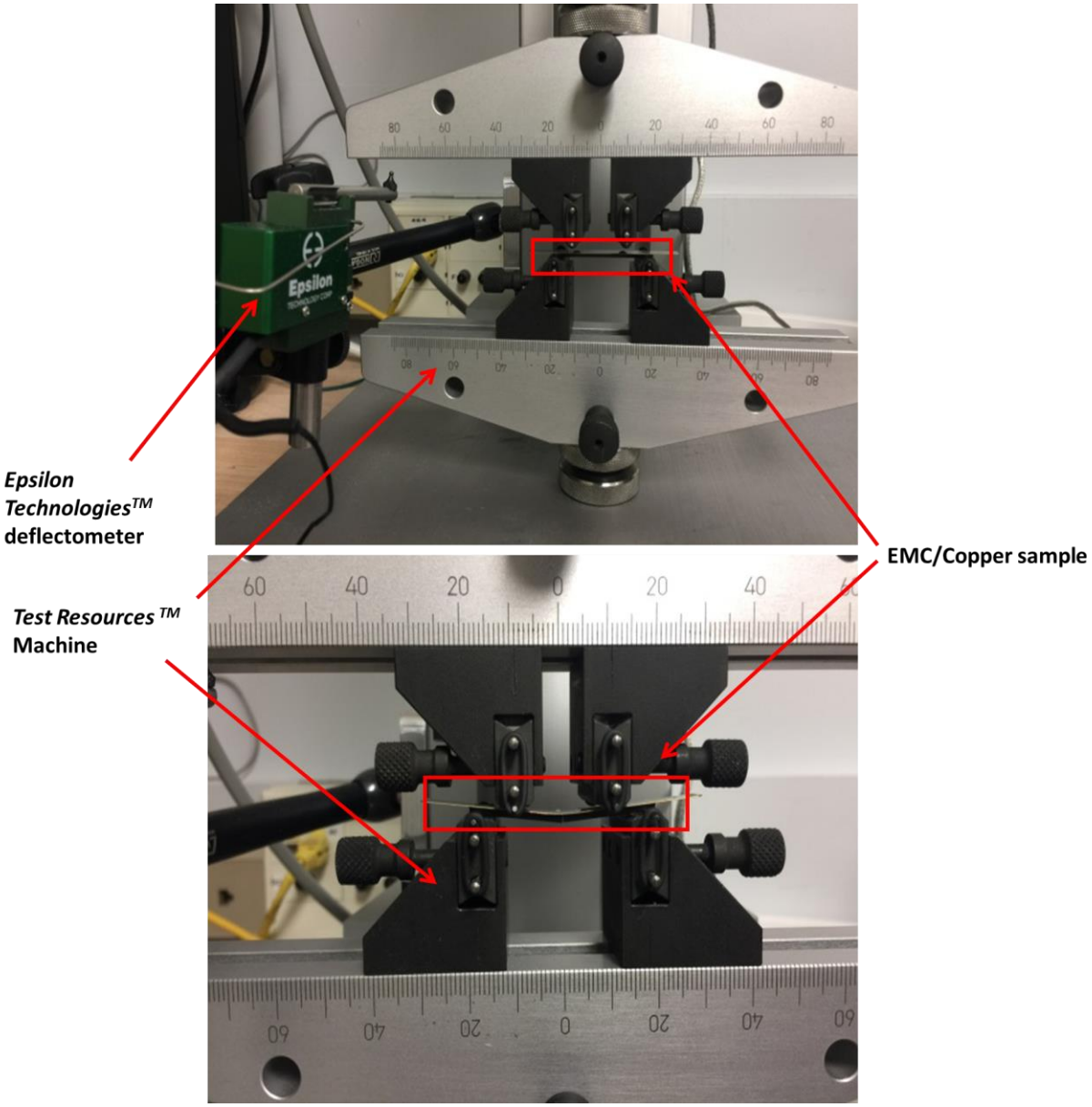

Figure 4.12 – FPB experiment in progress

Figure 4.13 shows a typical load vs. displacement graph obtained after doing FPB testing on an as-received EMC/Copper sample. The load increases with respect to displacement until at some critical point the crack propagates through the EMC notch. At

this point, the crack starts propagating on one side of the EMC/Copper interface at a steady $P_{critical}$ value. After the crack on that side of the EMC notch has propagated some distance, the crack stops increasing in size and delamination is introduced on the EMC/Copper interface on the other side of the EMC notch. Ideally both EMC/Copper interfaces on either side of the EMC notch should propagate simultaneously. Once the crack on other side of the EMC notch is initiated, the crack propagates at a steady load of 7.65 N.

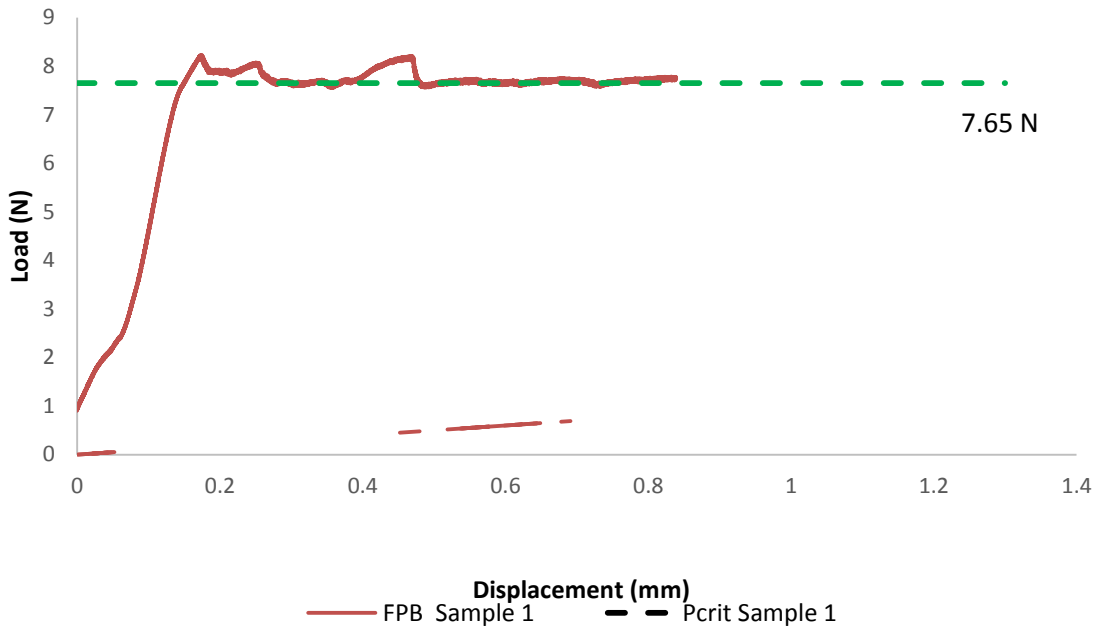

Figure 4.13 – Typical load vs. displacement graph obtained after conducting FPB testing on an as-received EMC/copper sample

FPB experiments are conducted on two as-received EMC/Copper sample. The load vs. displacement graphs obtained for the two samples tested are shown in Figure 4.14.

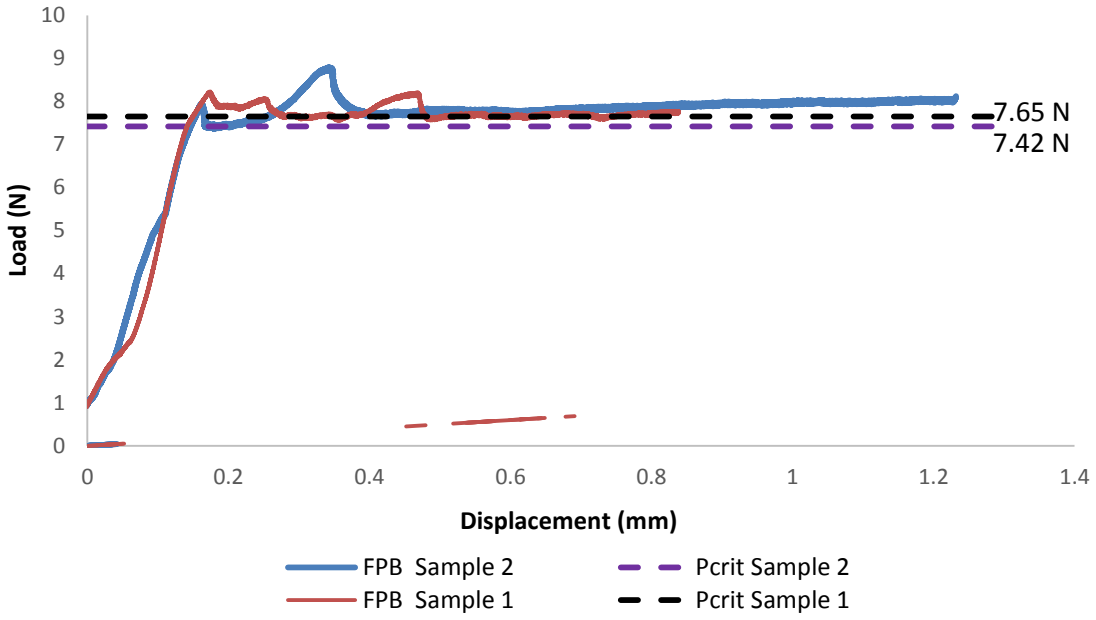

Figure 4.14 – Load vs. displacement graphs for two as-received FPB EMC/copper samples

The steady state load values at which delamination occurs for the as-received FPB EMC/Copper samples that were tested was $P_{critical}$ = 7.65 N and $P_{critical}$ = 7.42 N.

4.8 FPB Numerical Solution

Using the $P_{critical}$ values obtained from doing FPB testing on the as received EMC/Copper sample. FEM can be used to obtain the G_c value for the FPB geometry. VCCT is used to obtain the interfacial strength of the EMC/copper sample for FPB loading conditions. Figure 4.15 shows a schematic of the FPB geometry modeled using ANSYS™ version 14.0. Similar to the DCB geometry, a 2-D plane strain assumption is used to model the FPB geometry. In addition, a half-symmetry model is used for modeling the FPB set up to reduce computational time. The material properties used for the EMC and Copper are obtained from Table 4.1 and Table 4.2 . Since the load is equally distributed amongst the two pins, the $P_{critical}$ value applied on the EMC/Copper

sample is divided by 2. $P_{critical}$ is also divided by the width, b since the FEM model being used assumes 2-D plane strain.

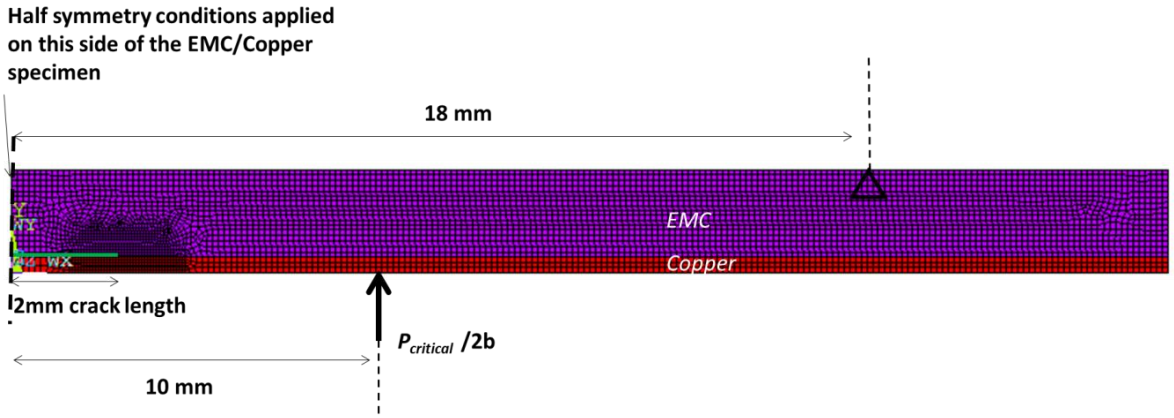

Figure 4.15 - 2D plane strain FPB model for EMC/copper sample

4.8.1 As-Received FPB EMC/Copper Sample Test Results

A total of two FPB tests were conducted on as received EMC/Copper specimen. Table 4.4 shows the SERR computed for the two $P_{critical}$ values obtained from FPB experiments.

Table 4.4 - G_c results for FPB as received EMC/copper samples

As Received EMC/Copper Specimen	$P_{criticial}$ (N)	Average G_c (J/m^2) (VCCT)
Sample 1	7.65	65.5
Sample 2	7.42	69.6
Average	7.54	**67.5±2.90**

The average G_c obtained through VCCT for a FPB EMC/Copper geometry is 67.5 J/m^2.

4.9 FPB Mode Mixity Calculation

The mode mixity of the FPB geometry is also calculated using the crack displacement method as described in Section 2.1.4. For this specific geometry, an as received sample with $P_{critical}$ value of 7.65 N is used to obtain the mode mixity, ψ of the EMC/Copper sample. Once again, nodal displacements, δ_y and δ_x are calculated for varying values of r ahead of the crack tip for this given geometry. G^* in this case is equal to G_c of the FPB setup which equals 65.5 J/m^2. Both sides of Equation 2.8 are plotted together on Figure 4.16 for two different values of r.

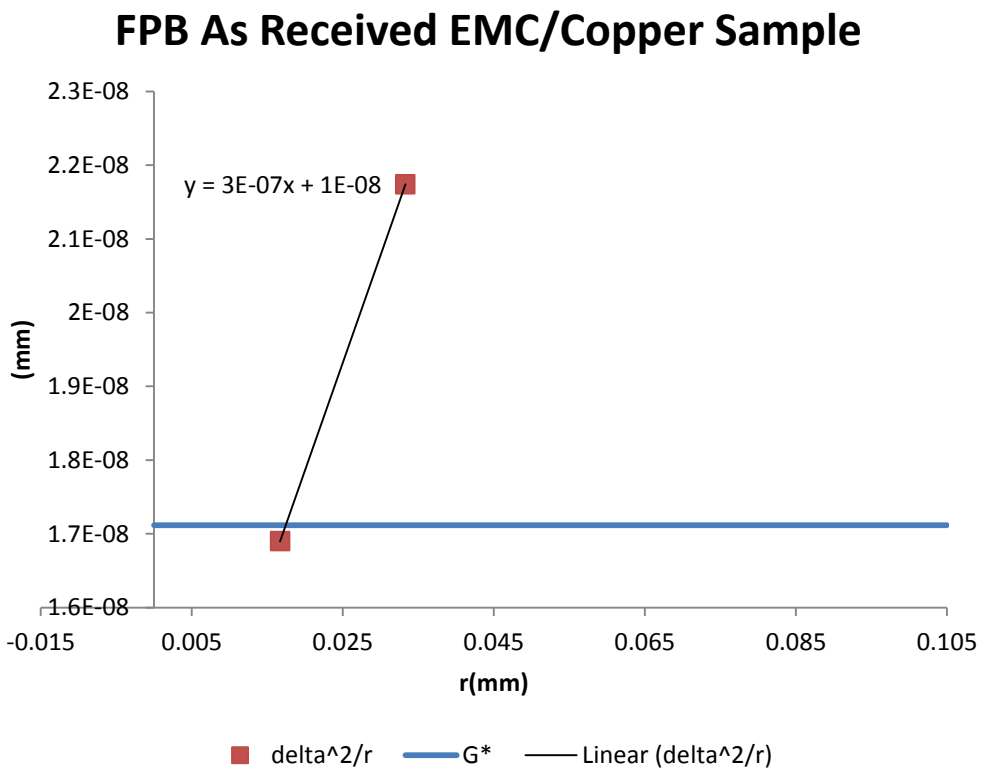

Figure 4.16 - Finding r to calculate ψ for an as received FPB EMC/copper sample

The intersection of the two graphs in Figure 4.16 gives an r value of 0.0237 mm. Inputting this value in Equation 2.7 gives a mode mixity, ψ of 35.7° for the as received FPB geometry.

4.10 FPB Analytical Solution

Charalambides et al. [44] obtained an analytical solution to calculate the SERR of a FPB geometry for a bi-material specimen. This analytical equation will be used to calculate G_c of a FPB geometry for the EMC/Copper sample. The equations used to obtain G_c for the FPB set up are shown as follows.

$$G = \frac{(1 - v_{Cu}^2)P^2L^2}{8E_{Cu}b^2}\left(\frac{1}{I_{Cu}} - \frac{\lambda}{I_C}\right) \quad 4.5$$

$$I_{Cu} = \frac{t^3{}_{Cu}}{12} \quad 4.6$$

$$\lambda = \frac{E_{Cu}(1 - v^2{}_{EMC})}{E_{EMC}(1 - v^2{}_{Cu})} \quad 4.7$$

$$I_C = \lambda I_{Cu} + \frac{t^3{}_{EMC}}{12} + \frac{\lambda t_{Cu} t_{EMC}\,(t_{Cu} + t_{EMC})^2}{4(\lambda t_{Cu} + t_{EMC})} \quad 4.8$$

I_C and I_{Cu} are the area moment of interia quantities for the entire beam and the copper leadframe respectively. λ is a non dimensionless term that describes a stiffness ratio between the copper leadframe and the EMC. The two $P_{critical}$ values obtained from the FPB experiments are inputted in the above analytical formula. The average G_c value calculated analytically for the FPB EMC/Copper geometry was 64.9 J/m^2. This value is in close agreement with the SERR value for the FPB geometry obtained using FEM.

4.11 Discussion of As-Received EMC/Copper FPB Simulation Results

Figure 4.17 shows the von Mises stress contours for an as-received EMC/Copper FPB geometry with a $P_{critical}$ value of 7.65 N.

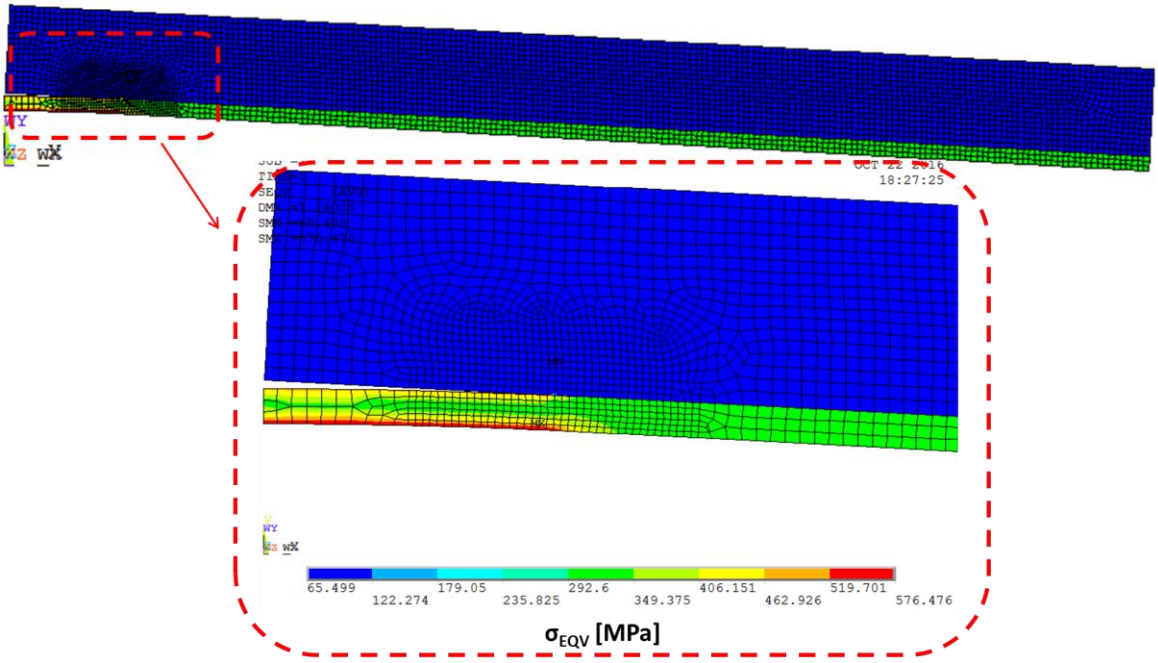

Figure 4.17 – von Mises stresses (σ_{eqv}) generated for an as-received FPB EMC/copper sample

Similar to the DCB EMC/Copper geometry, the maximum stress generated in the FPB sample occurs at the bottom edge of the copper leadframe strip and is around 576 MPa. This value is higher than the yield stress of the copper leadframe which is 334 MPa. However, the von Mises stresses at the interface are less than the copper leadframe yield stress value suggesting that like the DCB geometry, the plasticity in the model isn't significant and a linear elastic assumption is sufficient for the purposes of this study.

4.12 SERR vs. Mode Mixity relationshisp

The G_c and mode mixity, ψ that was obtained from DCB and FPB experiments can be fitted with the Hutchinson and Suo relationship as shown in Equation 2.10 [27].

In order to get reasonable fit, a sensible value of λ will be invoked such that it is between 0 and 1 since it relates to the ductility or brittleness of the surface under consideration. λ must be less than 1 because otherwise a nearly infinite G_c value at 90° will be obtained, which is not a reasonable estimation. A λ value of 0.90 is chosen which is mostly a brittle material while also minimizing the error between the predicted and experimenal G_c values obtained from DCB and FPB experiments. The G_c vs. mode mixity, ψ relationship obtained is shown as follows,

$$G_c = 42.6\{1 + tan^2(0.9\,\psi)\} \qquad 4.9$$

The G_c vs. mode mixity, ψ curve generated from Equation 4.9 is shown in Figure 4.18. The red points indicate the G_c and mode mixity, ψ values obtained from experimental DCB and FPB tests.

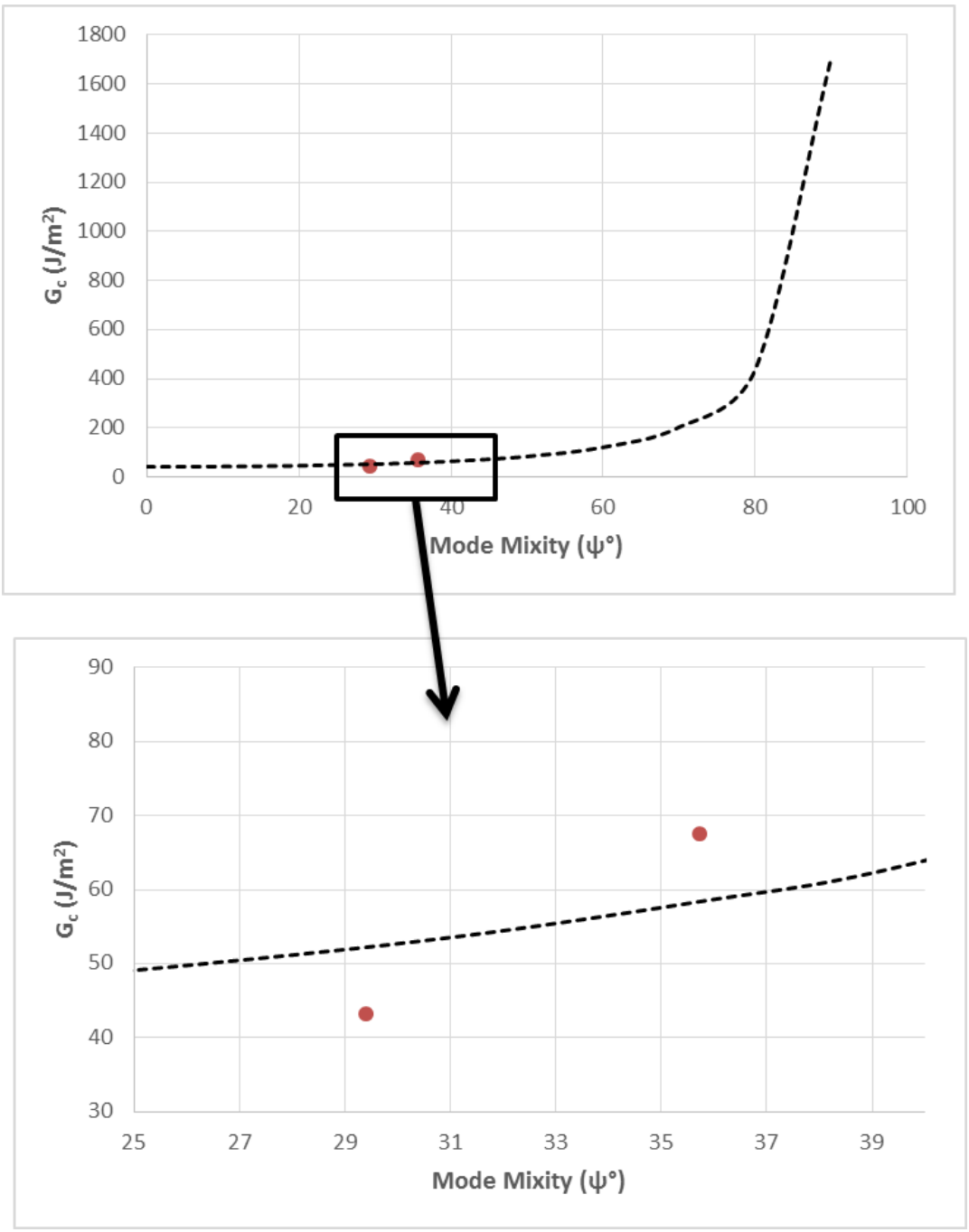

Figure 4.18 - G_c vs. ψ relationship obtained for EMC/copper sample

As can be seen from Figure 4.18, there is some error due to the spread of the experimental G_c values obtained from DCB testing. The G_c vs. mode mixity, ψ curve obtained overpredicts the G_c value for a DCB geometry and underpredicts the G_c value

for a FPB geometry as compared to the experimental DCB and FPB SERR values. Additional fracture mechanics tests need to be conducted at higher mode mixities ψ to obtain a better fit for the G_c vs. mode mixity, ψ° relationship.

The G_c vs. mode mixity, ψ relationship can be used to obtain G_c values for pure Mode I and Mode II conditions for the EMC/Copper specimen. The G_{IC} (Mode I) value obtained from Equation 4.9 is 42.6 J/m^2 and G_{IIC} (Mode II) value obtained is 1739 J/m^2. These values can be used to obtain cohesive zone parameters for as-received, thermally aged and moisture exposed EMC/Copper specimen as demonstrated in the next chapters.

CHAPTER 5. COHESIVE ZONE PARAMETERS FOR AS-RECEIVED EMC/COPPER SAMPLE

Cohesive Zone Parameters for the EMC/Copper sample are obtained by implementing cohesive zone elements in DCB and FPB geometries using FEM software. ANSYS™ version 14.0 is used to model the EMC/Copper sample. As mentioned in Section 2.3 the inverse method will be implemented in this study to obtain cohesive zone parameters. The inverse method involves fitting of certain CZ parameters in FEM software to obtain a simulated load vs. displacement for a DCB and FPB geometry. This result will then be compared and matched with experimental load vs. displacement data obtained by conducting interfacial fracture mechanics experiments. A bi-linear traction separation law will be used to characterize the EMC/Copper interface. The bilinear laws for CZM consist of Mode I and Mode II parameters.

5.1 Cohesive Zone Elements

Cohesive zone elements are placed in between the bonded region of the EMC and Copper Leadframe. 2-D plane-strain 6 node quadratic interface elements are used to model the cohesive zone layer between the EMC and Copper. A schematic representing the CZ elements between the EMC and Copper is shown in Figure 5.1.

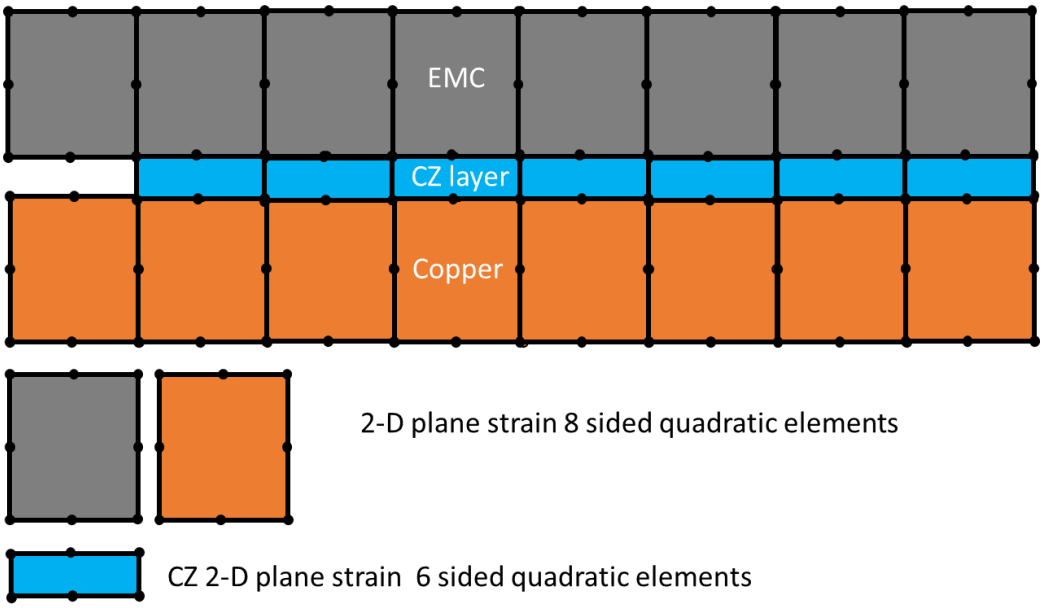

Figure 5.1 - Schematic of the CZ elements between the EMC and copper leadframe sample.

Prior to loading, the CZ elements have negligible thickness. Once the EMC/Copper sample is loaded, damage is incurred on the CZ elements.

5.2 DCB Cohesive Zone Model

Figure 5.2 shows a schematic of the EMC/Copper DCB geometry with cohesive zone elements modeled using ANSYS™ version 14.0. A 2D plane-strain assumption is implemented for the DCB model. In this particular DCB model, a crack length of 9.30 mm is used as shown in Figure 5.2.

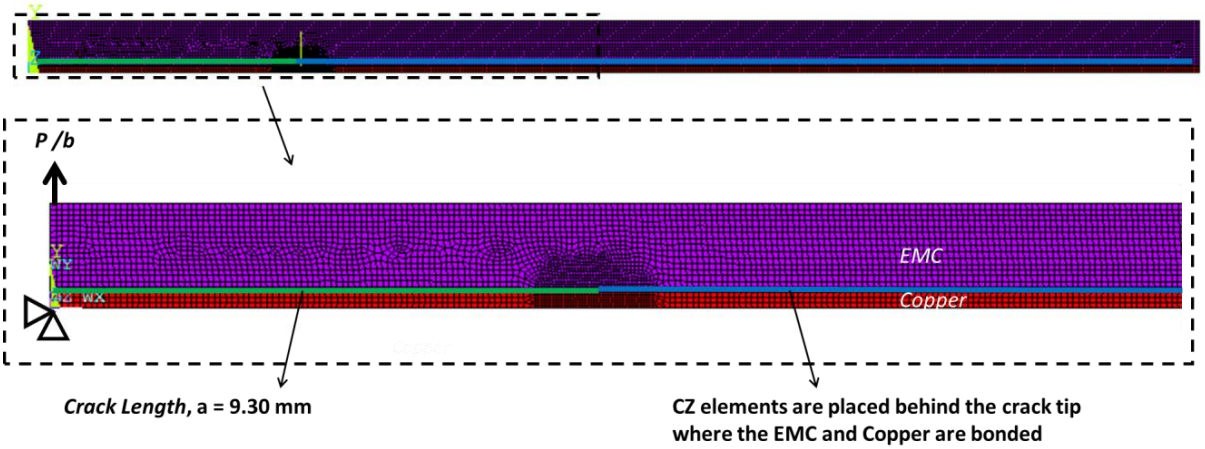

Figure 5.2 - Schematic of the EMC/copper DCB geometry with CZ elements

CZ elements are represented by the blue line in Figure 5.2. This region represents the segment where the EMC and Copper are bonded. The green line represents the crack length of the EMC/Copper ahead of the crack tip. A displacement applied to the DCB model to obtain a simulated load vs. displacement graph for a given set of CZ parameters.

5.3 FPB Cohesive Zone Model

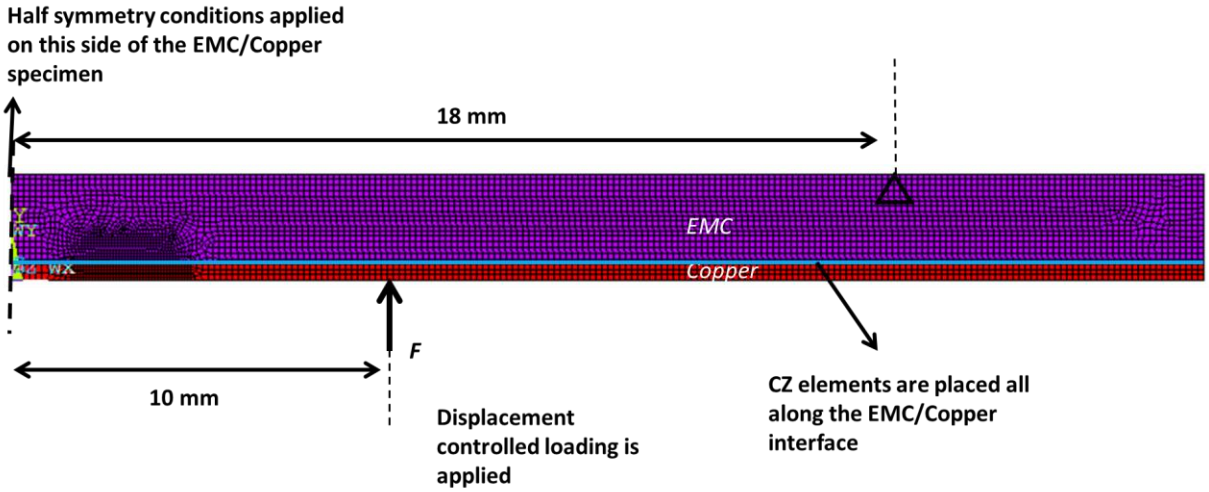

Figure 5.3 - Schematic of the EMC/copper FPB geometry with CZ elements

A 2D plane strain model is implemented for the FPB geometry. Half-symmetry is applied to the model to reduce computational time. CZ elements are represented by the blue line in Figure 5.3 and are placed in the all along the EMC/Copper interface. A displacement is applied to the FPB model and the force obtained from the model at the location where the displacement is applied will be equal to half the force from the experiment scaled by the width of the sample. A simulated load vs. displacement graph is obtained for a given set of CZ Parameters applied to the FPB geometry.

5.4 CZ Simulation Results for As Received EMC/Copper Sample

A bilinear traction separation law is used to obtain the simulated load vs. displacement graphs for the EMC/Copper DCB and FPB geometries. The traction separation laws are adjusted until the simulated and experimental load vs. displacement curves match. A few important points should be considered while obtaining the CZ parameters.

1. According to Equation 2.12 the area under the bi-linear traction triangle equals $G_{c.}$ So increasing the maximum traction σ_{max} for Mode I, will result in a decrease in the maximum interfacial separation, δ_c in order to keep G_c for Mode I constant. The same principle applies for Mode II parameters.
2. As mentioned in Section 2.2.3 the mesh used around the crack tip region in the FEM software has an impact on the model. Alfano and Crisfield [35] mention that increasing the σ_{max} to higher values might require the mesh around the crack tip region to be refined as well. Not doing so will lead to discretization errors in the simulated load vs. displacement data and oscillatory behavior during delamination as shown in Figure 2.6. For σ_{max} values which are too high for a given mesh density and result in discretization errors and oscillatory behavior, sufficiently

increasing the mesh density around the crack tip will reduce the discretization errors and smooth out the curve. In this study, as different values of σ_{max} are fitted, the mesh density is altered as required for higher maximum traction values to avoid these discretization errors.

3. Increasing the maximum traction σ_{max} too much for a given mesh density for either Mode I or Mode II can result in incorrect $P_{critical}$ values. This is because as the maximum interfacial traction, σ_{max} is increased, the maximum interfacial separation, δ_c is decreased to ensure G_c is kept constant as mentioned in the first point. The interplay between the length scale of the mesh density and the maximum separation, and that of the maximum traction and the order of the stress field which is impacted by the choice of cohesive parameters can result in either an over or under prediction of $P_{critical}$ depending on the relative influences of these factors. For a given G_c as δ_c is reduced, δ^* also decreases if α is kept constant.
4. The ratio $\alpha = \delta^* / \delta_c$ for either Mode I or Mode II can have a small effect on the initial slope of the load vs. displacement graph. α can also influence the extent of (if any) curvature of the load vs. displacement line depending on the choices of the other CZ parameters. Both of these dependencies however are not omnipresent for all CZ parameter selections.

Using the above guidelines the CZ parameters are determined for Mode I and Mode II.

5.4.1 DCB CZ simulation results

The G_c vs. mode mixity, ψ relationship overpredicts the G_c value for the DCB geometry. The DCB G_c value obtained from Equation 4.9 is 53.1 J/m^2 as compared to the average experimental DCB value obtained which is 45.1 J/m^2. This means that the

simulated load vs. displacement graph obtained for an as-received DCB EMC/Copper sample will have a higher $P_{critical}$ value and delamination path compared to the experimental DCB value. Figure 5.5 shows the simulated load vs. displacement graph for an as received DCB EMC/Copper sample. The simulation is run for two different crack lengths of 9.30 mm and 13.6 mm. The average G_c value obtained for this sample after running a DCB VCCT simulation was 47.8 J/m^2. This represents a 10% difference between the experimental G_c value and the G_c value obtained from Equation 4.9. Figure 5.4 shows how the simulated load vs. displacement graph compares with the experimental load vs. displacement graph for this as-received EMC/Copper DCB sample.

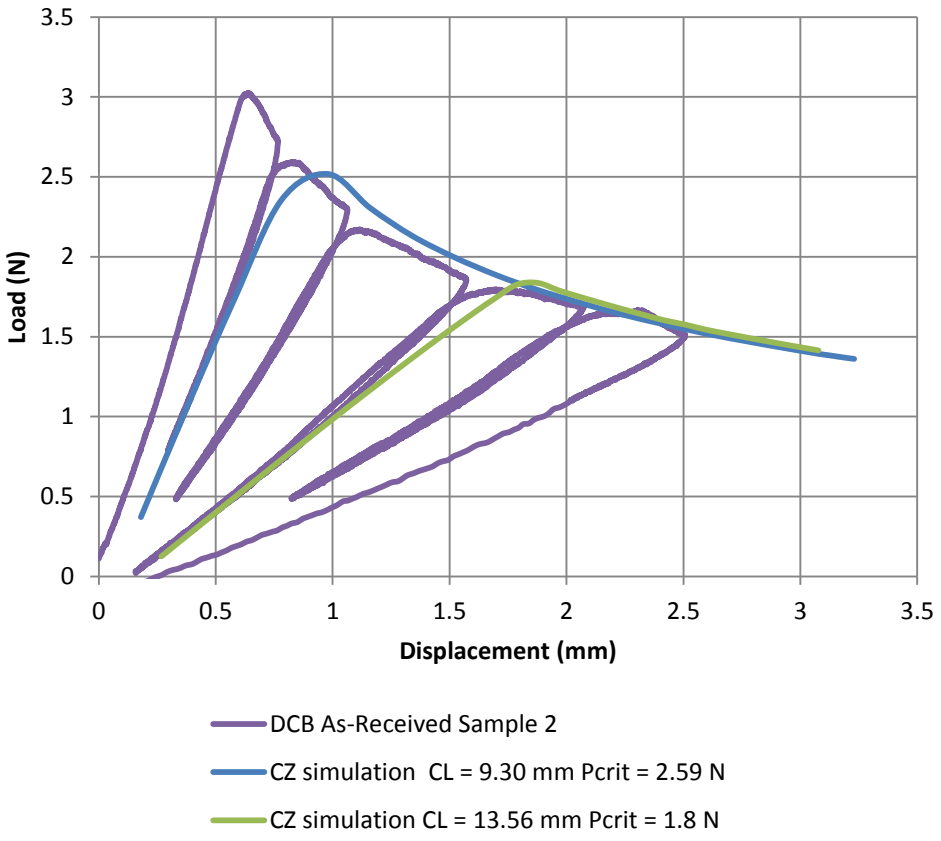

Figure 5.4- DCB CZ simulation compared with experimental DCB data for as-Received EMC/copper sample

As can be seen in Figure 5.4 the initial slope for both simulated load vs. displacement graphs match the slope of the experimental load vs. displacement graph. In addition, the simulated load vs. displacement graphs slightly overpredicts the $P_{critical}$ value for delamination at both crack lengths due to the 10% difference between the experimental G_c value and the G_c value obtained from Equation 4.9 . The simulated load vs. displacement graphs shows delamination or debonding in the EMC/Copper specimen as the CZ elements at the interface start acquiring damage past $P_{critical.}$. This process is repeated for another as-received DCB sample as shown in Figure 5.5.

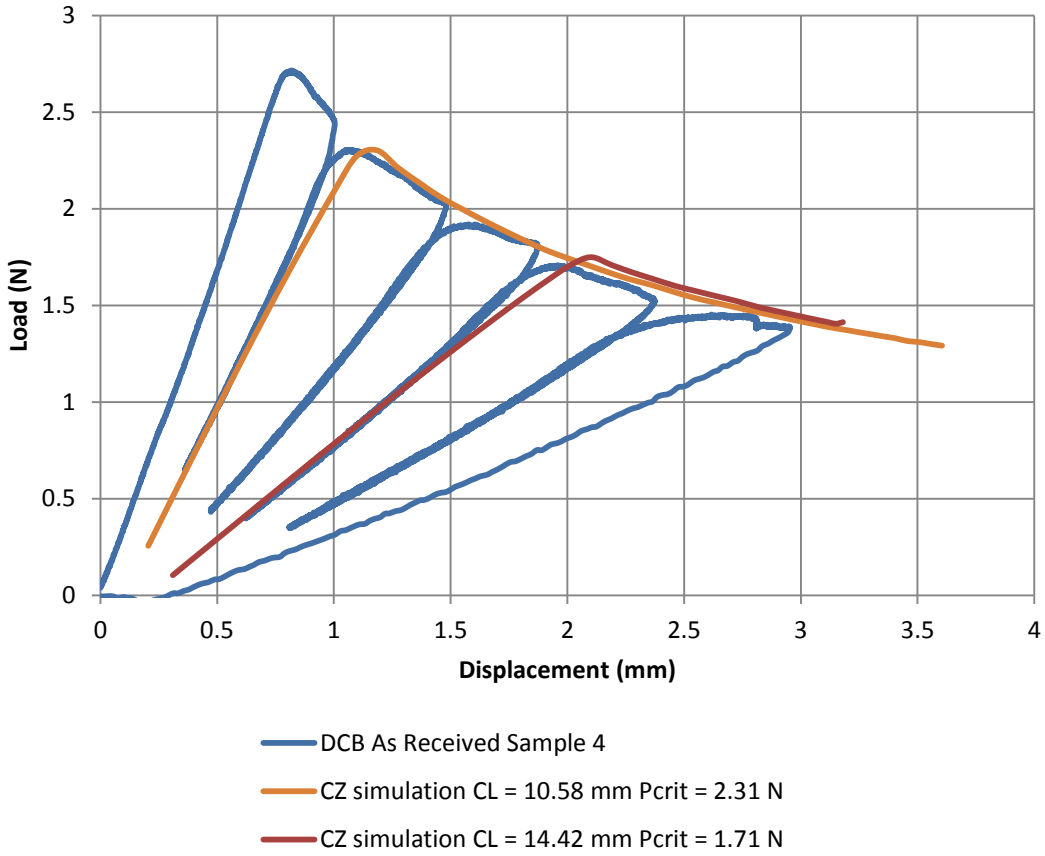

Figure 5.5- DCB CZ simulation compared with experimental DCB data for as-received EMC/copper sample.

The average G_c value obtained for this sample after running a DCB VCCT simulation was 47.30 J/m^2 representing a 10.9 % difference between experimental G_c value and the G_c value obtained from Equation 4.9. This difference is once again noticed in Figure 5.5 as the simulated load vs. displacement graphs slightly overpredicts the $P_{critical}$ value for delamination at both crack lengths.

5.5 FPB CZ simulation results

The G_c value obtained from Equation 4.9 underpredicts the G_c value compared to the G_c value obtained from the experimental as-received FPB data as shown in Figure 4.18. The FPB G_c value obtained from Equation 4.9 is 59.4 J/m^2 as compared to the average experimental DCB value obtained which is 67.4 J/m^2. This represents a 13.4% difference between the experimental FPB G_c value and the G_c value obtained from Equation 4.9. This means that the CZ simulated load vs. displacement graph obtained for an as-received FPB EMC/Copper specimen will have a lower $P_{critical}$ value and delamination path compared to the experimental FPB data.

Figure 5.6 shows the simulated load vs. displacement graph for the EMC/Copper FPB geometry. These graphs are compared with the two as received FPB experimental load vs. displacements graphs.

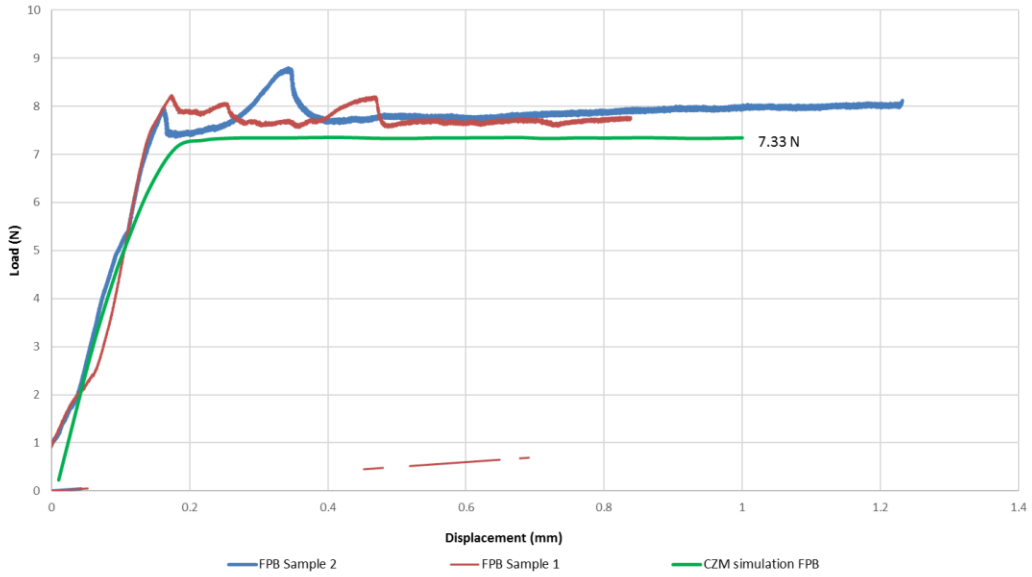

Figure 5.6- FPB CZ simulation compared with experimental FPB data for as-Received EMC/copper sample.

The initial slope of the FPB simulated load vs. displacement graph is in good agreement with the slope of the FPB experimental load vs. displacement graphs. The FPB geometry doesn't simulate crack propagation through the EMC notch so it is not shown in the simulated FPB graph. In addition, the simulated FPB graph underpredicts the $P_{critical}$ value at which steady state delamination of the FPB geometry occurs due to the 13.4% difference in the experimental . G_c value and the G_c value obtained from Equation 4.9. The $P_{critical}$ value is 7.33 N for the simulated FPB model. Once the $P_{critical}$ value is reached CZ elements begin incurring damage and this leads to steady state crack propagation at the EMC/Copper interface.

5.6 As-Received EMC/Copper CZ Parameters

The CZ parameters obtained for the as-received EMC/Copper sample are show in Table 5.1. The Mode I and Mode II bilinear traction separation triangles obtained are shown in Figure 5.7 and Figure 5.8 respectively. These CZ parameters can be used to

model crack initiation and propagation in an As Received EMC/Copper specimen for DCB and FPB geometries.

Table 5.1 –CZ parameters for as-received EMC/copper sample

As-Received EMC/Copper Bi-linear Traction Separation Laws		
	Mode I	**Mode II**
σ_{max} (MPa)	6.41	513
δ_c (μm)	5.46	2.79
δ^* (μm)	0.546	0.279
G_C (J/m^2)	17.5	715

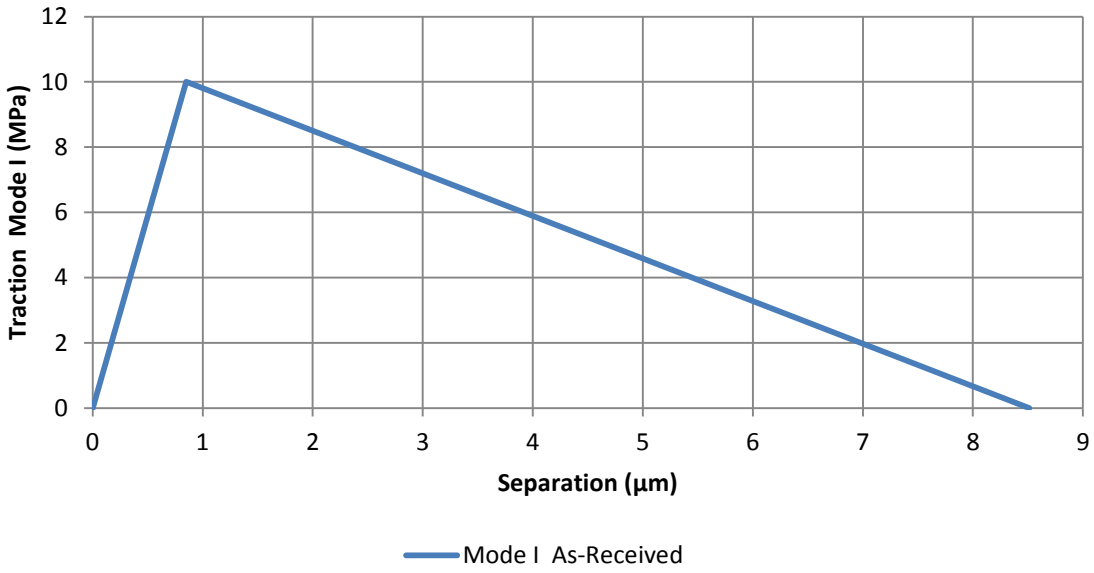

Figure 5.7 – Mode I bilinear traction separation triangle for as-received EMC/copper sample

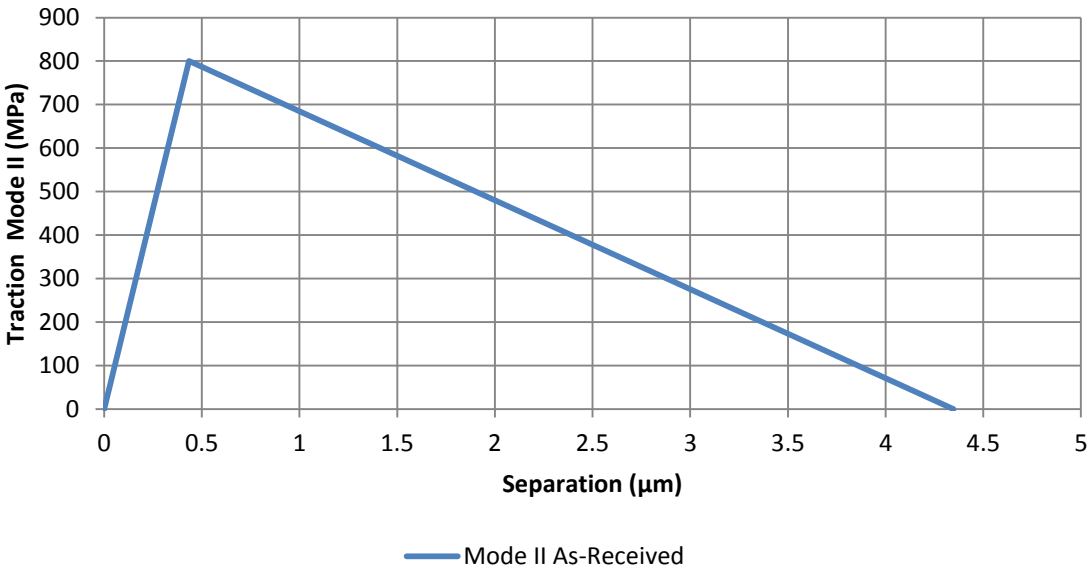

Figure 5.8 - Mode II bilinear traction separation triangle for as-received EMC/copper sample

CHAPTER 6. EXPERIMENTAL STUDY OF HUMIDITY-CONDITIONED SAMPLES

The EMC/Copper samples are exposed to different humidity conditions at different temperatures and durations. These conditions are based on stress test qualifications for packaged integrated circuits used by industry [45] The EMC/Copper samples are first prebaked at 125 °C for 24 hours to remove existing moisture content from the specimen. The samples then go through a moisture preconditioning step at 30 °C and 60 % R.H. for 192 hours. These conditions stimulate the storage conditions of a microelectronic package and represent the time allowed for the package to be left open before excessive moisture uptake affects the package's performance. These two steps are performed as a precursor before the humidity conditioning tests are conducted. DCB tests are performed after conducting these two steps to investigate how moisture preconditioning affects interfacial adhesion.

Humidity conditioning tests are conducted on samples at 85% R.H and 110°C for 264hrs and 528hrs and 85% R.H and 130 °C for 96hrs and 192hrs. The humidity conditioning tests are done at *NXP semiconductor*. DCB tests are then performed at room temperature on humidity-conditioned samples and the G_c values are obtained. Modified cohesive zone parameters can be obtained using the G_c value obtained for humidity conditioned EMC/Copper samples.

6.1 Experimental DCB results for humidity conditioned samples

Table 6.1 shows the average G_c value obtained for 4 EMC/Copper samples after doing DCB testing after a prebake and moisture preconditioning step. EMC/Copper samples are exposed to 60% R.H and 30 °C for 192hrs. Crack Length for the humidity

conditioned EMC/Copper samples are obtained using the compliance vs. crack length relationship shown in Section 4.3.1. $P_{critical}$ is taken to be the maximum load for each load curve. The average G_c value for each humidity conditioned EMC/Copper sample is obtained through VCCT.

Table 6.1 - G_c values for DCB EMC/copper samples exposed to 60 %R.H and 30 °C for 192 hours

Sample Number	G_c (J/m^2) (VCCT) after humidity conditioning at 60% R.H. and 30°C for 192hrs.
1	43.9
2	44.0
3	40.7
4	45.8
Average	**43.6±2.00**

The average G_c value of the EMC/Copper specimen after humidity preconditioning is 43.6 J/m^2. There is no substantial change in the interfacial adhesion of the EMC/Copper specimen after exposing the samples to 60 % R.H and 30 °C for 192 hours. This clearly suggests that humidity conditioning as low as 60 % R.H. shows no significant reduction in G_c. This shows that when EMC/Copper samples are exposed to 60% RH at 30 °C for 192 hours, there is no significant reduction in G_c.

6.1.1 DCB test results for EMC/Copper samples exposed to 85% R.H and 110 °C for 264hrs and 528 hrs

Table 6.2 shows the average G_c value obtained from DCB testing after exposing the EMC/Copper sample to 85% R.H and 110 °C for 264hrs and 528 hrs. A total of two

samples are tested for each condition. Crack Length for the humidity conditioned EMC/Copper samples are obtained using the compliance vs. crack length relationship shown in section 4.3.1. $P_{critical}$ is taken to be the maximum load for each load curve. The average G_c value for each humidity conditioned EMC/Copper sample for this condition is obtained through VCCT using FEM.

Table 6.2 - G_c values for DCB EMC/copper samples exposed to 85% R.H and 110 °C for 264hrs and 528 hrs

Sample Number	G_c (J/m^2) (VCCT) after humidity conditioning at 85% R.H. & 110°C for 264hrs	G_c (J/m^2) (VCCT) after humidity conditioning at 85% R.H. & 110°C for 528hrs
1	26.0	24.3
2	24.2	21.6
Average	**25.1±1.09**	**23.0±1.66**

The average G_c value obtained after humidity conditioning at 85% R.H.and 110°C for 264 hrs is 25.1 J/m^2.This shows that on increasing the moisture exposure level to 85% R.H. and ramping the temperature to 110°C there is a 44.3% reduction in the interfacial adhesion of the EMC/Copper sample from its as-received DCB value of 45.1 J/m^2. Increasing the exposure time to 528hrs for this humidity condition results in an average G_c value of 23.0 J/m^2 for the DCB EMC/Copper sample. This suggests that increasing the duration of exposure at this condition had a small effect on the already reduced interfacial strength of the EMC/Copper sample and resulted in 49.0 % drop in the interfacial adhesion of the EMC/Copper sample from its as-received DCB value of 45.1 J/m^2.

6.1.2 DCB test results for EMC/Copper samples exposed to 130 °C and 85% R.H for 264hrs and 528 hrs

Table 6.3 shows the G_c value obtained from DCB testing after exposing the EMC/Copper sample to 85% R.H and 130 °C for 96hrs and 192hrs. A total of two samples are tested for each condition. Crack Length for the humidity conditioned EMC/Copper samples are obtained using the compliance vs. crack length relationship shown in Section 4.3.1. $P_{critical}$ is taken to be the maximum load for each load curve. The average G_c value for each humidity conditioned EMC/Copper sample for this condition is obtained through VCCT using FEM.

Table 6.3- G_c values for DCB EMC/copper samples exposed to 85% R.H and 110 °C for 96hrs and 192hrs

Sample Number	G_c (J/m^2) (VCCT) after humidity conditioning at 85% R.H. and 130°C for 96hrs	G_c (J/m^2) (VCCT) after humidity conditioning at 85% R.H. and 130°C for 192hrs
1	17.6	18.1
2	17.6	18.9
Average	**17.6±1.14**	**18.5±1.09**

The average G_c value obtained after humidity conditioning at 85% R.H and 130°C for 96hrs is 17.6 J/m^2. These results suggest that increasing the temperature exposure to 130°C from 110°C further reduces the interfacial strength of the EMC/Copper sample. There is a 61.0% reduction in the interfacial adhesion of the EMC/Copper sample from its as-received DCB value of 45.1 J/m^2 when the sample is humidity conditioned at 85% R.H and 130°C for 96hrs. Increasing the duration of exposure to 192hrs at this humidity

condition results in a G_c value of 18.5 J/m^2 for the EMC/Copper sample. This suggests that increasing the exposure time at this humidity condition resulted in almost no change in the already reduced interfacial strength of the EMC/Copper sample. There is a 59.0% reduction in the interfacial adhesion of the EMC/Copper sample from its as-received DCB average experimental value of 45.1 J/m^2 when the sample is humidity conditioned at 85% R.H and 130°C for 192hrs.

6.2 Discussion of DCB results for humidity conditioned EMC/copper samples

Figure 6.1 shows a plot of G_c vs. time for all the different humidity conditioned samples. As can be seen from the graph, moisture exposure at 85 % R.H. results in a reduction in the interfacial strength of the EMC/Copper sample. This is in agreement with the results from Shirangi et al. and Ferguson et al. who demonstrate that exposure at 85°C and 85 % R.H. for various exposure times results in a clear reduction in the interfacial adhesion of the EMC/Copper sample [9, 36]. The graph also suggests that temperature with humidity conditioning has an impact on the interfacial adhesion. Increasing the temperature exposure from 110°C to 130°C further reduced the interfacial strength of the EMC/Copper sample by approximately 8%

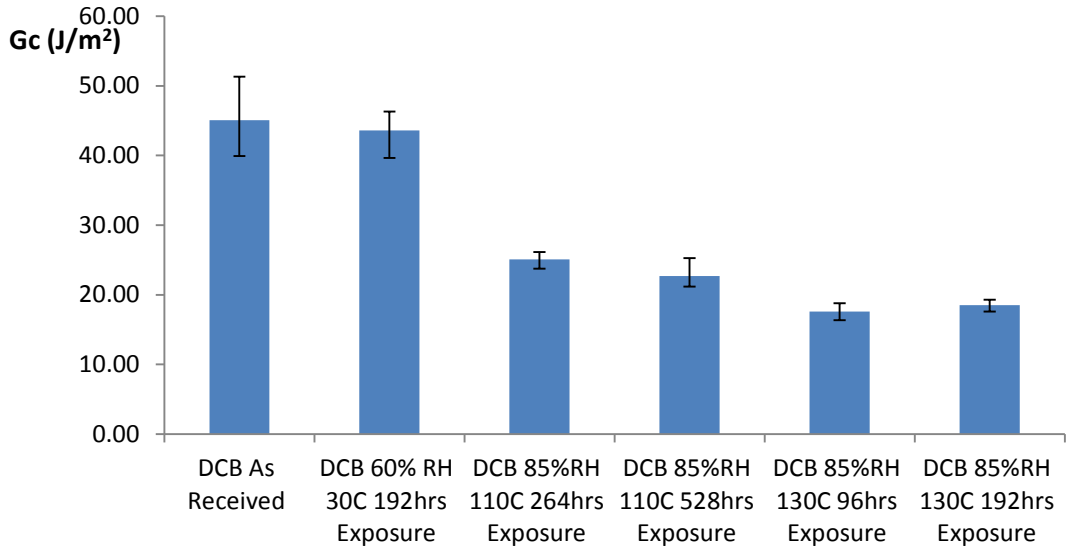

Figure 6.1- Plot of DCB G_c values for all humidity conditioned EMC/copper samples with as-received EMC/Copper G_c value

Increasing the exposure time at a given humidity condition doesn't seem to have much effect on the interfacial adhesion. This is in good agreement with moisture studies done by Shirangi et al. on EMC/Copper samples where it is shown that the biggest drop in interfacial adhesion at 85% R.H and 85°C occurs after 168hrs (1 week). The interfacial strength show little change after continued exposure at 85% R.H and 85°C for longer durations [36].

As mentioned in Section 2.3, there are several reasons for the drop in G_c seen at the humidity condition levels investigated on the EMC/Copper sample.

1. Moisture exposure might be resulting in chemical degradation of the adhesive bonds at the EMC/copper interface [9].

2. Humidity conditioning for longer durations, seems to be resulting in a permanent damage in the adhesion bonds of the EMC/Copper that cannot be reversed [36].
3. The EMC used might have a high moisture diffusion rate and most of the absorption could have occurred within the initial 96/264hrs of humidity conditioning. This would explain why subsequent humidity conditioning at longer durations of 192/528hrs did not lead to any further change in G_c. It is important to keep track of the mass of the EMC during humidity conditioning. Shirangi et al. [36] investigated the change in mass at regular intervals during moisture conditioning and observed that after a set amount of time and for given RH and temperature conditions, the mass reaches a saturation value. Most of the moisture absorption of the EMC could therefore have occurred during humidity exposure at 85% R.H. and 110°C for 264hrs and 85% R.H. and 130°C for 96hrs. Preliminary humidity conditioning tests on EMC/Copper samples showed that after removing the EMC/Copper samples from the humidity chamber some of the moisture mass was retained. The mass of the EMC measured was greater than the original mass of the EMC prior to any moisture conditioning. This suggests that some moisture absorption was retained and therefore could have played a role in affecting the interfacial strength of the EMC/Copper interface. As mentioned by Ferguson and Qu [9] increased moisture absorption of the EMC could be causing a reduction in adhesion strength through the displacement of the EMC, hence reducing Van der Waals forces at the interface.

6.3 CZ Parameters for humidity conditioned EMC/Copper samples

The G_c values obtained for the humidity conditioned samples can be used to develop modified CZ parameters that characterize the interfacial behavior of the EMC/Copper sample. Since no FPB tests are conducted on the moisture conditioned samples the percentage drop in the DCB G_c value after humidity conditioning will be applied to the G_{IC} and G_{IIC} values obtained from the G_c vs. ψ relationship shown in Figure 4.18. The guidelines mentioned in Section 5.4 are then followed to obtain modified mode I CZ parameters for the humidity conditioned EMC/Copper samples.

6.3.1 CZ Parameters for EMC/Copper samples exposed to 85% R.H and 110°C for 264hrs

The DCB G_c value for an EMC/Copper sample humidity conditioned at 85% R.H. and 110° for 264 hrs drops from an as-received G_c value of 45.1 J/m^2 to 25.1 J/m^2. This represents a 44.3 % drop in G_c. Table 6.4 shows the new G_{IC} and G_{IIC} values obtained after invoking this percentage drop on the as received G_{IC} and G_{IIC} values for the EMC/Copper sample.

Table 6.4: Modified G_{IC} and G_{IIC} values for EMC/copper sample conditioned at 85% R.H. and 110°C for 264hrs

	As Received	**85%RH & 110°C humidity conditioning for 264hrs exposure**
G_{IC} (J/m^2)	42.6	23.7
G_{IIC} (J/m^2)	1739	967

After obtaining the new G_{IC} and G_{IIC} values for the humidity conditioned EMC/Copper sample, the guidelines in Section 5.4 are followed to obtain the modified CZ parameters that accurately mimic the behavior of the EMC/Copper samples

conditioned at 85% R.H. and 110 °C for 264hrs. Figure 6.2 shows the simulated load vs. displacement graph for EMC/Copper sample conditioned at 85% R.H. and 110 °C for 264hrs at two different crack lengths.

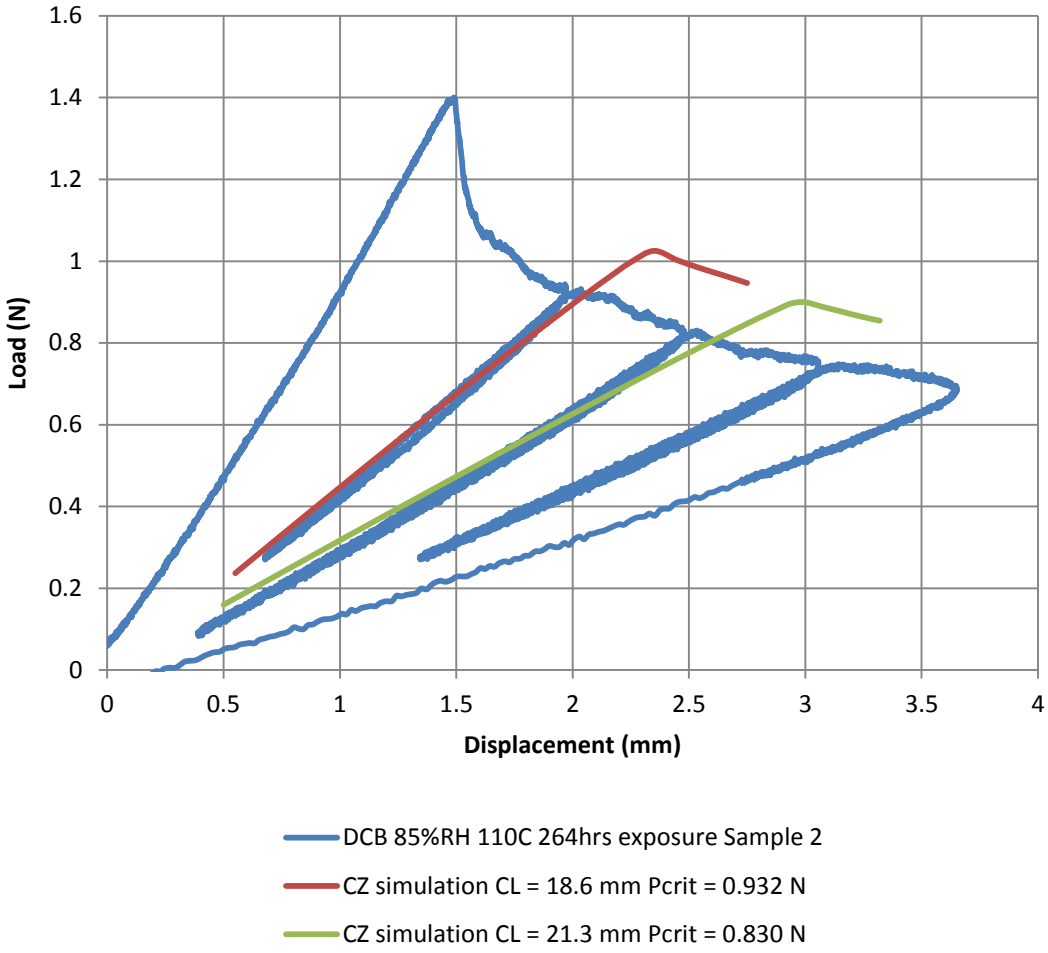

Figure 6.2 - DCB CZ simulation compared with experimental DCB data for EMC/copper sample conditioned at 85 % R.H. and 110 °C for 264hrs

As can be seen in Figure 6.2, the simulated load vs. displacement graph for the humidity conditioned sample overpredicts the $P_{critical}$ value at which delamination occurs. Since the experimental as received DCB G_c value underpredicts the G_c value obtained from Equation 4.9, this error is carried forward in subsequent calculations for humidity

and temperature conditioned samples. The modified CZ parameters obtained for EMC/Copper samples conditioned at 85% R.H. and 110 °C for 264hrs are shown inTable 6.5. Figure 6.3 and Figure 6.4 shows a plot of Mode I and Mode II modified bilinear traction separation triangles for this humidity condition respectively.

Table 6.5 - CZ parameters for EMC/Copper sample conditioned at 85% R.H. and 110 °C for 264hrs.

Bi-linear Traction Separation Laws 85% R.H and 110 °C for 264hrs		
	Mode I	**Mode II**
σ_{max} (MPa)	7.46	596
δ_c (µm)	6.35	3.24
δ* (µm)	0.635	0.324
G_C (J/m^2)	23.7	967

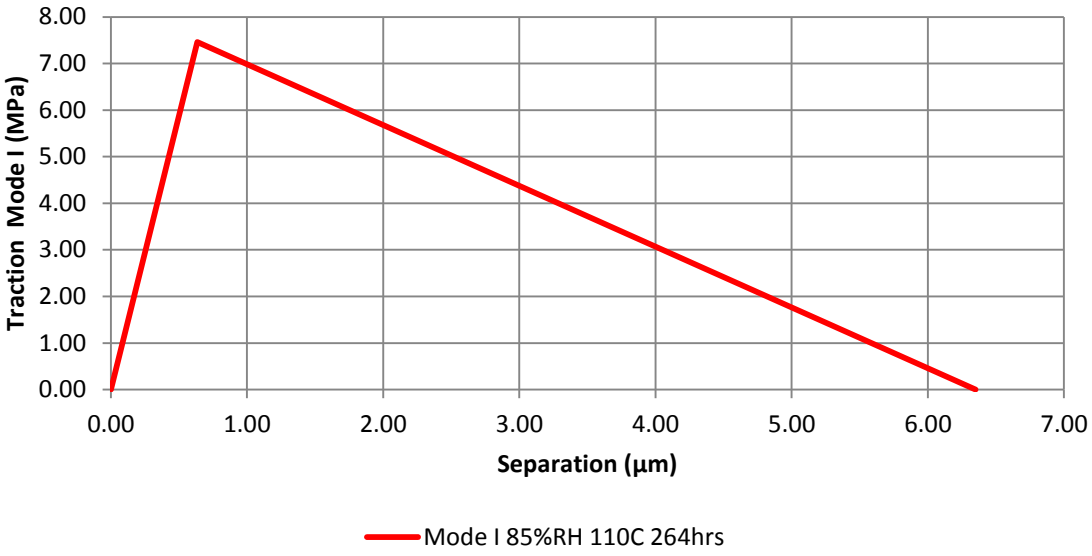

Figure 6.3 - Mode I CZ bilinear traction separation triangles for EMC/Copper Specimen conditioned at 85% R.H. and 110 °C for 264hrs.

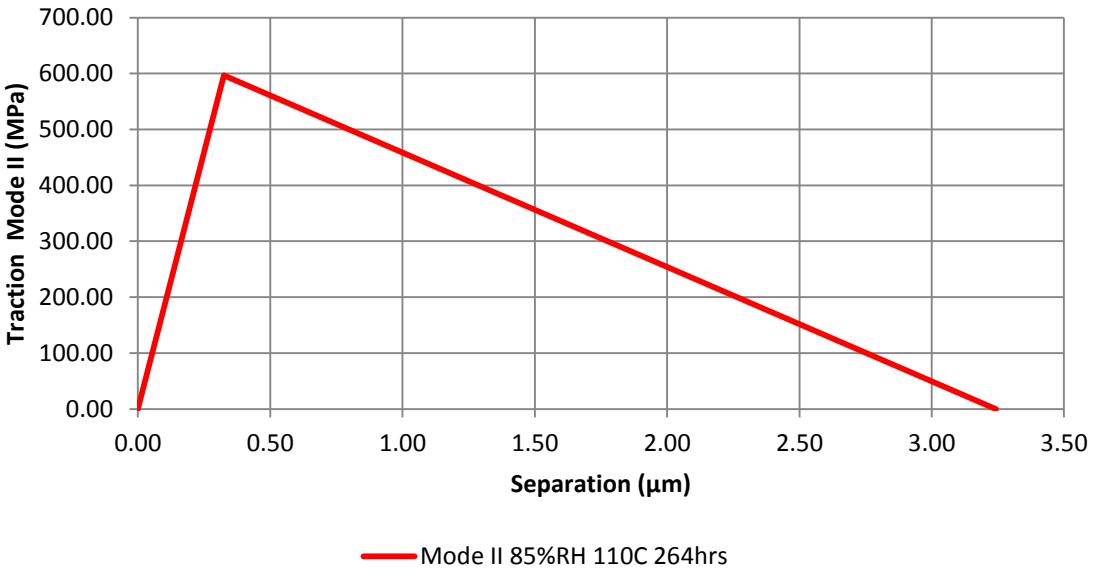

Figure 6.4 - Mode II CZ bilinear traction separation triangles for EMC/copper sample conditioned at 85% R.H. and 110 °C for 264hrs.

6.3.2 CZ Parameters for EMC/Copper samples exposed to 85% R.H and 110°C for 528hrs

The DCB G_c value for an EMC/Copper sample exposed to 85% R.H. and 110°C for 528hrs drops from an as-received G_c value of 45.1 J/m^2 to 22.7 J/m^2. This represents a 49.6 % drop in G_c. Table 6.6 shows the new G_{IC} and G_{IIC} values obtained after invoking this percentage drop on the as received G_{IC} and G_{IIC} values for the EMC/Copper sample.

Table 6.6- CZ Parameters for EMC/copper sample conditioned at 85% R.H. and 110 °C for 528hrs.

	As Received	85%RH and 110°C for 528hrs exposure
G_{IC} (J/m^2)	42.6	21.5
G_{IIC} (J/m^2)	1739	876

After obtaining the new G_{IC} and G_{IIC} values for the humidity conditioned EMC/Copper sample, the guidelines in Section 5.5 are followed to obtain the modified CZ parameters that accurately mimic the behavior of the EMC/Copper samples conditioned at 85% R.H and 110 °C. for 528hrs. Figure 6.4 shows the simulated load vs. displacement graph for EMC/Copper sample conditioned at 85% R.H and 110 °C for 528hrs at two different crack lengths.

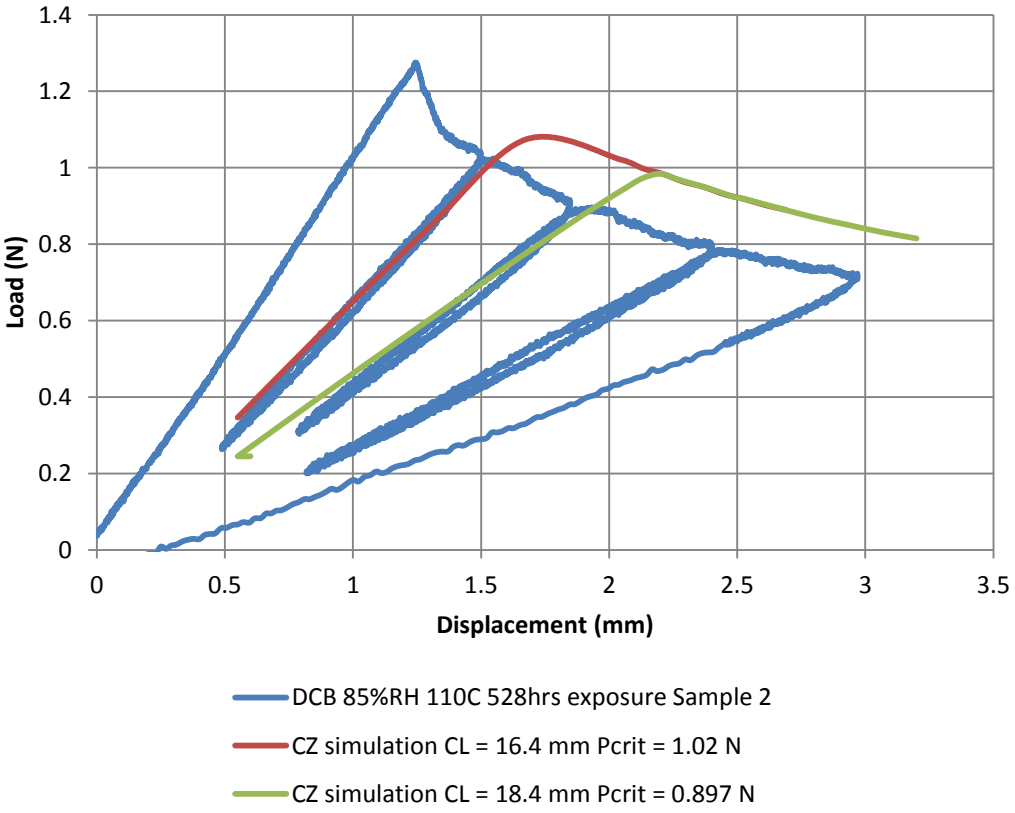

Figure 6.5 - DCB CZ simulation compared with experimental DCB data for EMC/copper sample conditioned at 85% R.H. and 110 °C for 528hrs.

Like the previous CZ DCB simulation graphs the simulated load vs. displacement graph overpredicts the $P_{critical}$ value at which delamination occurs. The modified CZ parameters obtained for EMC/Copper samples conditioned at 85% R.H and 110 °C for 528hrs are

shown in Table 6.7. Figure 6.6 and Figure 6.7 shows a plot of Mode I and Mode II modified bilinear traction separation triangles for this humidity condition respectively.

Table 6.7 - CZ parameters for EMC/copper sample conditioned at 110 °C and 85% R.H. for 528hrs.

Bilinear Traction Separation Laws 85% R.H and 110 °C for 528hrs		
	Mode I	**Mode II**
σ_{max} (MPa)	7.10	568
δ_c (µm)	6.04	4.35
δ^* (µm)	0.604	0.435
G_C (J/m^2)	21.5	876

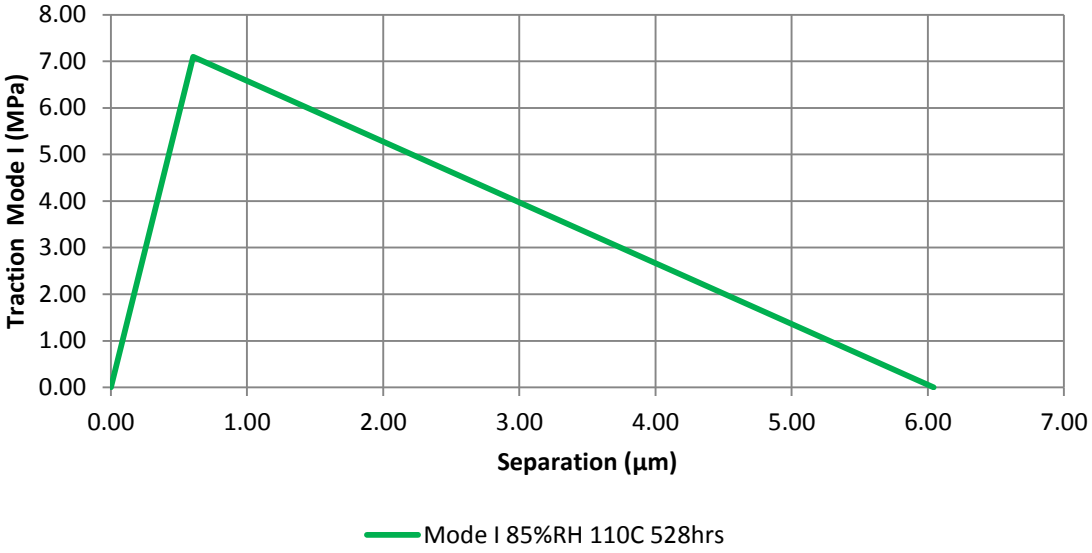

Figure 6.6 - Mode I CZ bilinear traction separation triangles for EMC/copper sample conditioned at 85% R.H. and 110 °C for 528hrs.

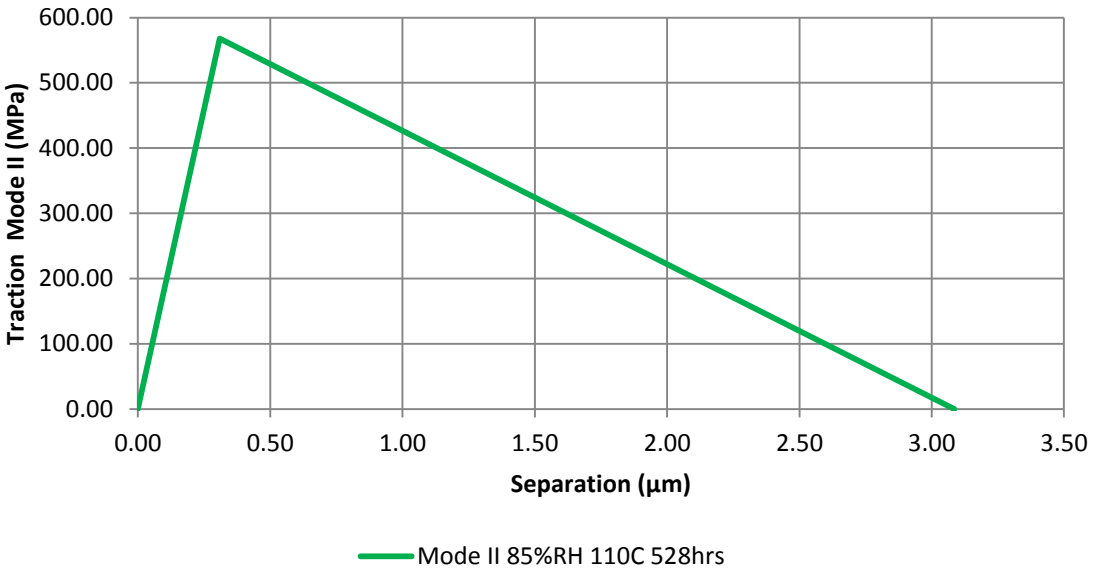

Figure 6.7 - Mode II CZ bilinear traction separation triangles for EMC/copper sample conditioned at 85% R.H. and 110 °C for 528hrs.

6.3.3 CZ Parameters for EMC/Copper samples exposed to 85% R.H. and 130°C for 96hrs

The DCB G_c value for an EMC/Copper sample exposed to 85% R.H and 130°C for 96hrs drops from an as-received G_c value of 45.1 J/m^2 to 17.6 J/m^2. This represents a 61.0 % drop in G_c. Table 6.8 shows the new G_{IC} and G_{IIC} values obtained after invoking this percentage drop on the as received G_{IC} and G_{IIC} values for the EMC/Copper sample.

Table 6.8 - Modified G_{IC} and G_{IIC} values for EMC/copper sample conditioned at 85% R.H. and 130°Cfor 96hrs

	As Received	85%RH and 130°C for 96hrs exposure
G_{IC} (J/m^2)	42.6	16.6
G_{IIC} (J/m^2)	1739	678

After obtaining the new G_{IC} and G_{IIC} values for the humidity conditioned EMC/Copper sample, the guidelines in Section 5.5 are followed to obtain the modified CZ parameters that accurately mimic the behavior of the EMC/Copper samples conditioned at 85% R.H. and 130 °C for 96hrs. Figure 6.8 shows the simulated load vs. displacement graph for the EMC/Copper sample conditioned at 85% R.H and 130 °C and for 96hrs at two different crack lengths.

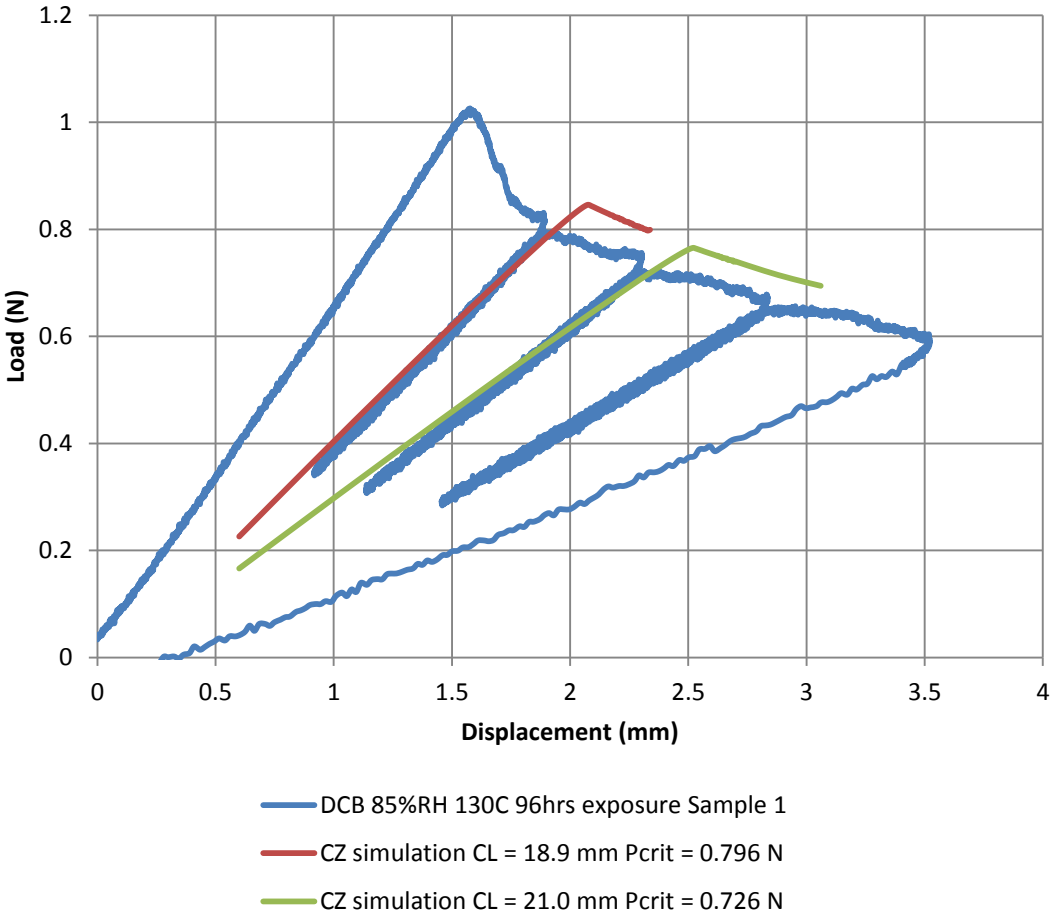

Figure 6.8 - DCB CZ simulation compared with experimental DCB data for EMC/copper sample conditioned at 85% R.H. and 130 °C for 96hrs.

Like the previous CZ DCB simulation graphs the simulated load vs. displacement graph overpredicts the $P_{critical}$ value at which delamination occurs. The modified CZ

parameters obtained for EMC/Copper samples conditioned at 85% R.H. and 130 °C for 192hrs are shown in Table 6.9. Figure 6.9 and Figure 6.10 shows a plot of Mode I and Mode II modified bilinear traction separation triangles for this humidity condition respectively.

Table 6.9 - CZ Parameters for EMC/copper sample conditioned at 85% R.H. and 130 °C for 96hrs.

Bilinear Traction Separation Laws 85% R.H and 130 °C for 96hrs		
	Mode I	**Mode II**
σ_{max} (MPa)	6.24	500
δ_c (µm)	5.32	2.72
δ* (µm)	0.532	0.272
G_C (J/m^2)	16.6	678

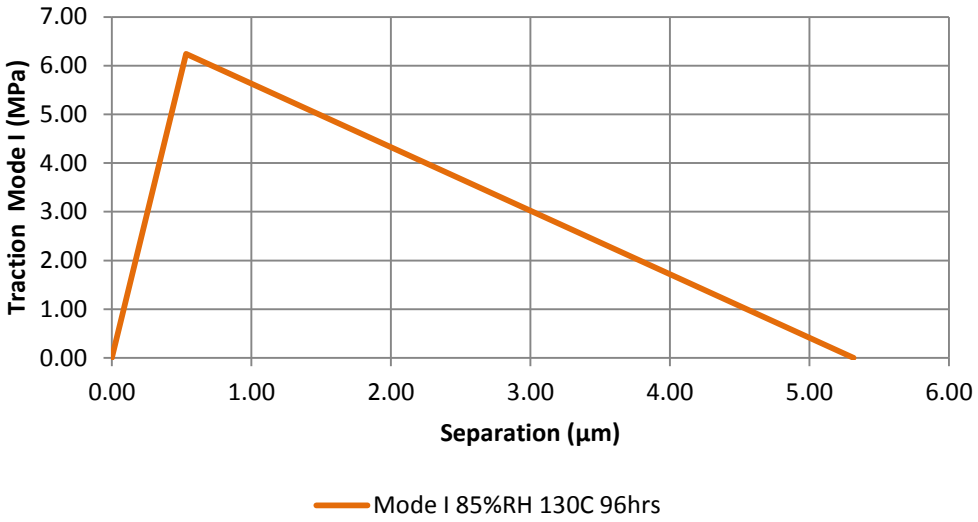

Figure 6.9 - Mode I CZ bilinear traction separation triangles for EMC/copper sample conditioned at 85% R.H. and 130 °C for 96hrs.

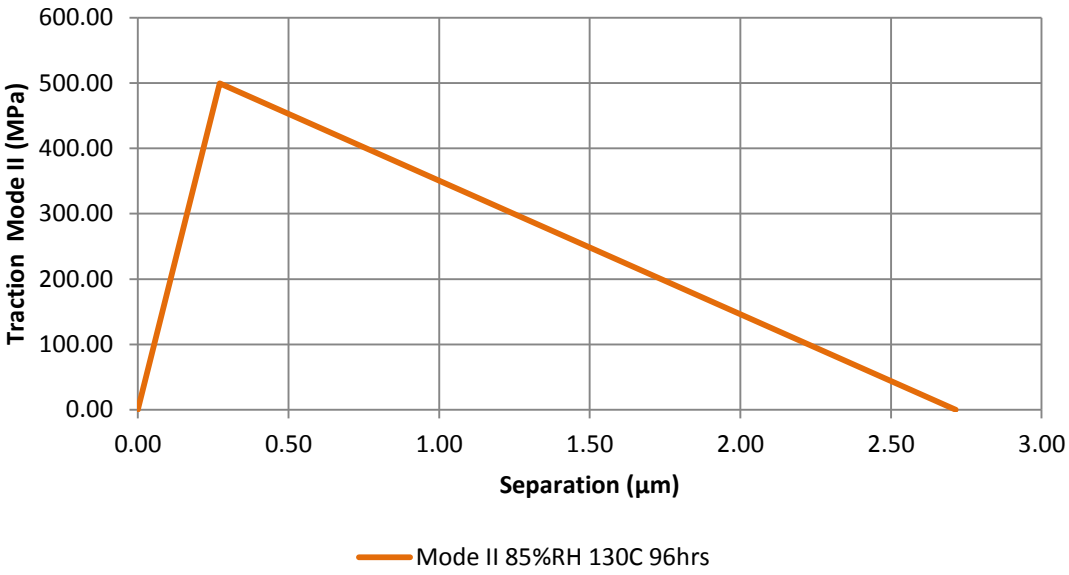

Figure 6.10- Mode II CZ bilinear traction separation triangles for EMC/copper sample conditioned at 85% R.H. and 130 °C for 96hrs.

6.3.4 CZ Parameters for EMC/Copper samples exposed to 130°C and 85% R.H. for 192hrs

The DCB G_c value for an EMC/Copper sample exposed to 85% R.H and 130°C for 192hrs drops from an as-received G_c value of 45.1 J/m^2 to 18.5 J/m^2. This represents a 58.9 % drop in G_c. Table 6.10 shows the new G_{IC} and G_{IIC} values obtained after invoking this percentage drop on the as received G_{IC} and G_{IIC} values for the EMC/Copper sample.

Table 6.10 - Modified G_{IC} and G_{IIC} values for EMC/copper sample conditioned at 85% R.H. and 130°C for 192hrs

	As Received	85%RH and 130°C for 192hrs exposure
G_{IC} (J/m^2)	42.6	17.5
G_{IIC} (J/m^2)	1739	715

After obtaining the new G_{IC} and G_{IIC} values for the humidity conditioned EMC/Copper sample, the guidelines in Section 5.5 are followed to obtain the modified CZ parameters that accurately mimic the behavior of the EMC/Copper samples conditioned at 85% R.H. and 130 °C for 192hrs. Figure 6.11 shows the simulated load vs. displacement graph for an EMC/Copper sample conditioned at 85% R.H. and 130 °C for 192hrs at two different crack lengths.

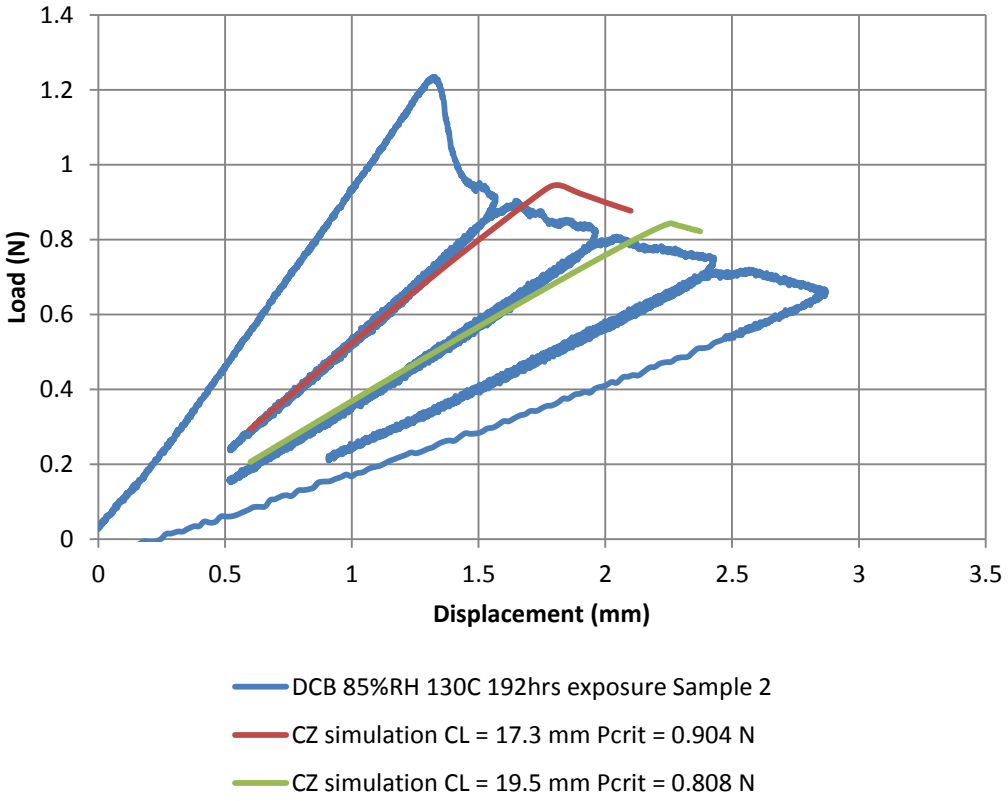

Figure 6.11 - DCB CZ simulation compared with experimental DCB data for EMC/copper sample conditioned at 85% R.H. and 130 °C for 192hrs.

Like the previous CZ DCB simulation graphs the simulated load vs. displacement graph overpredicts the $P_{critical}$ value at which delamination occurs. The modified CZ parameters obtained for EMC/Copper samples conditioned at 85% R.H. and 130 °C for 192hrs are shown in Table 6.11. Figure 6.12 and Figure 6.13 show a plot of Mode I and

Mode II modified bilinear traction separation triangles for this humidity condition respectively.

Table 6.11 - CZ Parameters for EMC/copper sample conditioned at 85% R.H. and 130 °C for 192hrs.

Bilinear Traction Separation Laws 130 °C and 85% R.H for 192hrs		
	Mode I	**Mode II**
σ_{max} **(MPa)**	6.41	513
δ_c **(µm)**	5.46	2.79
δ* (µm)	0.546	0.279
G_C **(J/m^2)**	17.5	715

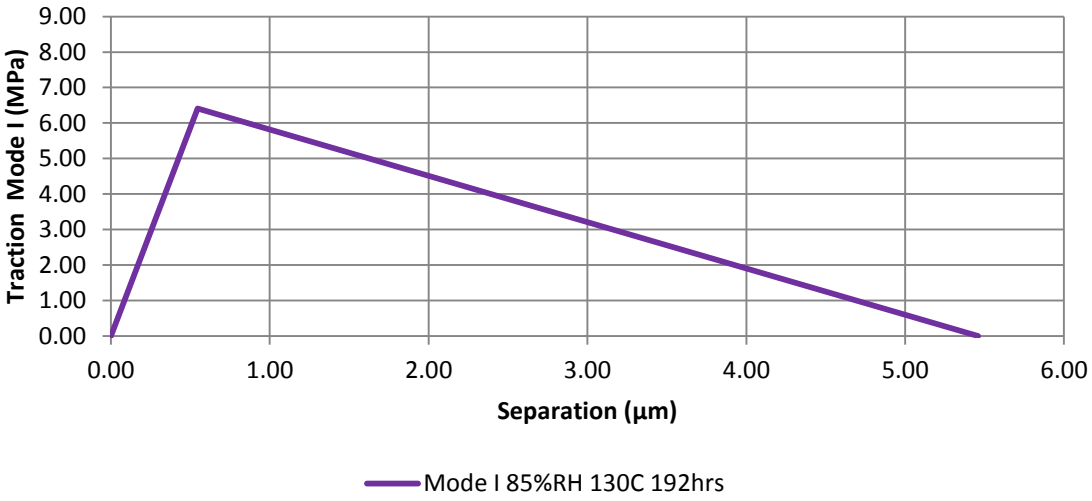

Figure 6.12 - Mode I CZ bilinear traction separation triangles for EMC/copper sample conditioned at 85% R.H. and 130 °C for 192hrs.

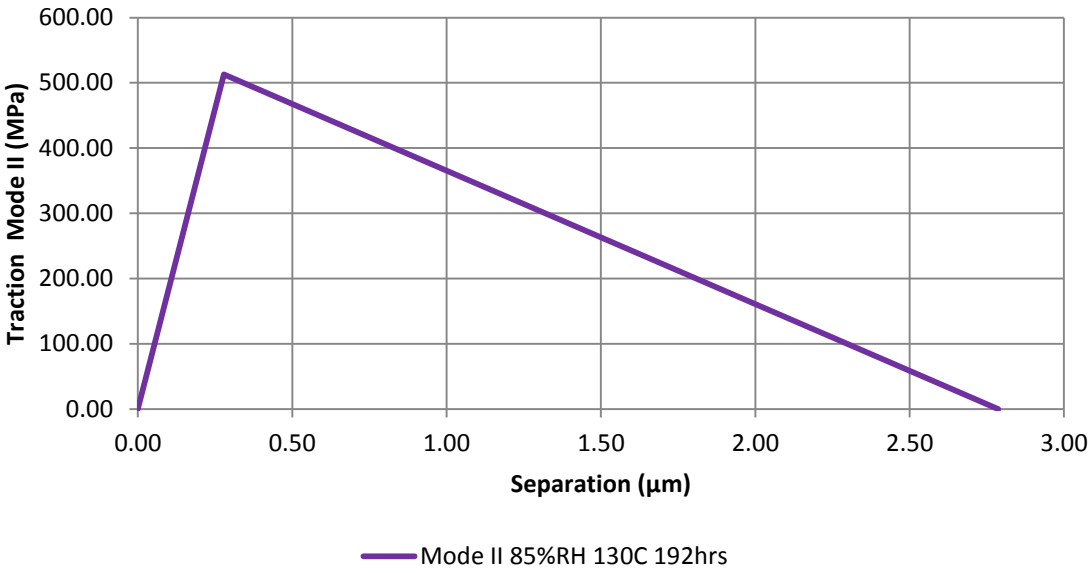

Figure 6.13 - Mode II CZ bilinear traction separation triangles for EMC/copper sample conditioned at 85% R.H. and 130 °C for 192hrs.

6.4 Discussion of the modified CZ Parameters obtained after humidity conditioning EMC/Copper samples.

Figure 6.14 shows all the modified Mode I CZ traction separation laws obtained after humidity conditioning the EMC/Copper sample at various levels. Figure 6.15 shows the same for Mode II CZ traction separation laws.

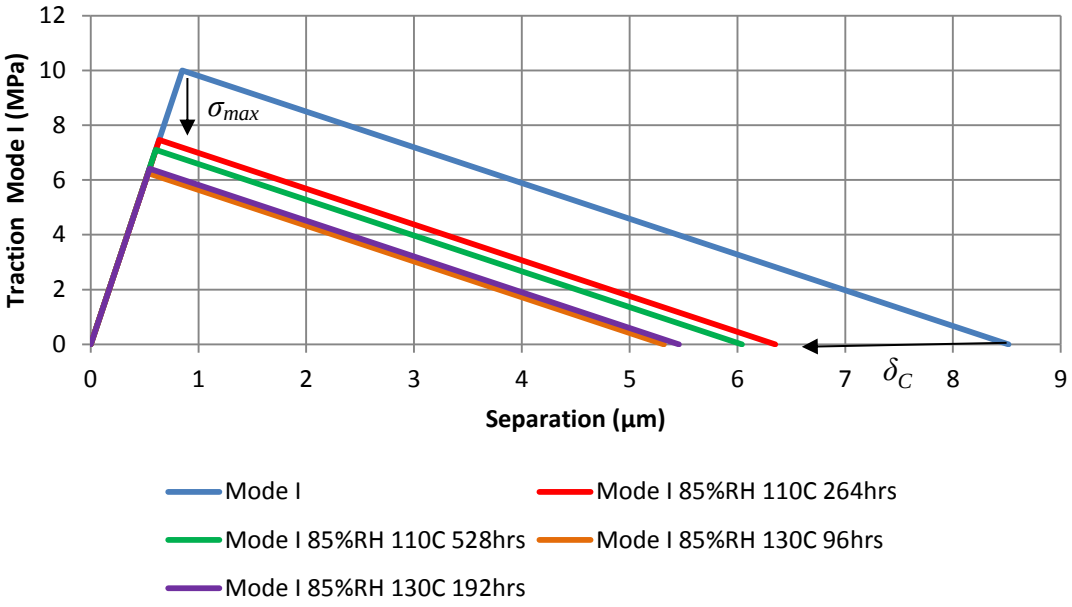

Figure 6.14- Mode I CZ bilinear traction separation triangles for EMC/copper sample exposed to different humidity condition levels

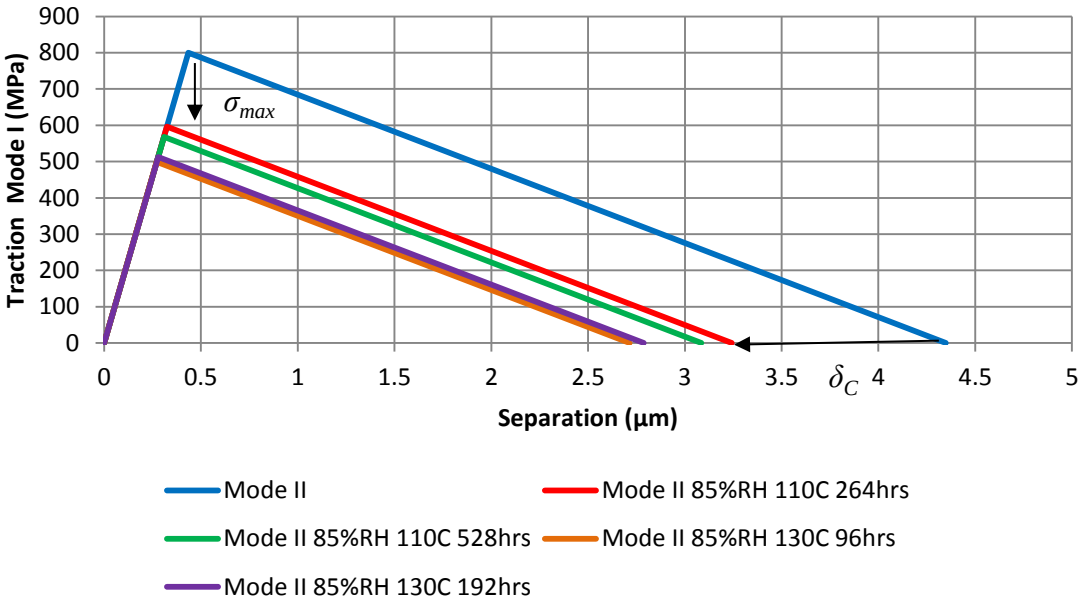

Figure 6.15- Mode II CZ bilinear traction separation triangles for EMC/copper sample exposed to different humidity condition levels

Figure 6.14 and Figure 6.15 both show that the reduction in the G_c value observed due to humidity conditioning at 85 % R.H and 110 °C and 85% R.H. and 130 °C is represented by a reduction in the maximum traction, σ_{max} and the maximum interfacial separation, δ_C of the as-received Mode I and Mode II CZ Parameters.

CHAPTER 7. EXPERIMENTAL STUDY OF ISOTHERMALLY AGED EMC/COPPER SAMPLES

EMC/Copper sample is exposed to different temperatures and durations. These conditions are based on stress test qualifications for packaged integrated circuits used by industry [45]. The conditions replicated are accelerated stress tests derived from reliability models that represent years of device operation.

EMC/Copper samples are exposed to temperatures of 150 °C and 175 °C for various durations. Modified cohesive zone parameters can be found using the G_c value obtained for thermally aged EMC/Copper samples.

7.1 Experimental DCB results for thermally aged EMC/Copper samples

EMC/Copper samples are exposed to temperatures of 150 °C and 175 °C for 168hrs, 504hrs and 1000hrs. DCB testing is conducted on the thermally aged EMC/Copper samples at room temperature. EMC/Copper samples are exposed to temperatures of 150 °C and 175 °C for 168hrs, 504hrs and 1000hrs. DCB testing is conducted on the thermally aged EMC/Copper samples at room temperature.

7.1.1 DCB test results for EMC/Copper samples exposed to 150°C for 168hrs, 504hrs and 1000hrs

Table 7.1 shows the average G_c value obtained after thermally aging EMC/Copper samples at 150°C. EMC/Copper samples are exposed to 150°C for 168hrs, 504hrs and 1000hrs. Crack Length for the temperature conditioned EMC/Copper samples are

obtained using the compliance vs. crack length relationship shown in Section 4.3.1. $P_{critical}$ is taken to be the maximum load for each load curve. The average G_c value for each temperature conditioned EMC/Copper sample is obtained through VCCT using FEM.

Table 7.1 - G_c values for DCB EMC/copper samples exposed to 150°C for 168hrs, 504hrs and 1000hrs

Sample Number	G_c (J/m^2) (VCCT) after isothermal aging at 150°C for 168hrs	G_c (J/m^2) (VCCT) after isothermal aging at 150°C for 504hrs	G_c (J/m^2) (VCCT) after isothermal aging at 150°C for 1000hrs
1	50.6	49.7	29.4
2	42.4	46.5	20.8
3	38.7	x	37.0
Average	**43.9±6.53**	**48.1±3.22**	**29.1±7.72**

As can be seen from Table 7.1, no significant change in interfacial adhesion is noticed after temperature conditioning at 150°C. The average G_c value obtained after isothermal aging at 150°C for 168hrs and 504hrs was 43.9 J/m^2 and 48.1 J/m^2 respectively. This clearly indicates that temperature conditioning at 150°C for 168hrs and 504hrs lead to no significant change in the G_c value. A decrease in G_c value is seen after thermally aging the EMC/Copper sample at 150°C for 1000hrs. The average G_c value obtained after isothermal aging at 150°C for 1000hrs is 29.1 J/m^2. There is a 35.5 % loss in the G_c value of the EMC/Copper sample from its as-received G_c value of 45.1 J/m^2 after thermal aging at 150°C for 1000hrs. This may be due to the fact that exposure for longer durations at 150°C leads to chemical degradation of the adhesive bonds at the EMC/Copper interface.

7.1.2 DCB test results for EMC/Copper samples exposed to 175°C for 168hrs, 504hrs and 1000hrs

Table 7.2 shows the average G_c value obtained after thermally aging EMC/Copper samples at 175°C. EMC/Copper samples are exposed to 175°C for 168hrs, 504hrs and 1000hrs. Crack Length for the temperature conditioned EMC/Copper samples are obtained using the compliance vs. crack length relationship shown in Section 4.3.1. $P_{critical}$ is taken to be the maximum load for each load curve. The average G_c value for each temperature conditioned EMC/Copper sample is obtained through VCCT using FEM.

Table 7.2 - G_c values for DCB EMC/copper samples exposed to 175°C for 168hrs, 504hrs and 1000hrs

Sample Number	G_c (J/m^2) (VCCT) after isothermal aging at 175°C for 168hrs	G_c (J/m^2) (VCCT) after isothermal aging at 175°C for 504hrs	G_c (J/m^2) (VCCT) after isothermal aging at 175°C for 100hrs
1	55.9	50.7	16.1
2	55.1	47.7	21.0
3	50.5	x	x
Average	**53.8±5.32**	**49.2±3.49**	**18.6±2.83**

As can be seen from Table 7.2, no significant change in interfacial adhesion is noticed after temperature conditioning at 175°C. The average G_c value obtained after isothermal aging at 175°C for 168hrs and 504hrs was 53.8 J/m^2 and 49.2 J/m^2 respectively. This clearly indicates that temperature conditioning at 175°C for 168hrs and 504hrs lead to no significant change in the G_c value of the EMC/Copper sample. A decrease in the G_c value is seen after thermally aging studies were conducted on the EMC/Copper sample at 175°C for 1000hrs. The average G_c value obtained after

isothermal aging at 175°C for 1000hrs is 18.6 J/m^2. There is a 58.8% loss in the G_c value of the EMC/Copper sample from its as-received G_c value of 45.1 J/m^2 after thermal aging at 175°C for 1000hrs. The loss in the G_c value was greater after thermal aging at 175°C for 1000hrs compared to the results obtained after testing at 150°C for 1000hrs. This clearly indicates that increasing the temperature to 175°C at 1000hrs conditioning introduced further chemical degradation of the EMC/Copper interface bonds compared to the loss incurred after thermal aging at 150°C for 1000hrs.

7.2 Discussion of DCB results for isothermally aged EMC/copper samples

Figure 7.1 and Figure 7.2 show a plot of G_c EMC/Copper samples thermally aged at 150°C and 175°C for 168hrs, 504hrs and 1000hrs respectively.

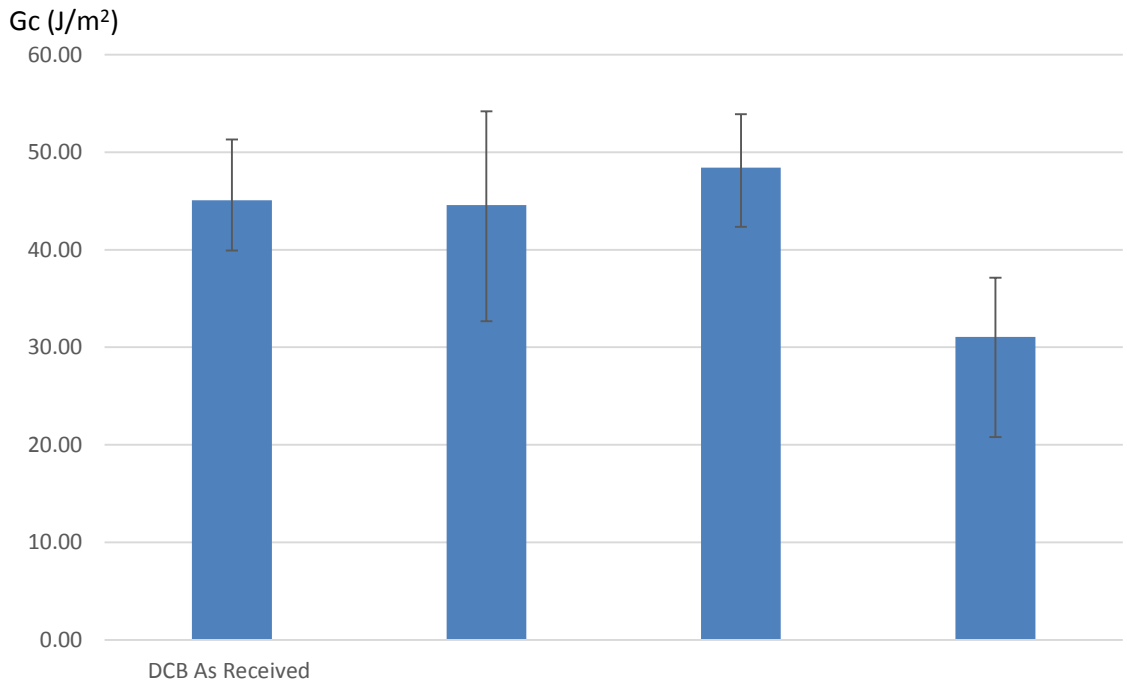

Figure 7.1 - Plot of DCB G_c values EMC/Copper samples thermally aged at 150 °C for 168hrs, 504hrs and 1000hrs.

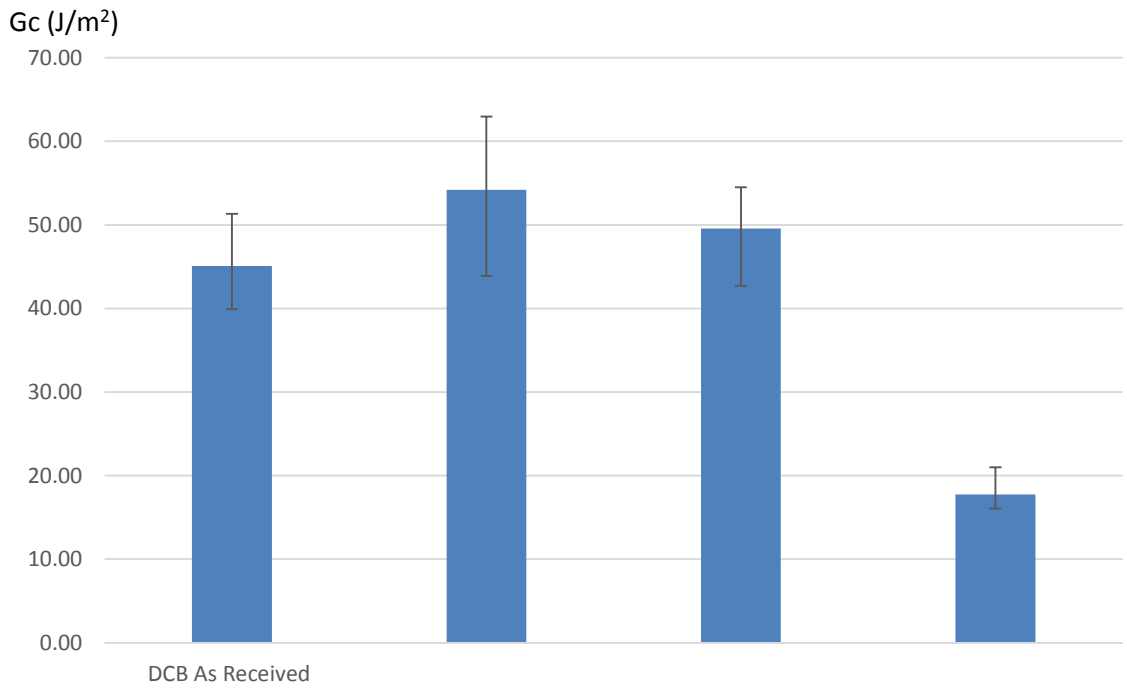

Figure 7.2 - Plot of DCB G_c values EMC/Copper samples thermally aged at 175 °C for 168hrs, 504hrs and 1000hrs.

The results obtained are in agreement with previous studies done to investigate the effect of isothermal aging on the interfacial adhesion of an EMC/Copper interface. Shirangi et al. showed in Section 2.3 that thermally aging an EMC/Copper sample at 175°C for 336 hours (2 weeks) there is a significant loss in interfacial adhesion [36].For the EMC/Copper sample investigated in this study, this loss in interfacial strength is occurring after thermally aging the samples for longer durations.

7.3 CZ Parameters for thermally aged EMC/Copper samples

The G_c values obtained for the thermally aged samples can be used to develop modified CZ parameters that characterize the interfacial behavior of the EMC/Copper sample. The same technique as mentioned in Section 6.3 is used to develop modified CZ

parameters for EMC/Copper samples thermally aged at 150°C and 175°C for 168hrs, 504hrs and 1000hrs.

7.3.1 CZ Parameters for EMC/Copper samples exposed to 150°C for 168hrs

The DCB G_c value for an EMC/Copper sample thermally aged at 150°C for 168hrs drops from an as-received G_c value of 45.1 J/m^2 to 44.6 J/m^2.This represents a 1.09% drop in G_c. Table 7.3 shows the new G_{IC} and G_{IIC} values obtained after invoking this percentage drop on the as received G_{IC} and G_{IIC} values for the EMC/Copper sample.

Table 7.3 - Modified G_{IC} and G_{IIC} values for EMC/Copper sample thermally aged at 150°C for 168hrs

	As Received	**150°C and 168hrs exposure**
G_{IC} (J/m^2)	42.6	42.1
G_{IIC} (J/m^2)	1739	1720

After obtaining the new G_{IC} and G_{IIC} values for the thermally aged EMC/Copper sample, the guidelines in Section 5.5 are followed to obtain the modified CZ parameters that accurately mimic the behavior of the EMC/Copper samples conditioned at 150°C. for 168hrs. Figure 7.3 shows the simulated load vs. displacement graph for EMC/Copper sample conditioned at 150°C. for 168hrs. at two different crack lengths.

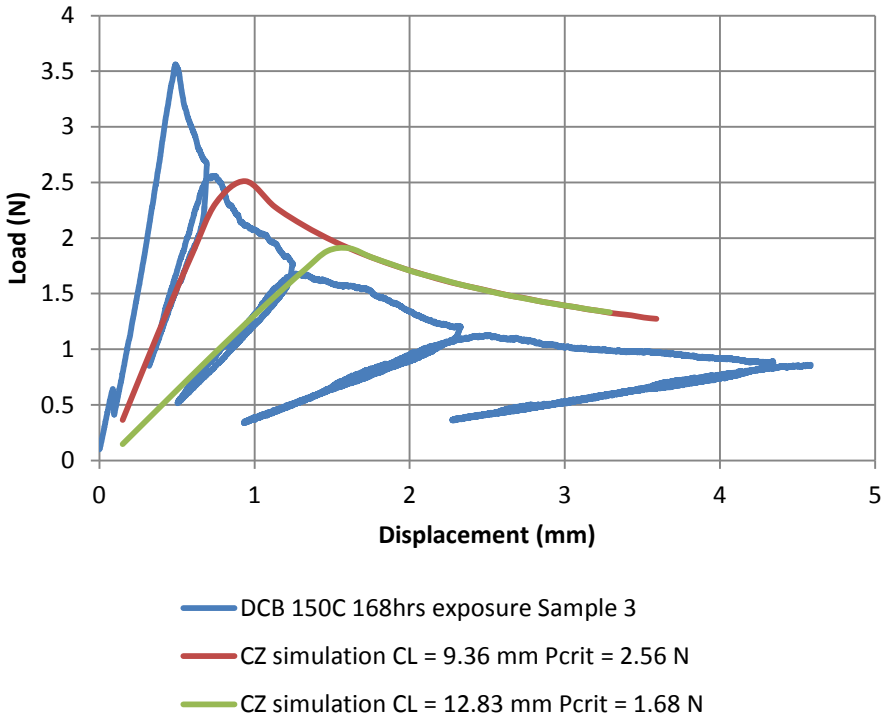

Figure 7.3 - DCB CZ simulation compared with experimental DCB data for EMC/copper sample thermally aged at 150°C for 168hrs

Like the previous CZ DCB simulation graphs the simulated load vs. displacement graph overpredicts the $P_{critical}$ value at which delamination occurs. The modified CZ parameters obtained for EMC/Copper samples thermally aged at 150°C for 168hrs are shown in Table 7.4. Figure 7.4 and Figure 7.5 shows a plot of Mode I and Mode II modified bilinear traction separation triangles for this thermally aged condition respectively.

Table 7.4 - CZ Parameters for EMC/copper sample thermally aged at 150°C for 168hrs

Traction Separation Laws 150C 168hrs		
	Mode I	**Mode II**
σ_{max} **(MPa)**	9.95	796
δ_c **(µm)**	8.47	4.32
δ* (µm)	0.847	0.432
G_C **(J/m^2)**	42.1	1720

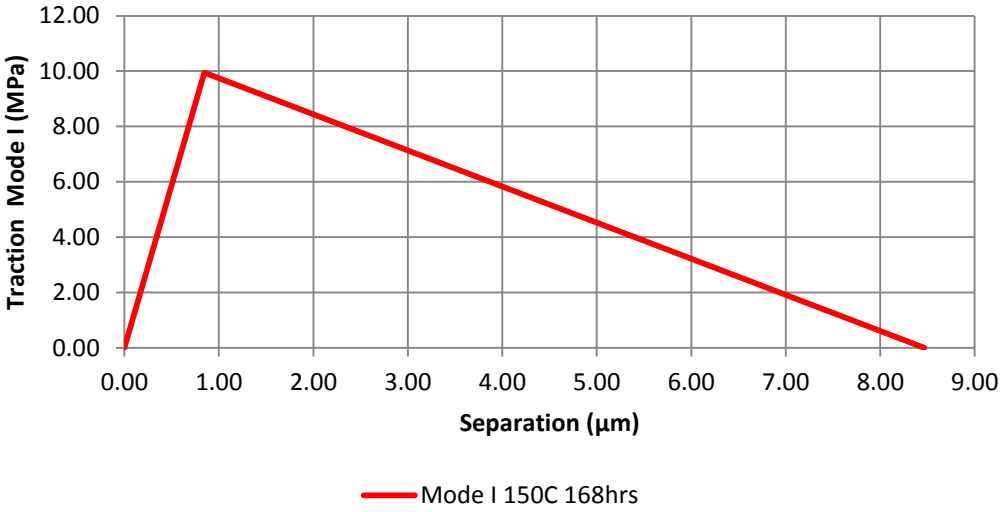

Figure 7.4 - Mode I CZ bilinear traction separation triangles for EMC/copper sample thermally aged at 150°C for 168hrs

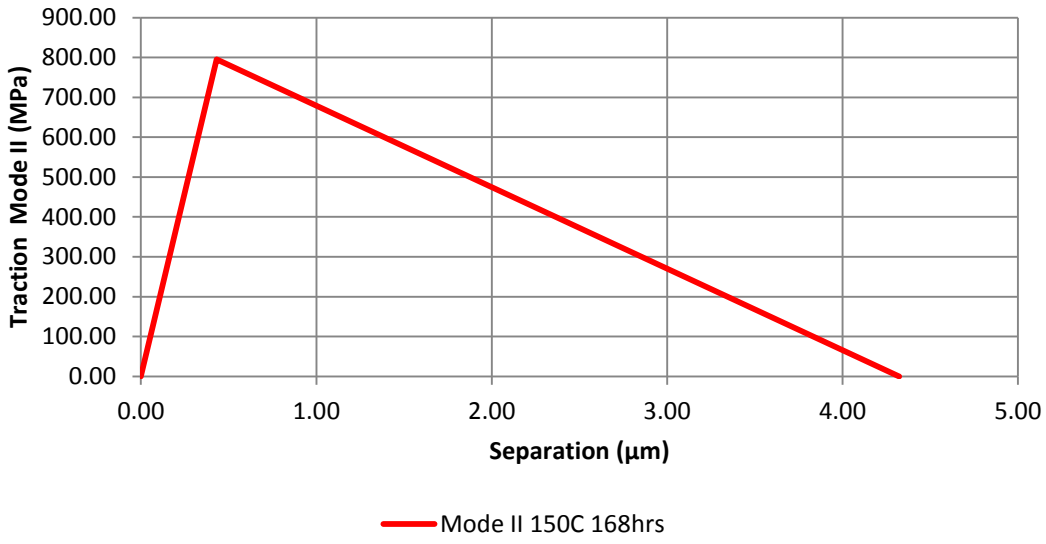

Figure 7.5 - Mode II CZ bilinear traction separation triangles for EMC/copper sample thermally aged at 150°C for 168hrs

7.3.2 CZ Parameters for EMC/Copper samples exposed to 150°C for 504hrs

The DCB G_c value for an EMC/Copper sample thermally aged at 150°C for 504hrs increases from an as-received G_c value of 45.1 J/m^2 to 48.4 J/m^2.This represents a 7.41% increase in G_c. Table 7.5 shows the new G_{IC} and G_{IIC} values obtained after invoking this percentage drop on the as received G_{IC} and G_{IIC} values for the EMC/Copper sample.

Table 7.5 - Modified G_{IC} and G_{IIC} values for EMC/copper sample thermally aged at 150°C for 504hrs

	As Received	150°C and 504hrs exposure
G_{IC} (J/m^2)	42.6	45.7
G_{IIC} (J/m^2)	1739	1868

After obtaining the new G_{IC} and G_{IIC} values for the thermally aged EMC/Copper sample, the guidelines in Section 5.5 are followed to obtain the modified CZ parameters

that accurately mimic the behavior of the EMC/Copper samples conditioned at 150°C. for 504hrs. Figure 7.6 shows the simulated load vs. displacement graph for EMC/Copper sample conditioned at 150°C. for 504hrs. at two different crack lengths.

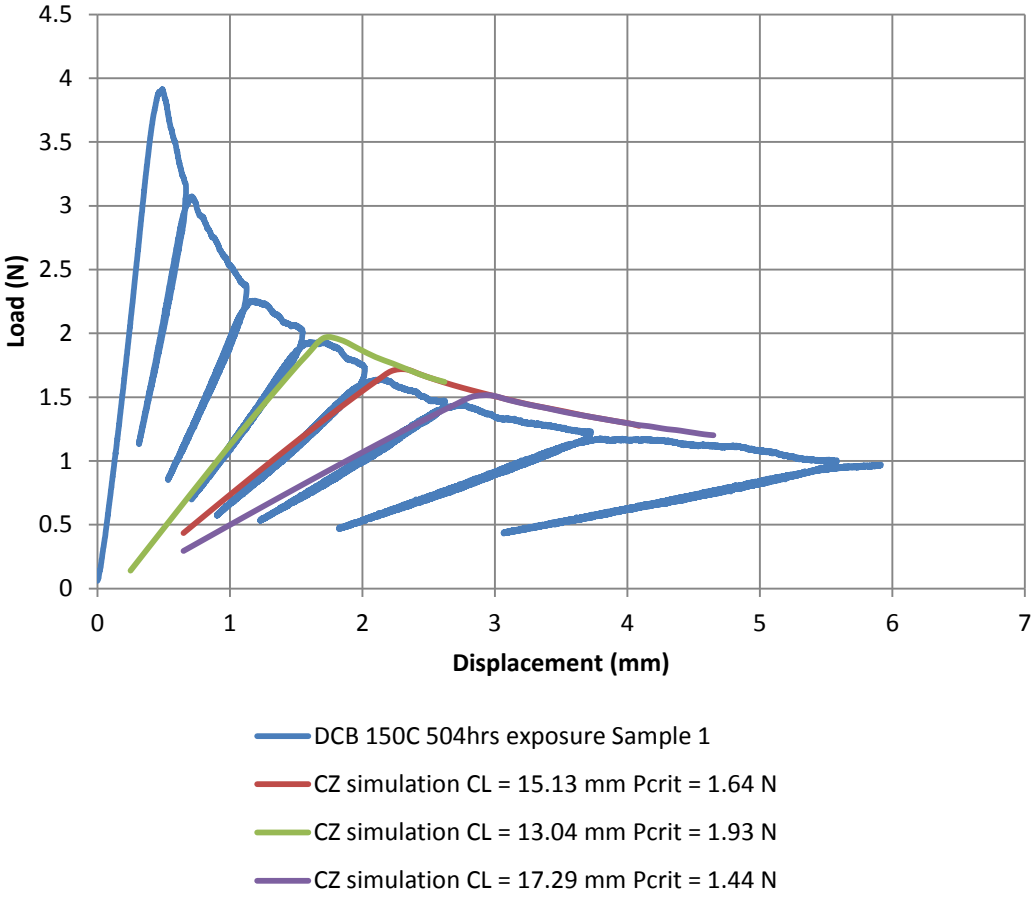

Figure 7.6 - DCB CZ simulation compared with experimental DCB data for EMC/copper sample thermally aged at 150°C for 504hrs

Like the previous CZ DCB simulation graphs the simulated load vs. displacement graph overpredicts the $P_{critical}$ value at which delamination occurs. The modified CZ parameters obtained for EMC/Copper samples thermally aged at 150°C for 504hrs are shown in Table 7.6. Figure 7.7 and Figure 7.8 shows a plot of Mode I and Mode II modified bilinear traction separation triangles for this thermally aged condition respectively.

Table 7.6 - CZ Parameters for EMC/copper sample thermally aged at 150°C for 504hrs

Traction Separation Laws 150C 504hrs exposure		
	Mode I	**Mode II**
σ_{max} **(MPa)**	10.4	829
δ_c **(µm)**	8.82	4.51
δ^* **(µm)**	0.882	0.451
G_C **(J/m^2)**	45.7	1868

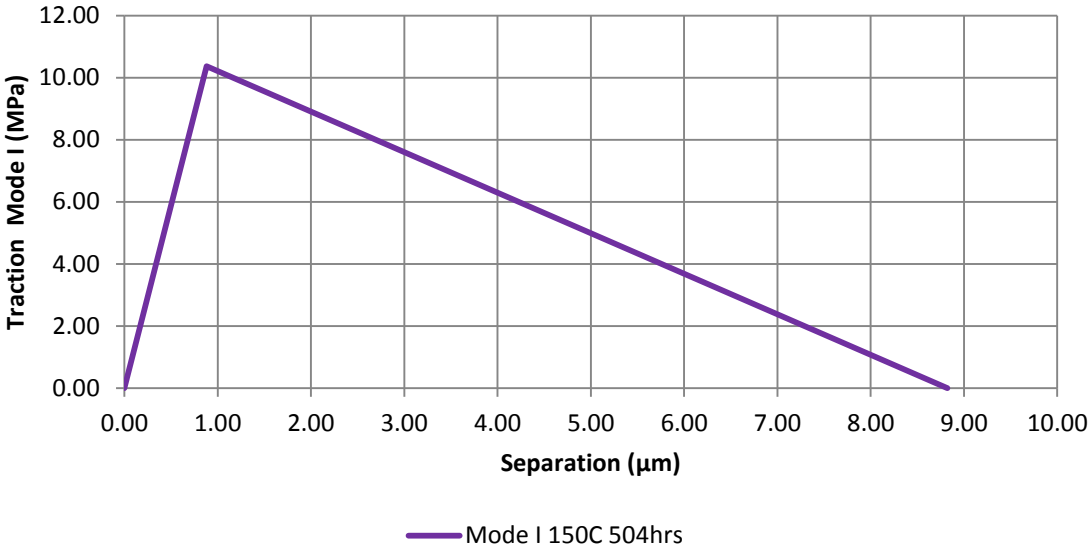

Figure 7.7 - Mode I CZ bilinear traction separation triangles for EMC/copper sample thermally aged at 150°C for 504hrs

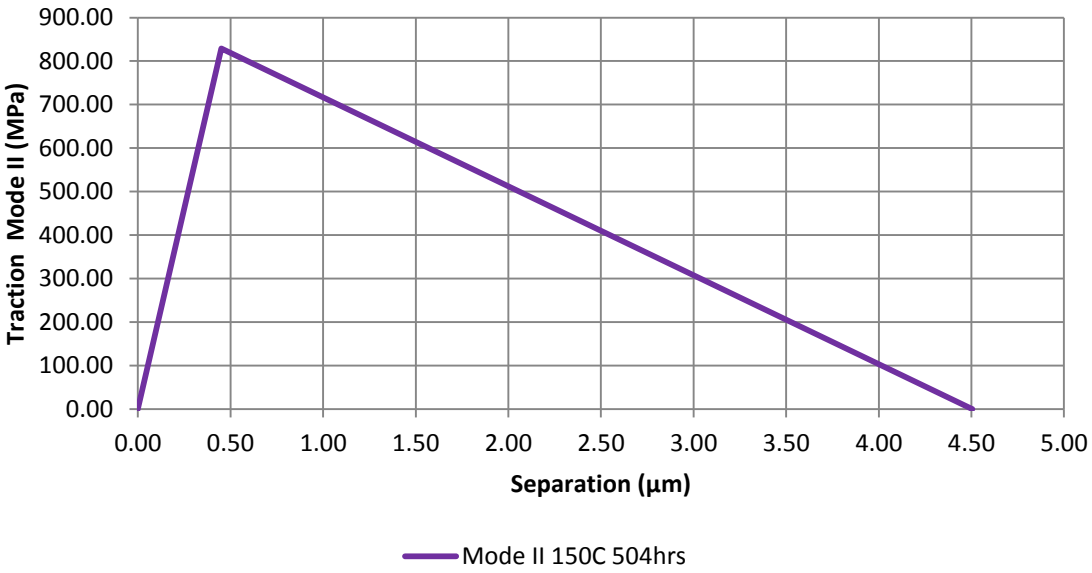

Figure 7.8 - Mode II CZ bilinear traction separation triangles for EMC/copper sample thermally aged at 150°C for 504hrs

7.3.3 CZ Parameters for EMC/Copper samples exposed to 150°C for 1000hrs

The DCB G_c value for an EMC/Copper sample thermally aged at 150°C for 1000hrs drops from an as-received G_c value of 45.1 J/m^2 to 31.1 J/m^2.This represents a 31.1% drop in G_c. Table 7.7 shows the new G_{IC} and G_{IIC} values obtained after invoking this percentage drop on the as received G_{IC} and G_{IIC} values for the EMC/Copper sample.

Table 7.7 - Modified G_{IC} and G_{IIC} values for EMC/copper sample thermally aged at 150°C for 504hrs

	As Received	150°C and 1000hrs exposure
G_{IC} (J/m^2)	42.6	29.3
G_{IIC} (J/m^2)	1739	1198

After obtaining the new G_{IC} and G_{IIC} values for the thermally aged EMC/Copper sample, the guidelines in Section 5.5 are followed to obtain the modified CZ parameters

that accurately mimic the behavior of the EMC/Copper samples conditioned at 150°C. for 1000hrs. Figure 7.9 shows the simulated load vs. displacement graph for EMC/Copper sample conditioned at 150°C. for 1000hrs. at two different crack lengths.

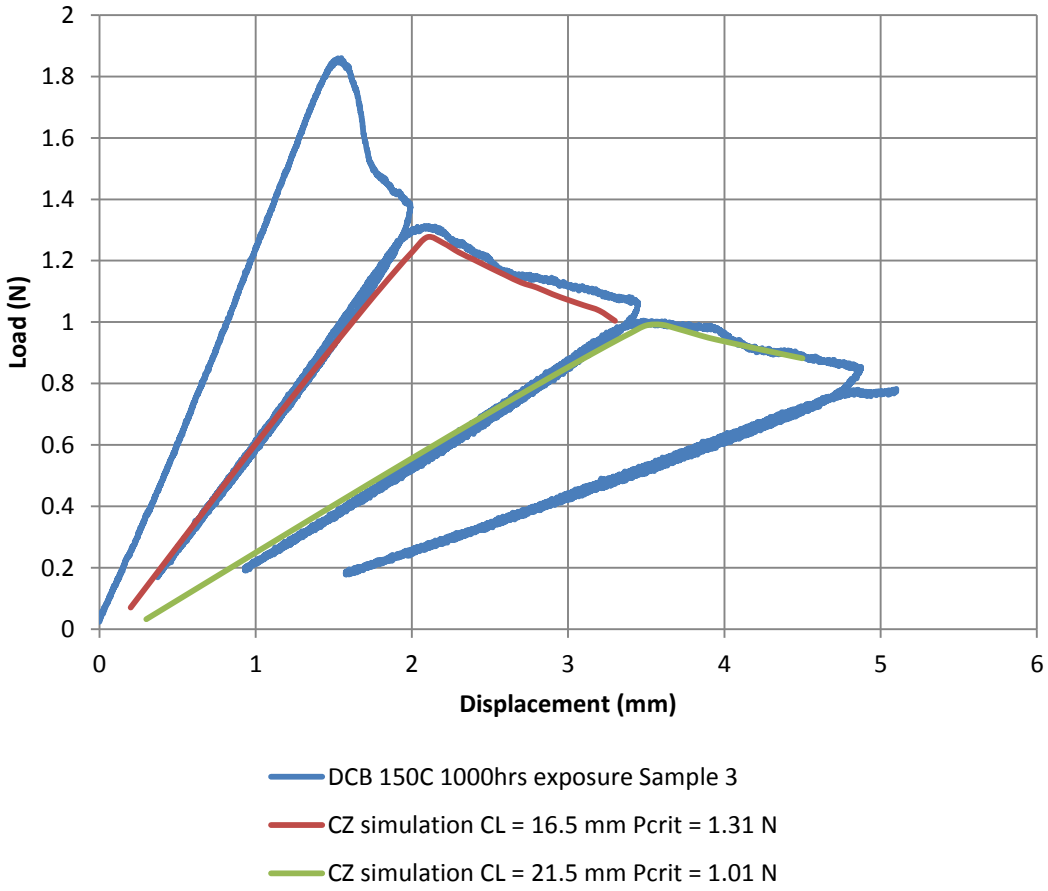

Figure 7.9 - DCB CZ simulation compared with experimental DCB data for EMC/copper sample thermally aged at 150°C for 1000hrs

Like the previous CZ DCB simulation graphs the simulated load vs. displacement graph overpredicts the $P_{critical}$ value at which delamination occurs. The modified CZ parameters obtained for EMC/Copper samples thermally aged at 150°C for 1000hrs are shown in Table 7.8Table 7.4. Figure 7.10 and Figure 7.11 shows a plot of Mode I and

Mode II modified bilinear traction separation triangles for this thermally aged condition respectively

Table 7.8 - CZ Parameters for EMC/Copper sample thermally aged at 150°C for 1000hrs

Traction Separation Laws 150C 1000hrs Exposure		
	Mode I	**Mode II**
σ_{max} (MPa)	8.30	664
δ_c (µm)	7.07	3.61
δ^* (µm)	0.707	0.361
G_C (J/m^2)	29.3	1198

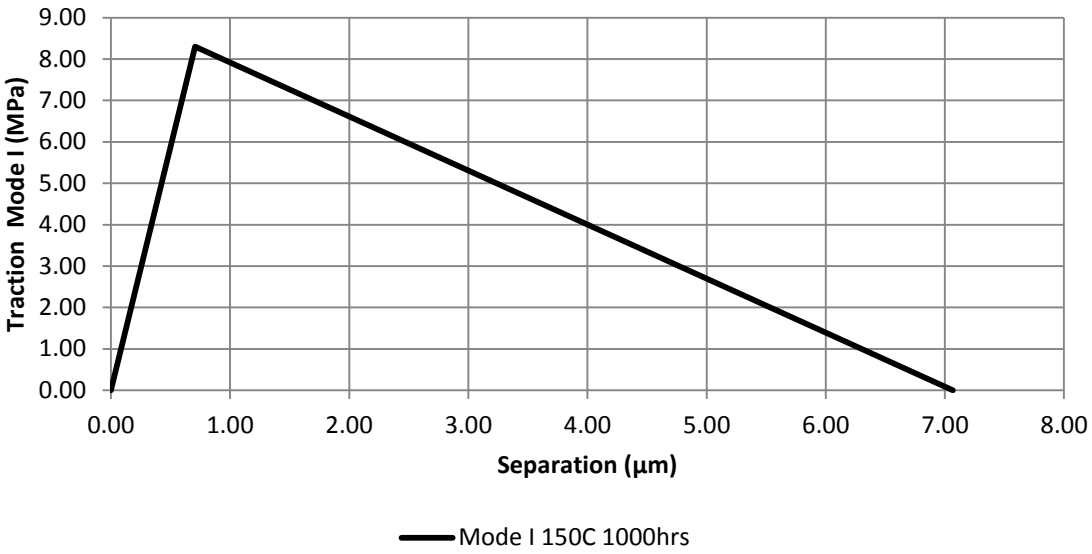

Figure 7.10 - Mode I CZ bilinear traction separation triangles for EMC/copper sample thermally aged at 150°C for 1000hrs

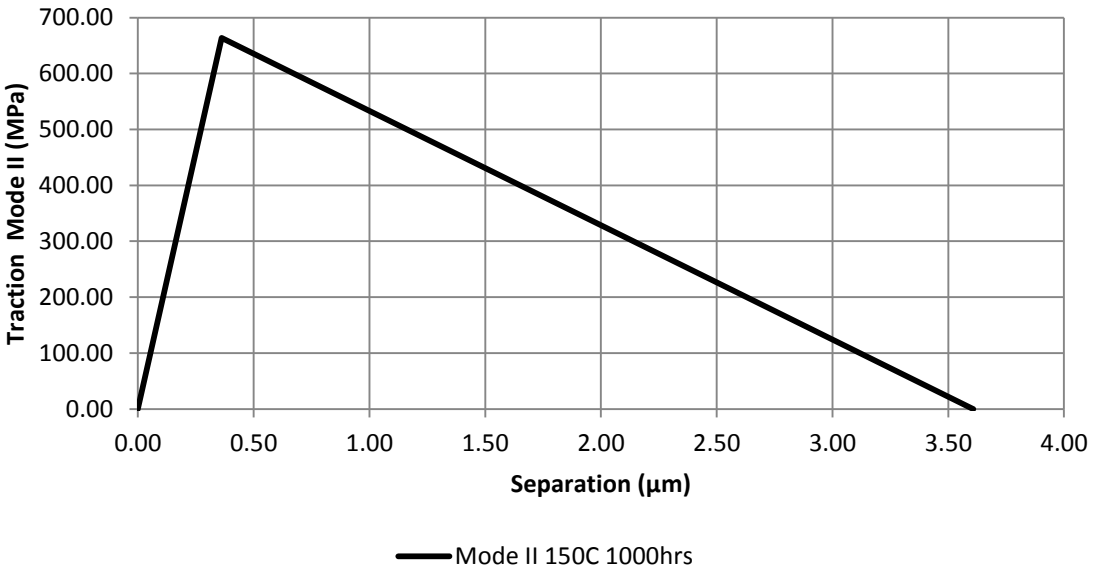

Figure 7.11 - Mode II CZ bilinear traction separation triangles for EMC/copper sample thermally aged at 150°C for 1000hrs

7.3.4 CZ Parameters for EMC/Copper samples exposed to 175°C for 168hrs

The DCB G_c value for an EMC/Copper sample thermally aged at 175°C for 168hrs increases from an as-received G_c value of 45.1 J/m^2 to 54.2 J/m^2.This represents a 20.2% increase in G_c. Table 7.3 shows the new G_{IC} and G_{IIC} values obtained after invoking this percentage drop on the as received G_{IC} and G_{IIC} values for the EMC/Copper sample.

Table 7.9 - Modified G_{IC} and G_{IIC} values for EMC/copper sample thermally aged at 175°C for 168hrs

	As Received	175°C and 168hrs exposure
G_{IC} (J/m^2)	42.6	51.2
G_{IIC} (J/m^2)	1739	2091

After obtaining the new G_{IC} and G_{IIC} values for the thermally aged EMC/Copper sample, the guidelines in Section 5.5 are followed to obtain the modified CZ parameters that accurately mimic the behavior of the EMC/Copper samples conditioned at 150°C. for 168hrs. Figure 7.12 shows the simulated load vs. displacement graph for EMC/Copper sample conditioned at 175°C. for 168hrs. at two different crack lengths.

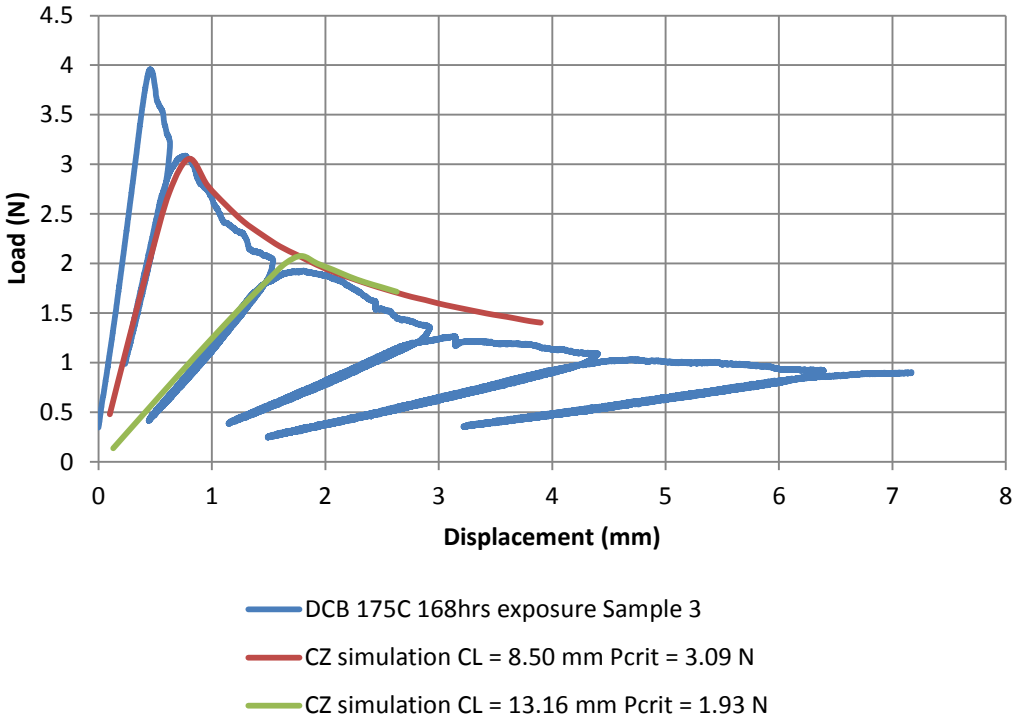

Figure 7.12 - DCB CZ simulation compared with experimental DCB data for EMC/Copper Sample thermally aged at 175°C for 168hrs

Like the previous CZ DCB simulation graphs the simulated load vs. displacement graph overpredicts the $P_{critical}$ value at which delamination occurs. The modified CZ parameters obtained for EMC/Copper samples thermally aged at 175°C for 168hrs are shown in Table 7.10. Figure 7.13 and Figure 7.14 show a plot of Mode I and Mode II

modified bilinear traction separation triangles for this thermally aged condition respectively.

Table 7.10 - CZ Parameters for EMC/copper sample thermally aged at 175°C for 168hrs

Traction Separation Laws 175C 168hrs		
	Mode I	**Mode II**
σ_{max} (MPa)	11.0	877
δ_c (µm)	9.34	4.77
δ* (µm)	0.934	0.477
G_C (J/m^2)	51.2	2091

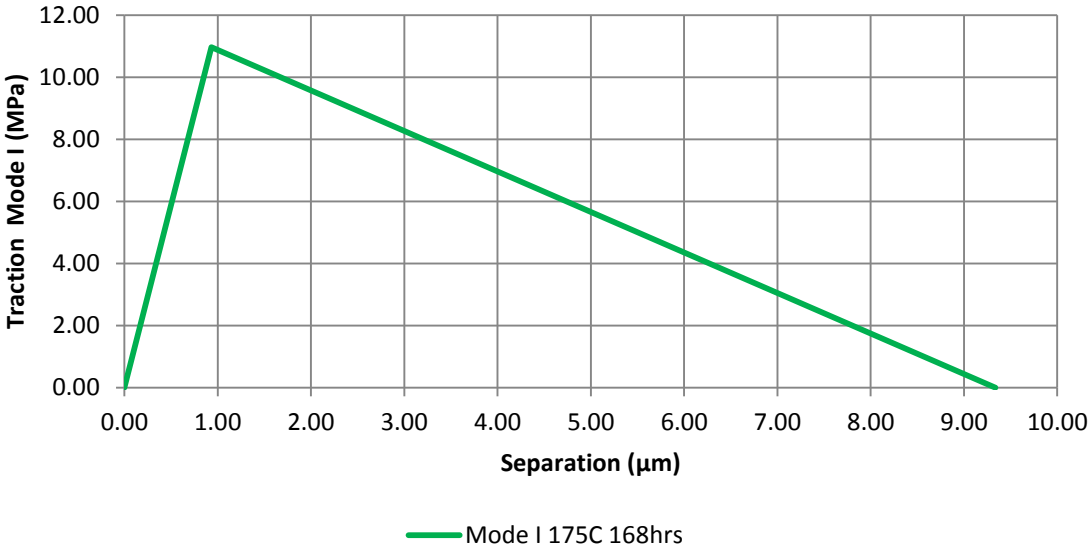

Figure 7.13 - Mode I CZ bilinear traction separation triangles for EMC/copper sample thermally aged at 175°C for 168hrs

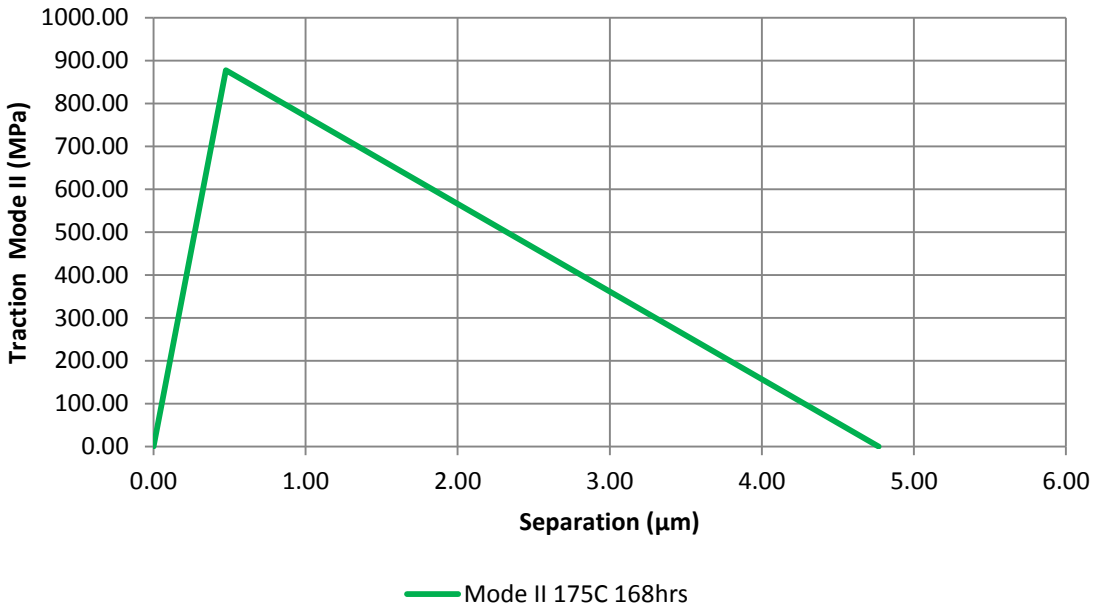

Figure 7.14 - Mode II CZ bilinear traction separation triangles for EMC/copper sample thermally aged at 175°C for 168hrs

7.3.5 CZ Parameters for EMC/Copper samples exposed to 175°C for 504hrs

The DCB G_c value for an EMC/Copper sample thermally aged at 175°C for 504hrs increases from an as-received G_c value of 45.1 J/m^2 to 49.6 J/m^2.This represents a 9.98% increase in G_c. Table 7.11shows the new G_{IC} and G_{IIC} values obtained after invoking this percentage drop on the as received G_{IC} and G_{IIC} values for the EMC/Copper sample.

Table 7.11- Modified G_{IC} and G_{IIC} values for EMC/copper sample thermally aged at 175°C for 504hrs

	As Received	175°C and 504hrs exposure
G_{IC} (J/m^2)	42.6	46.8
G_{IIC} (J/m^2)	1739	1912

After obtaining the new G_{IC} and G_{IIC} values for the thermally aged EMC/Copper sample, the guidelines in Section 5.5 are followed to obtain the modified CZ parameters that accurately mimic the behavior of the EMC/Copper samples conditioned at 175°C. for 504hrs. Figure 7.15 shows the simulated load vs. displacement graph for EMC/Copper sample conditioned at 175°C. for 504hrs. at two different crack lengths.

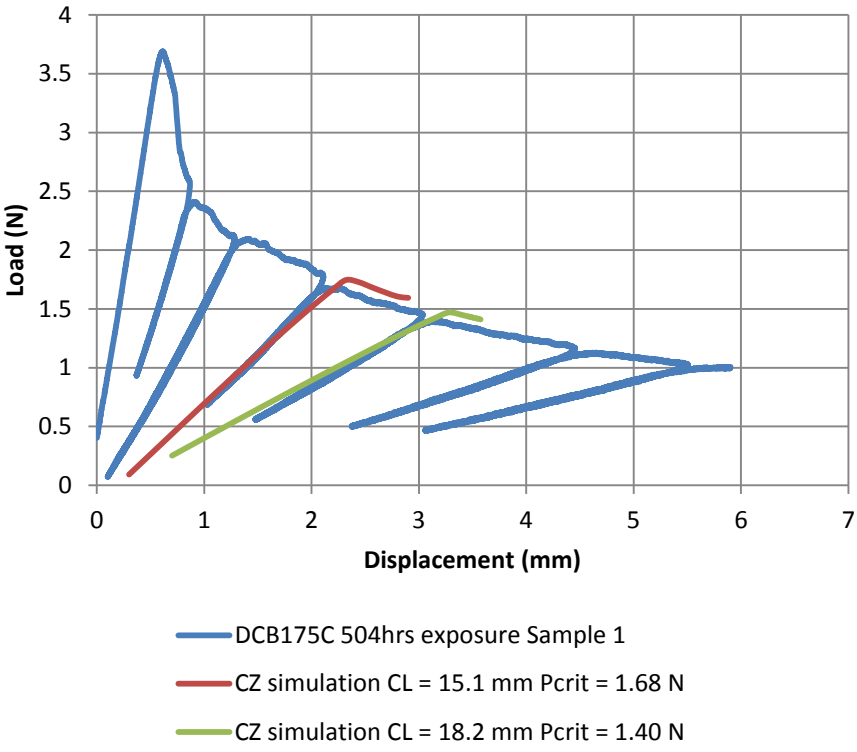

Figure 7.15 - DCB CZ simulation compared with experimental DCB data for EMC/copper sample thermally aged at 175°C for 504hrs

Like the previous CZ DCB simulation graphs the simulated load vs. displacement graph overpredicts the $P_{critical}$ value at which delamination occurs. The modified CZ parameters obtained for EMC/Copper samples thermally aged at 175°C for 504hrs are shown in Table 7.12. Figure 7.17 and Figure 7.17 show a plot of Mode I and Mode II

modified bilinear traction separation triangles for this thermally aged condition respectively.

Table 7.12 - CZ parameters for EMC/copper sample thermally aged at 175°C for 504hrs

Traction Separation Laws 175C 504hrs exposure		
	Mode I	**Mode II**
σ_{max} **(MPa)**	10.5	839
δ_c **(µm)**	8.93	4.56
δ* (µm)	0.893	0.456
G_C **(J/m^2)**	46.8	1913

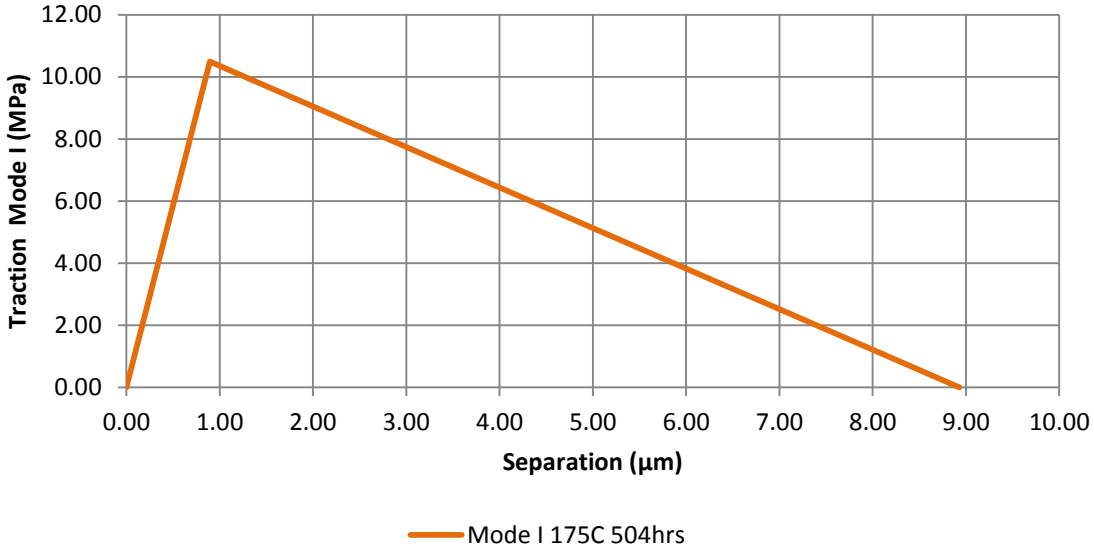

Figure 7.16 - Mode I CZ bilinear traction separation triangles for EMC/Copper Specimen thermally aged at 175°C for 504hrs

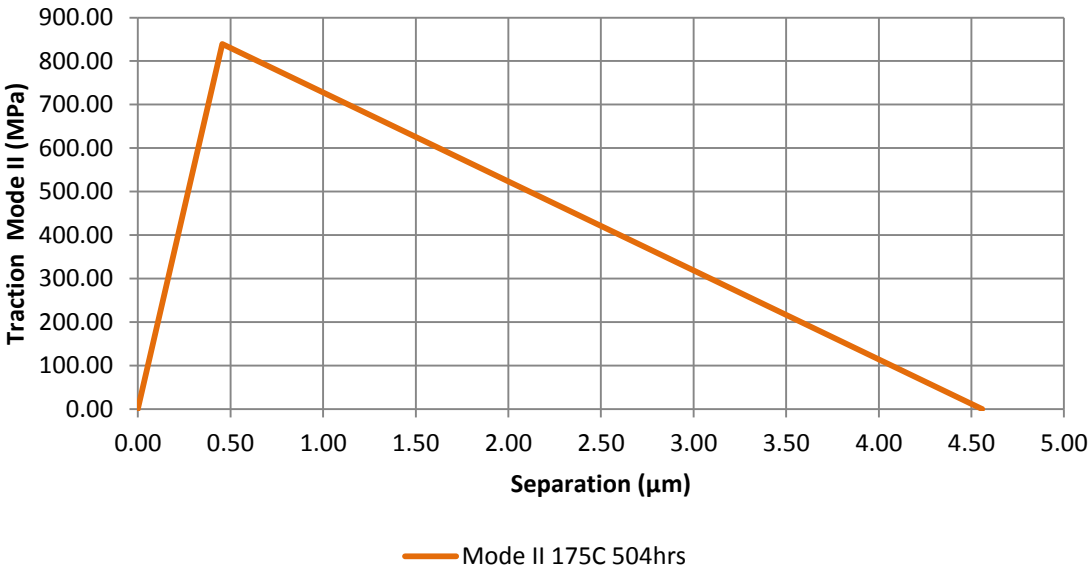

Figure 7.17- Mode I CZ bilinear traction separation triangles for EMC/copper sample thermally aged at 175°C for 504hrs

7.3.6 CZ Parameters for EMC/Copper samples exposed to 175°C for 1000hrs

The DCB G_c value for an EMC/Copper sample thermally aged at 175°C for 1000hrs drops from an as-received G_c value of 45.1 J/m^2 to 17.7 J/m^2.This represents a 60.7% drop in G_c. Table 7.13 shows the new G_{IC} and G_{IIC} values obtained after invoking this percentage drop on the as received G_{IC} and G_{IIC} values for the EMC/Copper sample.

Table 7.13 - Modified G_{IC} and G_{IIC} values for EMC/copper sample thermally aged at 175°C for 1000hrs

	As Received	175°C and 1000hrs exposure
G_{IC} (J/m^2)	42.6	16.7
G_{IIC} (J/m^2)	1739	684

After obtaining the new G_{IC} and G_{IIC} values for the thermally aged EMC/Copper sample, the guidelines in Section 5.5 are followed to obtain the modified CZ parameters

that accurately mimic the behavior of the EMC/Copper samples conditioned at 175°C. for 1000hrs. Figure 7.18 shows the simulated load vs. displacement graph for EMC/Copper sample conditioned at 175°C. for 1000hrs. at two different crack lengths.

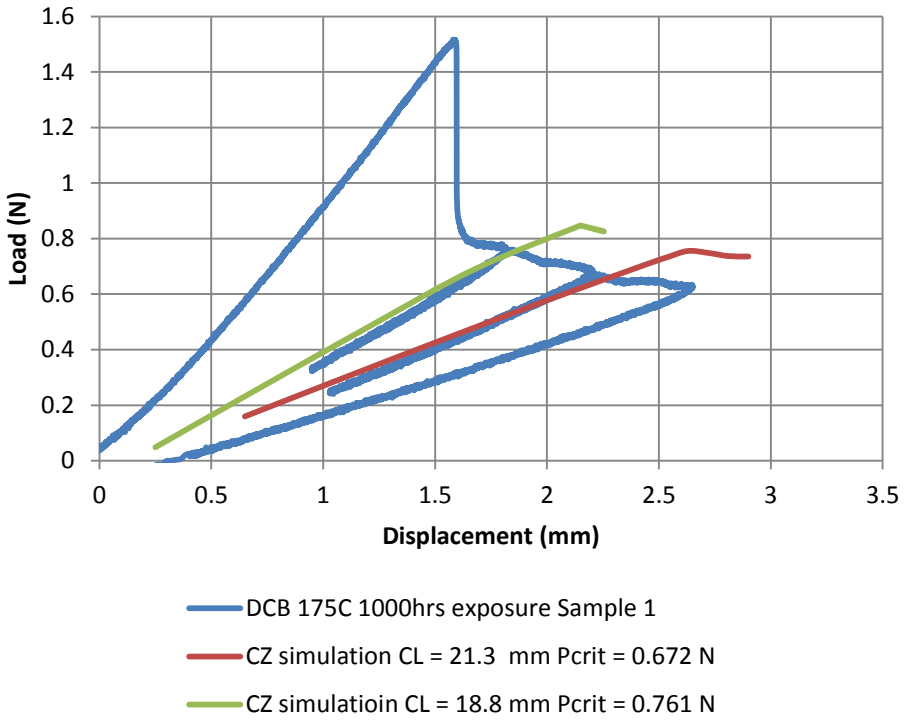

Figure 7.18 - DCB CZ simulation compared with experimental DCB data for EMC/copper sample thermally aged at 175°C for 504hrs

Like the previous CZ DCB simulation graphs the simulated load vs. displacement graph overpredicts the $P_{critical}$ value at which delamination occurs. The modified CZ parameters obtained for EMC/Copper samples thermally aged at 175°C for 1000hrs are shown in Table 7.14. Figure 7.19 and Figure 7.20 show a plot of Mode I and Mode II modified bilinear traction separation triangles for this thermally aged condition respectively.

Table 7.14 - CZ Parameters for EMC/copper sample thermally aged at 175°C for 1000hrs

Traction Separation Laws 175C 1000hrs exposure		
	Mode I	**Mode II**
σ_{max} (MPa)	6.27	502
δ_c (µm)	5.34	2.73
δ^* (µm)	0.534	0.273
G_C (J/m^2)	16.7	684

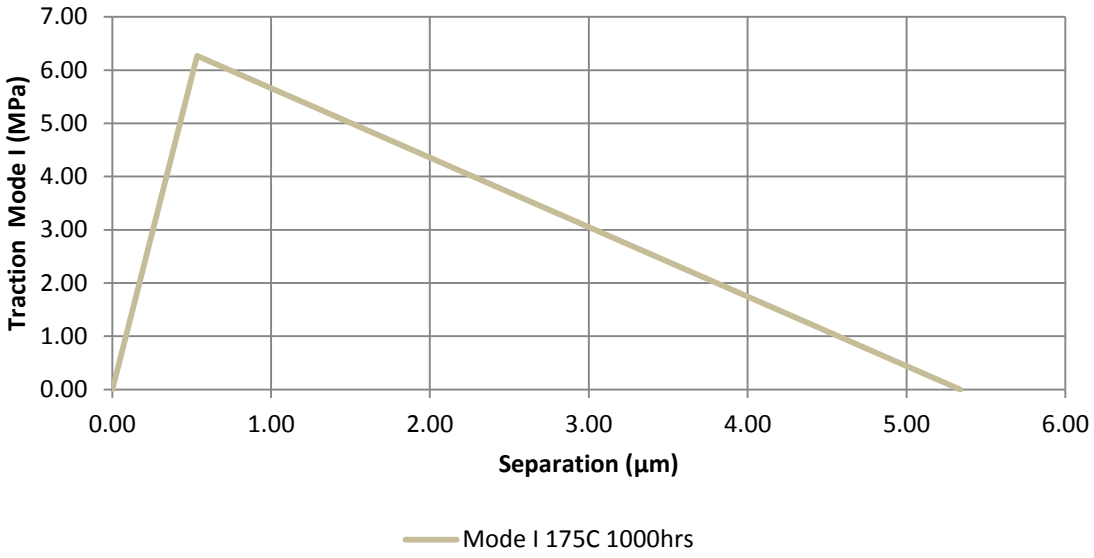

Figure 7.19- Mode I CZ bilinear traction separation triangles for EMC/copper sample thermally aged at 175°C for 1000hrs

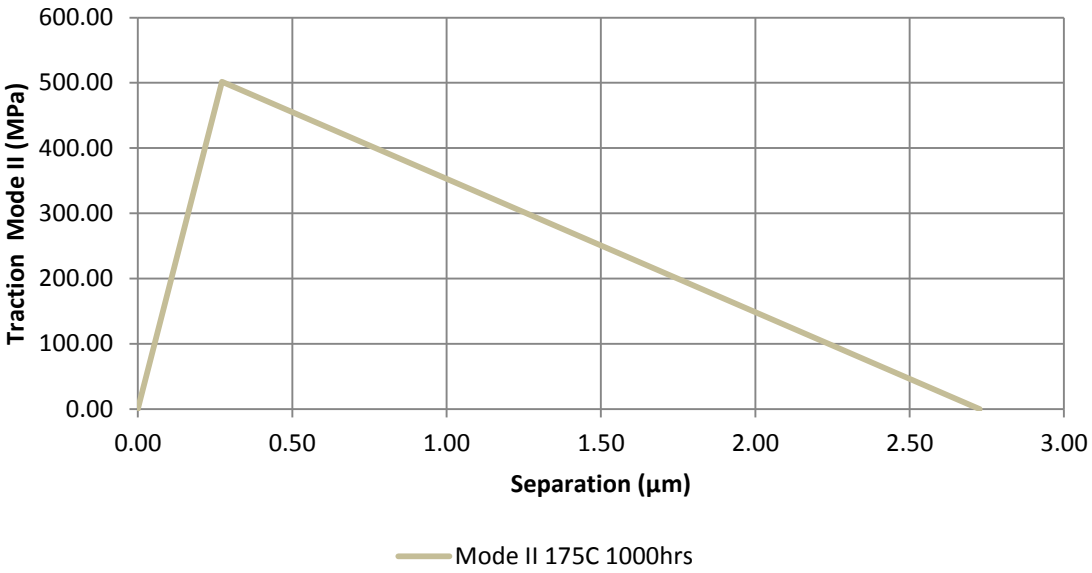

Figure 7.20 - Mode II CZ bilinear traction separation triangles for EMC/copper sample thermally aged at 175°C for 1000hrs

7.4 Discussion of the modified CZ Parameters obtained after thermally aging EMC/Copper samples.

Figure 7.21 and Figure 7.22 show the as received and modified Mode I and Mode II CZ bi-linear traction triangles obtained after thermally aging the EMC/Copper at 150°C for 168hrs, 504hrs and 1000hrs. There isn't much change in the CZ triangles after thermally aging the EMC/Copper sample at 150°C for 168hrs and 504hrs since there isn't much change in the interfacial adhesion at these conditions. Similar to the modified CZ triangles obtained for humidity conditioned EMC/Copper samples, the loss in adhesion seen at 150°C and 1000hrs is represented by a reduction in σ_{max} and δ_c of the as-received Mode I and Mode II CZ bi-linear traction triangles.

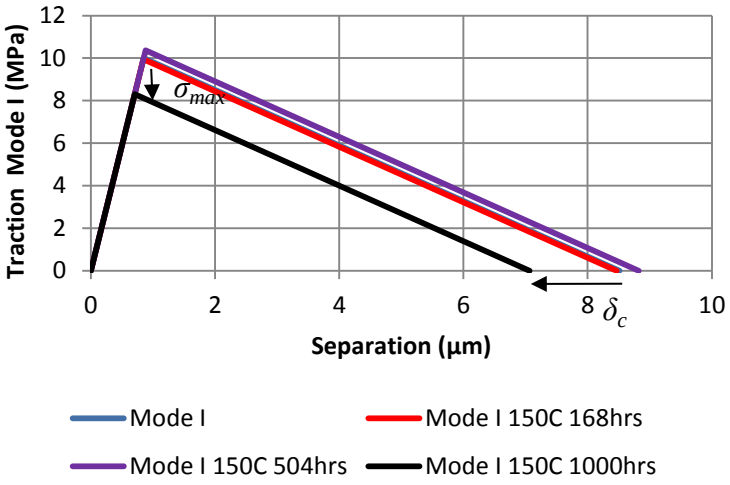

Figure 7.21 – Mode I CZ bilinear traction separation triangles for EMC/copper sample thermally aged at 150°C for 168hrs, 504hrs and 1000hrs

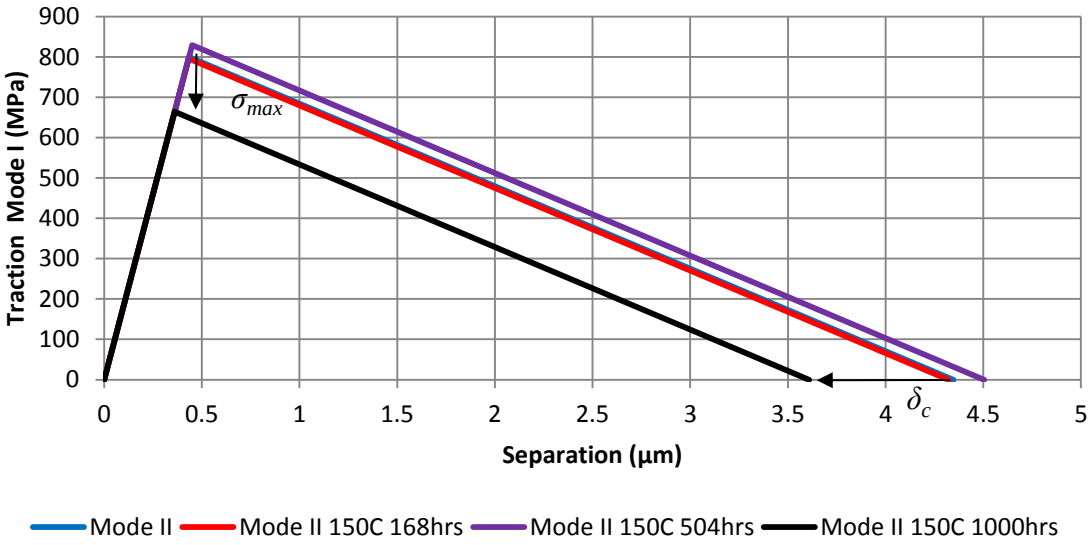

Figure 7.22 - Mode II CZ bilinear traction separation triangles for EMC/copper sample thermally aged at 150°C for 168hrs, 504hrs and 1000hrs

Figure 7.23 and Figure 7.24 show as received and modified Mode I and Mode II CZ bi-linear traction triangles obtained after thermally aging the EMC/Copper at 175°C for 168hrs, 504hrs and 1000hrs. There isn't much change in the CZ triangles after thermally

aging the EMC/Copper sample at 175°C for 168hrs and 504hrs since there isn't a loss in the interfacial adhesion at these conditions. There is an even greater loss in interfacial adhesion after thermally aging the EMC/Copper sample at 175°C for 1000hrs compared to the G_c value obtained after conditioning at 150°C for 1000hrs. This loss in interfacial strength is also represented by a reduction in as received Mode I and Mode II σ_{max} and δ_c CZ parameters.

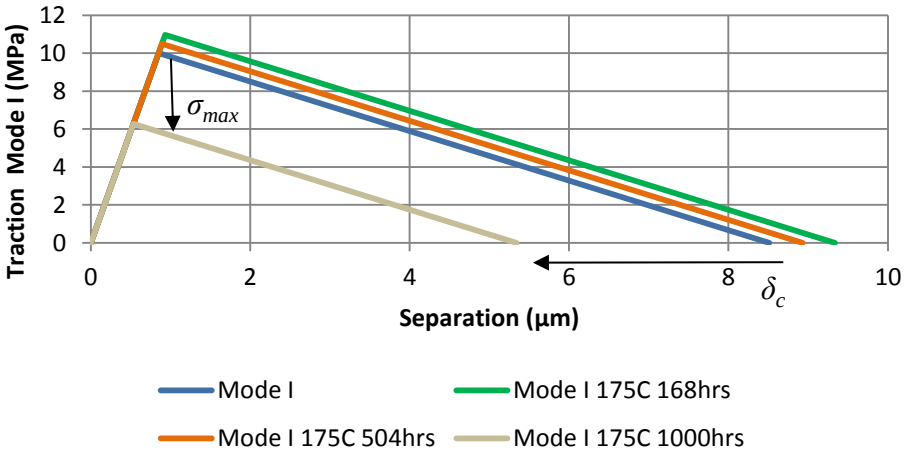

Figure 7.23 - Mode I CZ bilinear traction separation triangles for EMC/copper sample thermally aged at 175°C for 168hrs, 504hrs and 1000hrs

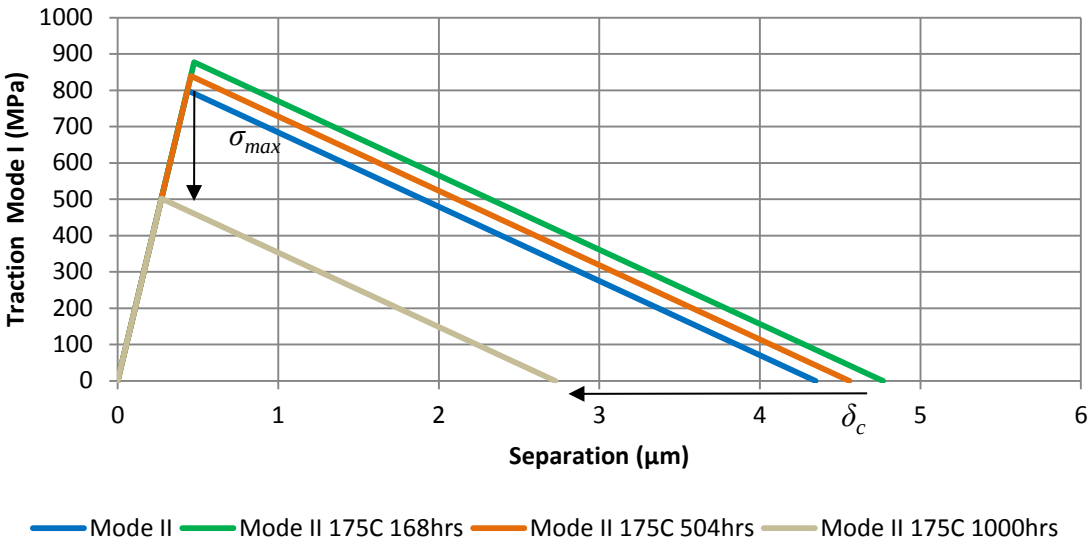

Figure 7.24 - Mode II CZ bilinear traction separation triangles for EMC/copper sample thermally aged at 175°C for 168hrs, 504hrs and 1000hrs

CHAPTER 8. CONCLUSIONS AND FUTURE WORK

The primary objective of this work was to develop mixed-mode CZ parameters that model the interfacial strength of thermally aged and humidity conditioned EMC/Copper samples.

DCB and FPB tests were conducted on EMC/Copper samples. Using the load vs. displacement data obtained from these tests, the critical SERR and mode mixity, ψ for each geometry was computed using FEM and analytical solutions. The Hutchinson and Suo [27] relationship was used to characterize the critical SERR as a function of ψ for an as-received EMC/Copper sample. Using this relationship, Mode I and Mode II CZ parameters were obtained by fitting the simulated load vs. displacement graphs obtained from FEM software with experimental load vs. displacement data from DCB and FPB tests. Isothermal aging and humidity conditioning tests were run on EMC/Copper samples based on stress test qualifications for packaged integrated circuits used by industry [45]. DCB tests were run on EMC/Coppers samples after thermal aging and humidity conditioning exposure. Modified Mode I and Mode II CZ Parameters were formulated by fitting simulated load vs. displacement graphs with experimental load vs. displacement data obtained by running DCB tests on thermally aged and humidity conditioned EMC/Copper samples. The following conclusions can be made from this study

8.1 G_c vs. mode mixity, ψ relationship for EMC/Copper interface

Using DCB and FPB tests, the interfacial strength of the EMC/Copper sample was characterized for two different loading conditions. The mode mixity of each loading condition was calculated using the crack-displacement method by Matos et al. [28]. The mode mixity obtained for the DCB test was 29.4°, whereas the mode mixity for the FPB test was 35.7°. Since, the mode mixities for both tests are so close to each other, more G_c values need to be experimentally determined at other mode mixities to get a stronger G_c vs. mode mixity, ψ fit for the EMC/Copper interface. Future work should look at developing and investigating fracture tests that characterize the interfacial strength of the EMC/Copper sample for mode mixities other than the ones discussed in this thesis.

8.2 Effect of humidity conditioning and thermal aging on EMC/Copper interface strength

Humidity conditioning tests were conducted on the EMC/Copper sample at 60% R.H and 30°C for 192hrs, 85% R.H and 110°C for 264hrs and 528hrs and 85% R.H and 130°C for 96hrs and 192hrs. Humidity conditioning at 60% R.H and 30°C for 192hrs revealed no loss in interfacial adhesion. Conditioning at 85% R.H and 110°C for 264hrs resulted in a 44.3% loss in the interfacial adhesion of the EMC/Copper sample. Increasing the duration of humidity exposure to 528hrs seemed to have minimal effect on the already reduced interfacial strength of the EMC/Copper sample.

Furthermore, conditioning at 85% R.H and 130°C for 96hrs resulted in a 61.0% reduction of the EMC/Copper interfacial strength. This showed that increasing the temperature from 110°C to 130°C further weakened the EMC/Copper interfacial adhesion. Increasing the duration of the humidity exposure to 192hrs for this humidity

condition also seemed to have minimal effect on the already reduced interfacial strength of the EMC/Copper sample.

The following conclusions can be made from the humidity conditioning tests conducted on the EMC/Copper sample.

1. 60% R.H at 30°C humidity exposure does not seem to affect the interfacial strength of the EMC/Copper sample.
2. Increasing the humidity exposure level to 85% R.H. at 110°C results in a reduction in the interfacial strength of the EMC/Copper sample.
3. Humidity conditioning tests at temperatures close to the glass transition temperature of the EMC have an effect on the interfacial adhesion since increasing the temperature from 110°C to 130°C at 85% R.H further weakened the EMC/Copper interfacial strength.
4. Interfacial adhesion of the EMC/Copper sample seems to be unaffected by humidity exposure at longer durations. For both humidity condition tests that were conducted, the interfacial strength of the EMC/Copper sample did not change when the exposure time was doubled.

Thermal aging tests were conducted on the EMC/Copper sample at 150°C and 175°C for 168hrs, 504hrs and 1000hrs. The results showed that the interfacial adhesion of the EMC/Copper sample was unaffected at temperatures of 150°C and 175°C after exposure for 168hrs and 504hrs. A significant decrease in the interfacial strength of the EMC/Copper sample was seen after aging for 1000hrs at both these temperatures. There is a 35.5 % loss in the interfacial adhesion of the EMC/Copper sample from its as-

received value after thermal aging at 150°C for 1000hrs. There is a 58.8% loss in the interfacial adhesion of the EMC/Copper sample from its as-received value after thermal aging at 175°C for 1000hrs. The main conclusion that can be made from these tests is that for temperature conditioning at 150°C and 175°C permanent degradation is only seen at the EMC/Copper interface for longer durations in excess of a 1000hrs.

8.3 Determination of As-Received and modified CZ Parameters

8.3.1 As-Received CZ Parameters

CZ Parameters were successfully obtained for as-received, thermally aged and humidity conditioned copper/EMC samples. The G_c vs. mode mixity, ψ fit over-predicted the DCB critical SERR value and under-predicted the FPB value. Consequently, CZ parameters showed a good fit between simulated and experimental load vs. displacement data but over-predicted the critical delamination load value for DCB tests and under-predicted this value for FPB tests. The initial loading slope prior to delamination for the simulated load vs. displacement graph and the experimental data showed a good fit for both tests.

8.3.2 Modified CZ Parameters

Modified CZ Parameters were obtained to model the interfacial strength of the humidity conditioned and thermally aged EMC/Copper samples. The simulated graphs obtained from the modified CZ parameters over-predicted the critical delamination load when compared with the experimental data, similar to the as-received simulation graphs. Like the as-received CZ graphs, the initial slope of the simulated load vs. displacement

graphs for the modified CZ parameters matched the slope of the experimental load vs. displacement graphs. A loss in interfacial adhesion in the EMC/Copper sample is represented by a reduction in the maximum interfacial traction, σ_{max} and the maximum interfacial separation, δ_c for both Mode I and Mode II as-received CZ parameters. This is seen for all modified CZ parameters obtained for humidity conditioned and thermally aged EMC/Copper samples that show a significant loss in interfacial strength.

These modified CZ parameters can be used in EMC/Copper interfaces present in flip chip packages, 3-D IC packages, SOIC packages and multichip modules to keep track of the damage incurred at the interface. Interfacial damage and debonding due to accelerated stress life tests and qualifications in packages with EMC/Copper interfaces can be modeled with these modified CZ parameters.

8.4 Future Work

Future work on the effect of isothermal aging and humidity conditioning on EMC/Copper mold compound interfacial adhesion and the modified CZ parameters will be done with the following next steps in mind.

1. FPB tests and other fracture mechanics tests will be conducted on as-received, thermally aged and humidity conditioned EMC/Copper samples to obtain a better G_c vs. mode mixity, ψ fit for the interface. By doing so, the CZ parameters obtained will better match the experimental load vs. displacement data obtained.
2. Studies by Ferguson and Qu [9] showed that the Young's modulus of the EMC, E_{EMC} is affected by moisture exposure. Future work will investigate the change in the E_{EMC} after humidity conditioning tests. An updated mode mixity for DCB and

FPB geometries can be evaluated using the new $E_{EMC.}$ This value can be used to obtain a new Hutchinson and Suo[27] fit for the geometry as well the updated CZ parameters.

3. Future studies will also investigate the effect of stress relaxation and creep on the EMC due to thermal aging. E_{EMC} will be computed as a function of time at different temperatures and this information will be used to generate a master stress relaxation curve and prony series for the EMC. A viscoelastic material model for the EMC can be created with this information and be used to calculate the effect of both temperature and time on the E_{EMC}. Stress relaxation and creep effects should have an effect on the E_{EMC} especially at longer durations (1000hrs). The new E_{EMC} and G_c value obtained from this study can be used to obtain updated CZ parameters for the thermally aged EMC/Copper samples.
4. Future work will also investigate the crack front shape. Visual inspections of thermally-aged copper leadframe surfaces reveal a straight crack front that is curved on the edges. At the edges, the sample experiences stress tri-axiality as the width of the sample is not large enough to obey the plain strain criterion. As the width increases, the sample obeys the plain strain criterion in the middle of the sample where the crack front is flat or straight. Three-dimensional FE analysis of the interfacial strength at the crack front will be investigated in future studies. C-Mode Scanning Acoustic Microscopy (C-SAM) imaging will also be used in addition to visual inspection to investigate the shape of the crack-front of the EMC/Copper sample during future delamination and debonding studies.

5. Future studies will also investigate how sub-critical loading as a function of time affects the interfacial strength of the EMC/Copper sample for different interfacial fracture experiments including DCB and FPB testing. Samples will be loaded and held with a sub-critical load prior to any delamination. Displacement-controlled experiments will be carried out, the change in the force will be investigated as a function of time.
6. As discussed earlier, existing literature[9] shows that the copper oxide formation during thermal aging leads to the displacement of the EMC at the interface resulting in a loss in interfacial strength. Thermal aging studies will be conducted in a nitrogen, N_2 (inert) chamber to investigate whether or not the formation of copper oxide is a driver for the loss in interfacial strength.
7. Preliminary X-ray Photoelectron Spectroscopy (XPS) studies were conducted on copper leadframe surface to investigate the copper oxide deposition. Future work will perform XPS studies and depth profile measurements to investigate the type of oxide and the thickness of oxide after thermally aging the EMC/Copper samples for different durations.
8. Future work will also investigate the effect of adding an adhesion promoter at the EMC/Copper interface and how that enhances the interfacial strength of the sample.

APPENDIX A. EXPERIMENTAL LOAD VS. DISPLACEMENT GRAPHS OBTAINED FOR AS-RECEIVED, THERMALY AGED AND HUMIDITY CONDITIONED EMC/COPPER SAMPLES

This appendix illustrates the experimental load vs. displacement graphs obtained for DCB tests conducted on as-received, thermally aged and humidity conditioned EMC/Copper samples.

A.1 As-Received DCB data

The following figures illustrate the experimental load vs. displacement graphs obtained from DCB tests conducted on as-received EMC/Copper samples.

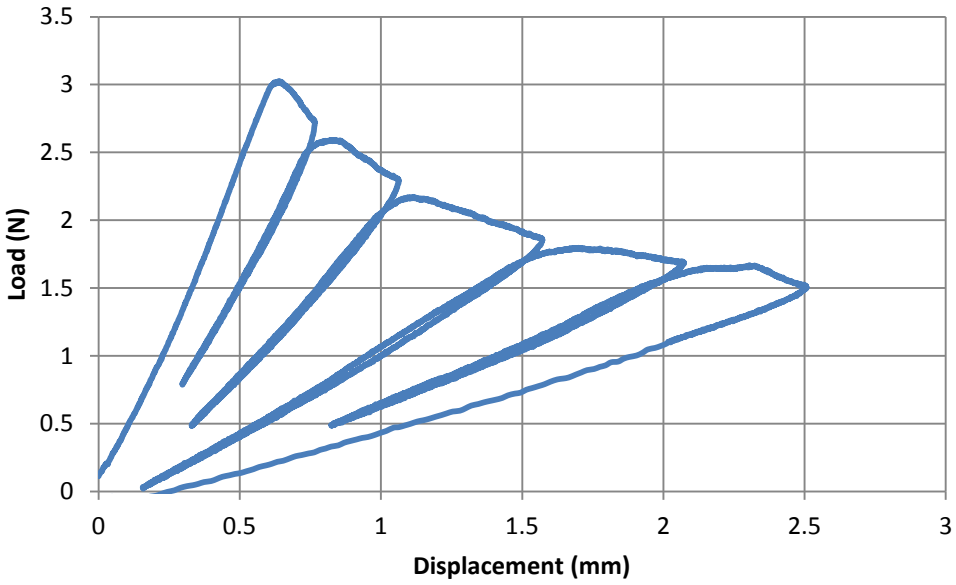

Figure A.1 – Experimental load vs. displacement data as-received EMC/copper sample 1

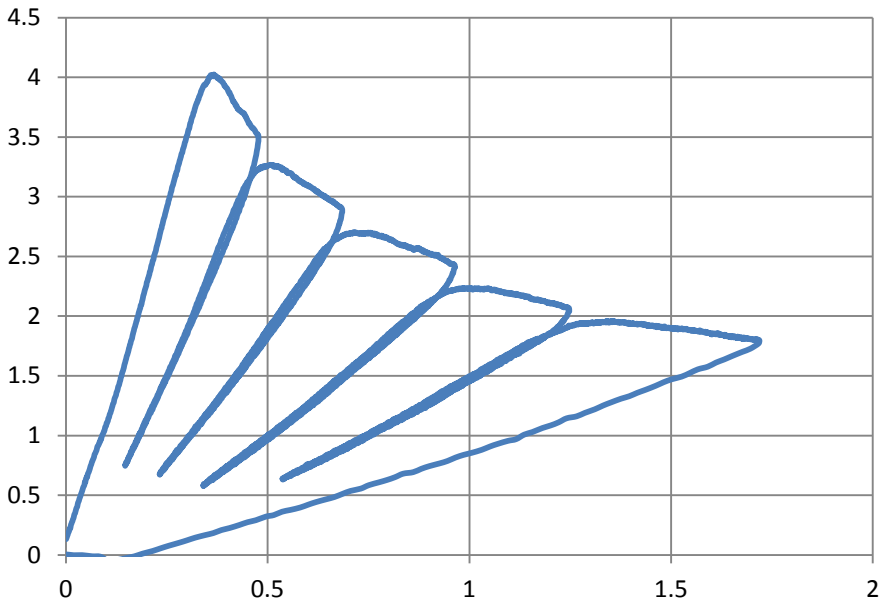

Figure A.2 - Experimental load vs. displacement data as-received EMC/copper sample 2

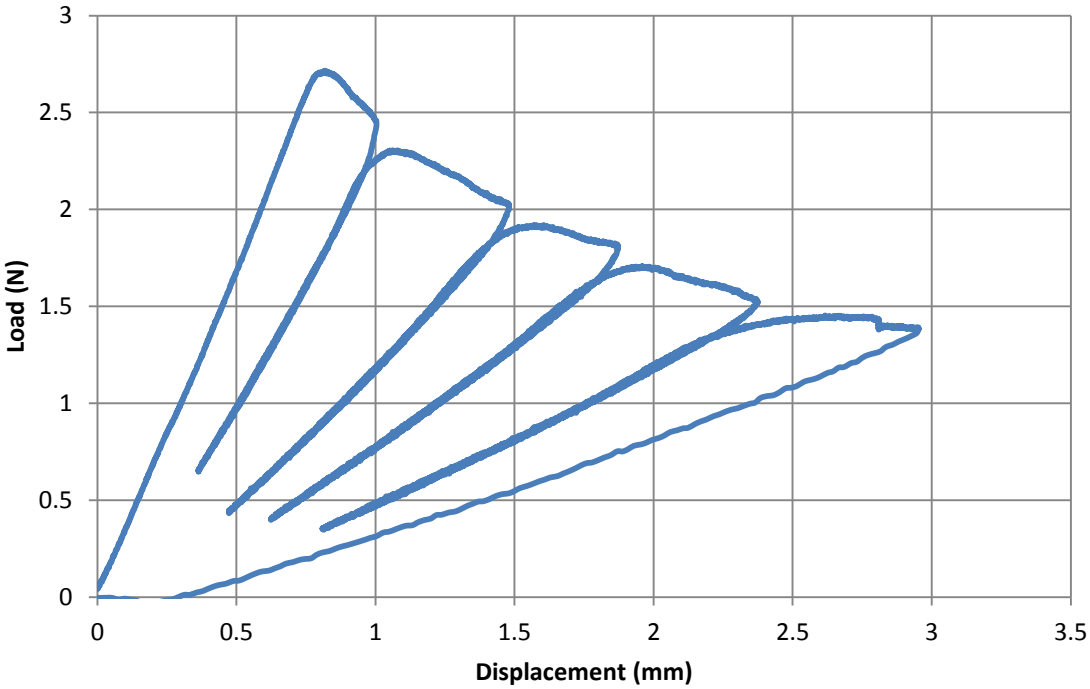

Figure A.3 - Experimental load vs. displacement data as-received EMC/copper sample 3

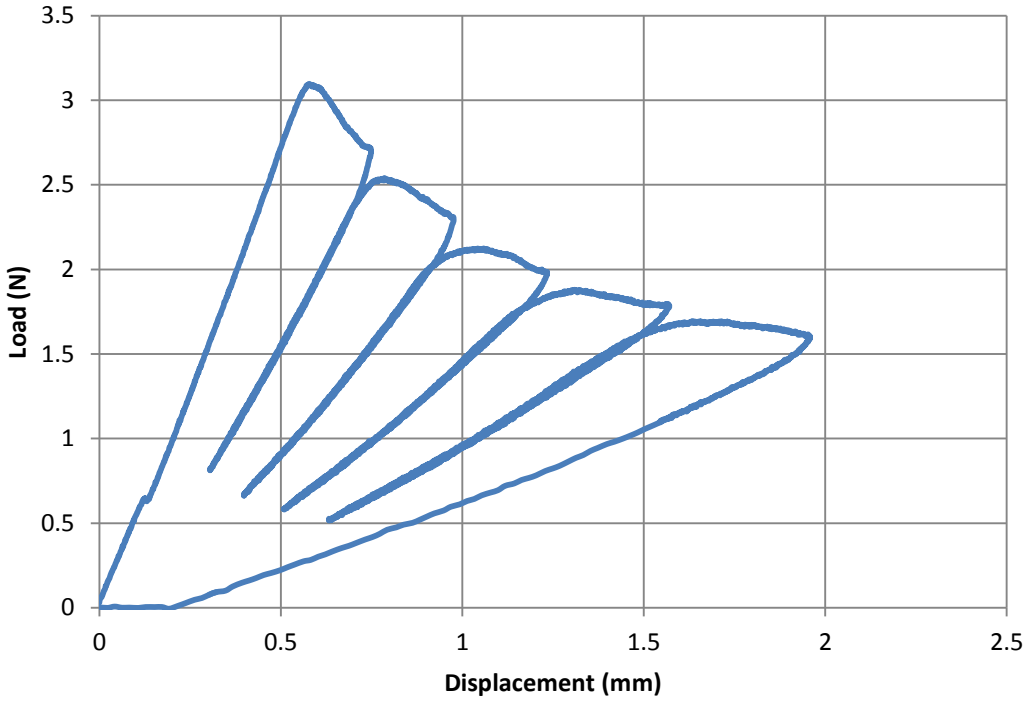

Figure A.4 - Experimental load vs. displacement data as-received EMC/copper sample 4

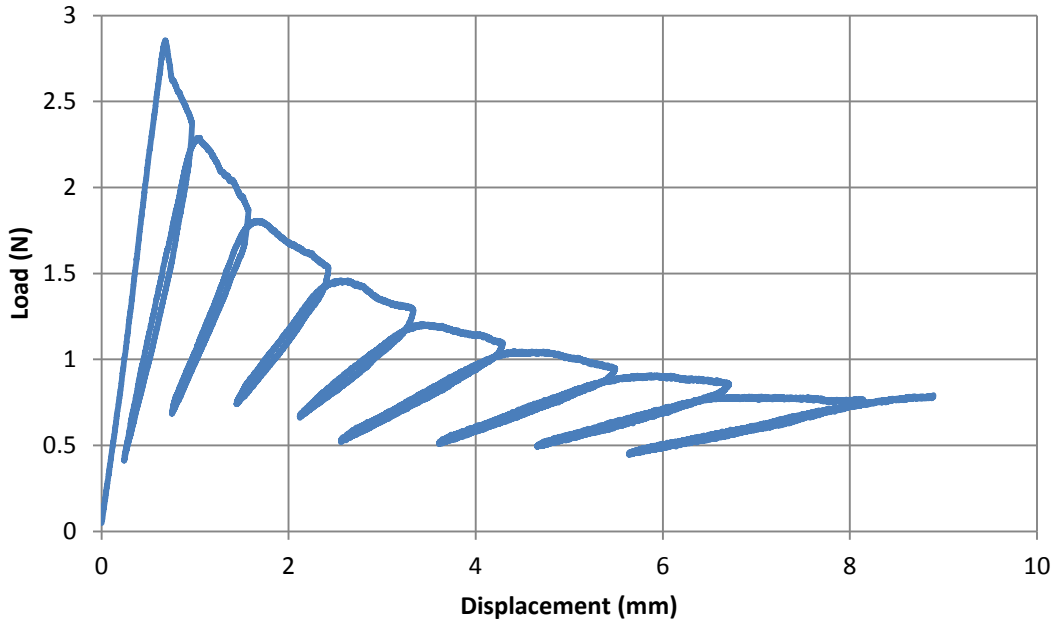

Figure A.5 - Experimental load vs. displacement data as-received EMC/copper sample 5

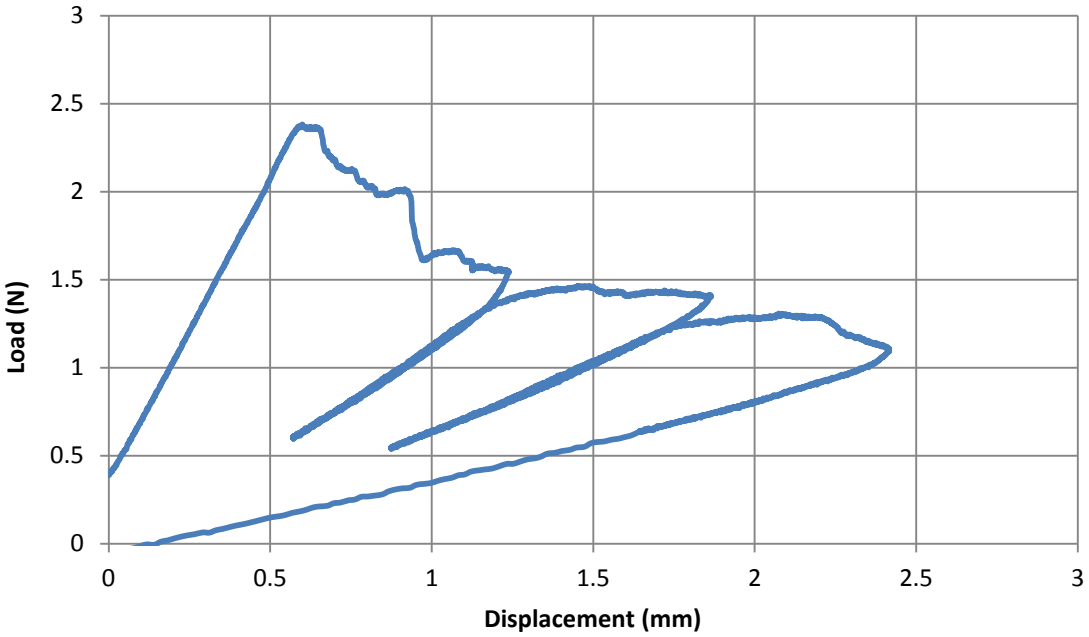

Figure A.6 - Experimental load vs. displacement data as-received EMC/copper sample 6

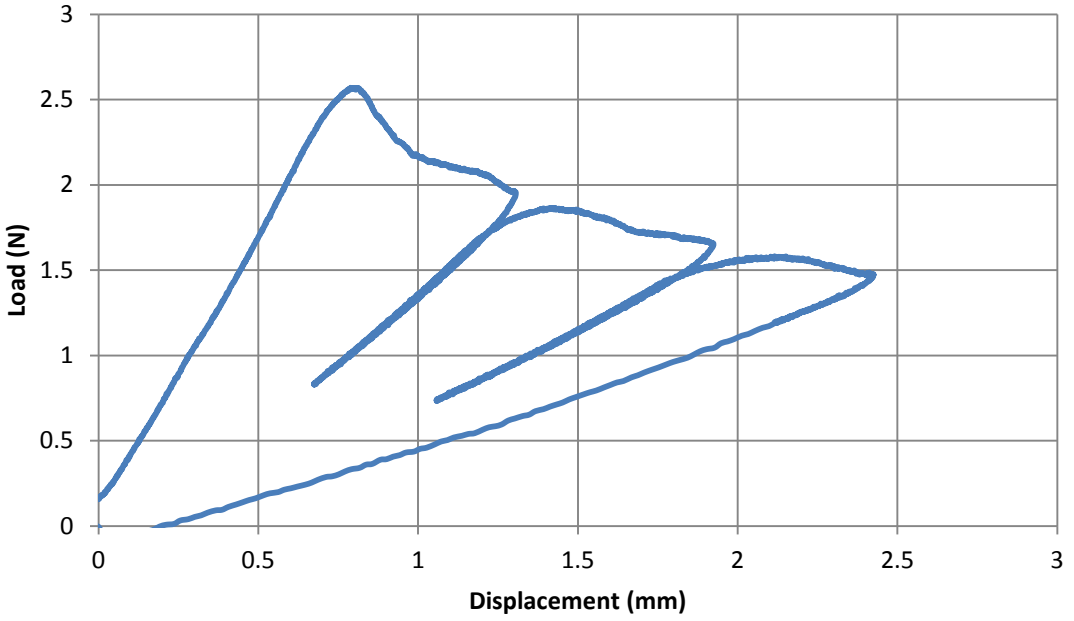

Figure A.7 - Experimental load vs. displacement data as-received EMC/copper sample 7

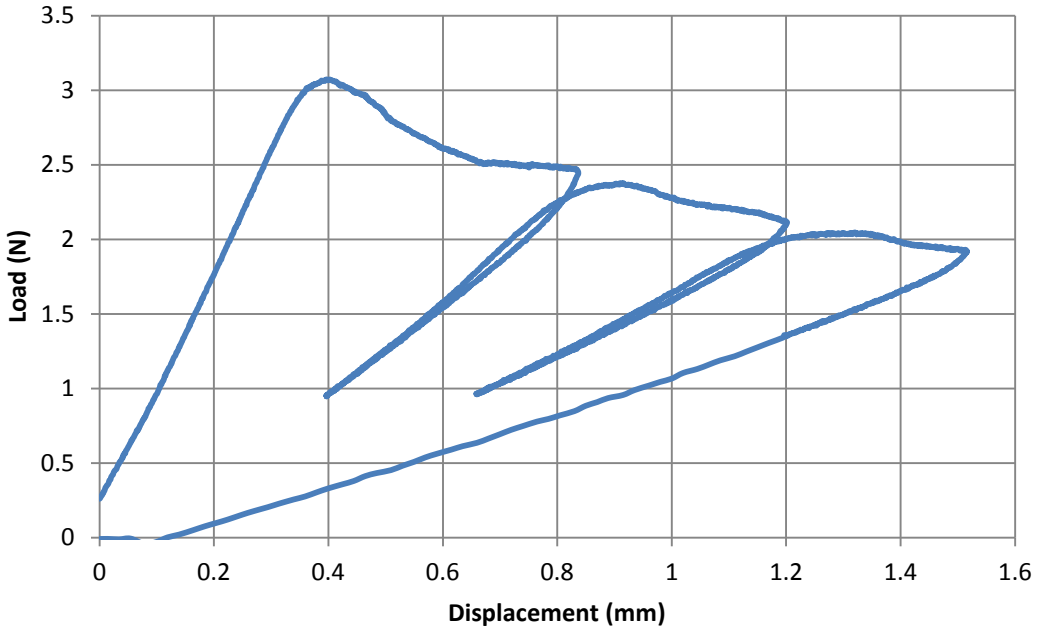

Figure A.8 - Experimental load vs. displacement data as-received EMC/copper sample 8

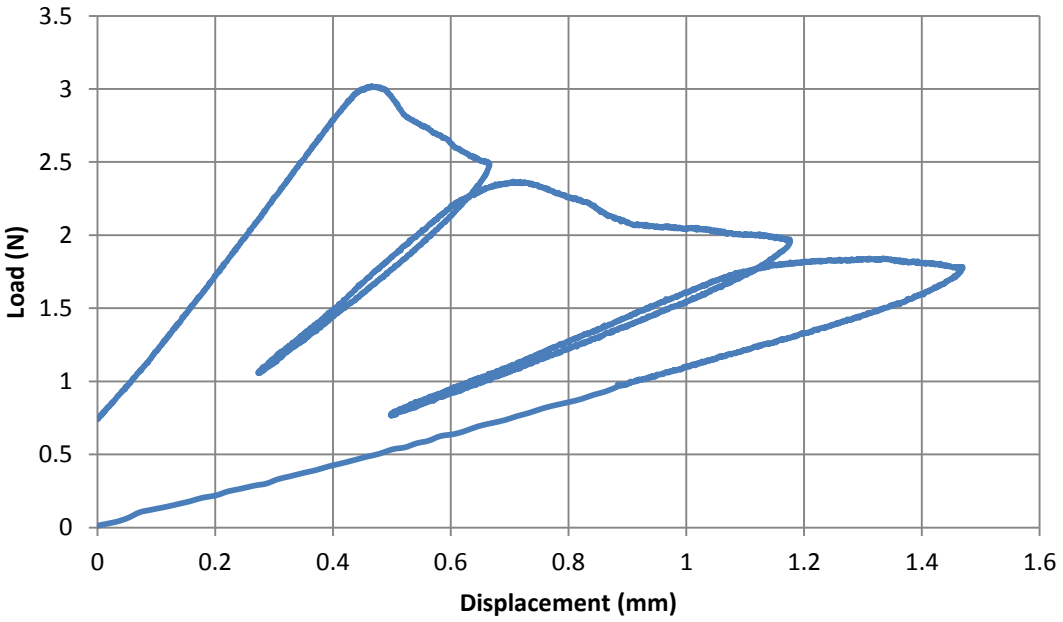

Figure A.9 - Experimental load vs. displacement data as-received EMC/copper sample 9

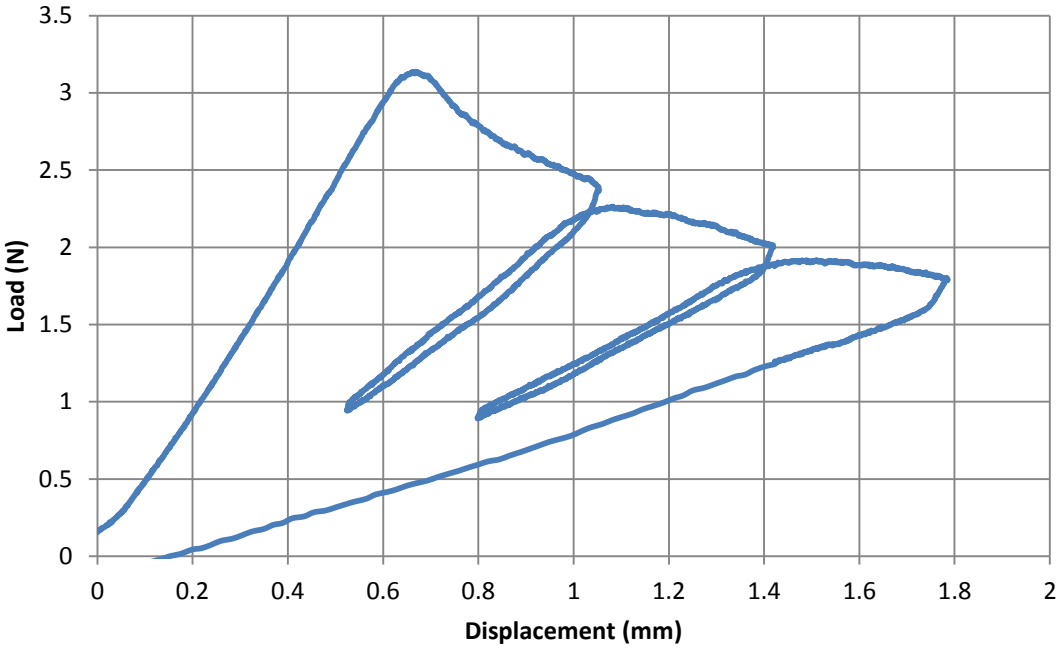

Figure A.10 - Experimental load vs. displacement data as-received EMC/copper sample 10

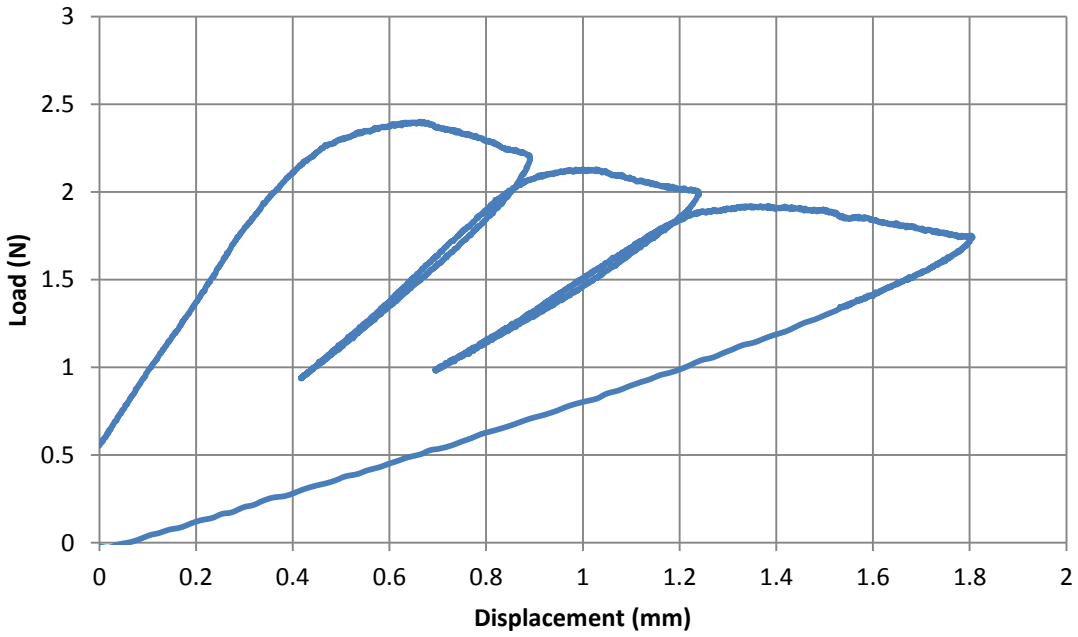

Figure A.11- Experimental load vs. displacement data as-received EMC/copper sample 11

A.2 Humidity conditioned DCB data

The following figures illustrate the experimental load vs. displacement graphs obtained from DCB tests conducted on humidity conditioned EMC/Copper samples.

A.2.1 DCB data for EMC/Copper samples humidity conditioned at 60%R.H & 30°C for 192hrs

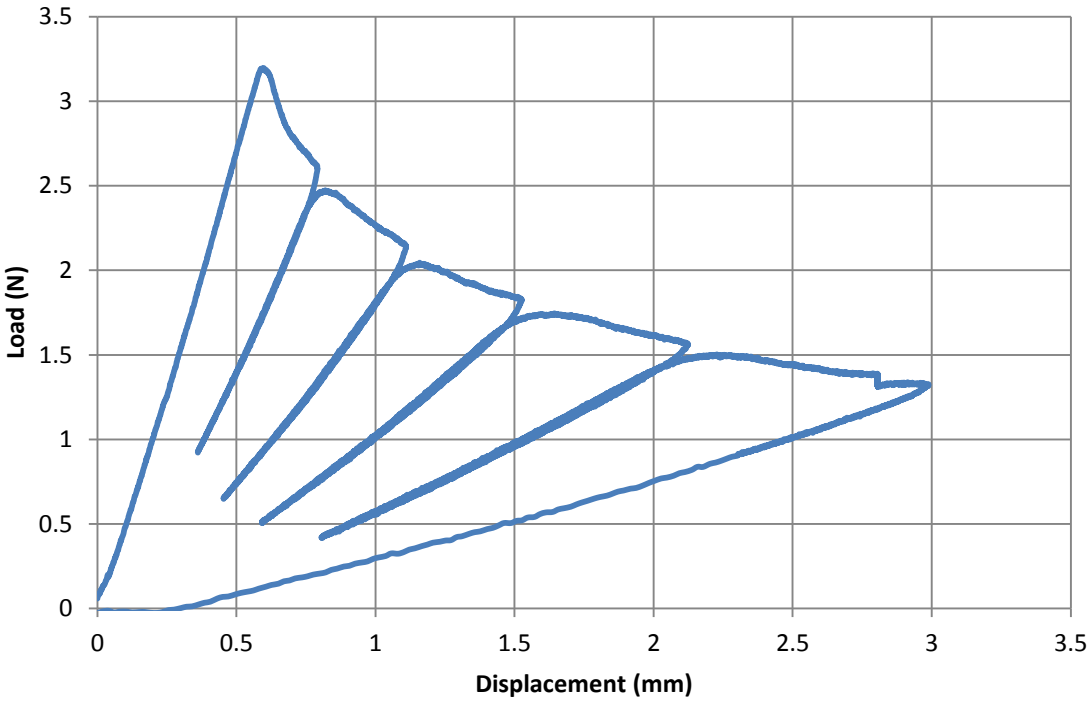

Figure A.12 - Experimental load vs. displacement data for EMC/copper sample conditioned at 60%R.H. & 30°C for 192hrs, sample 1

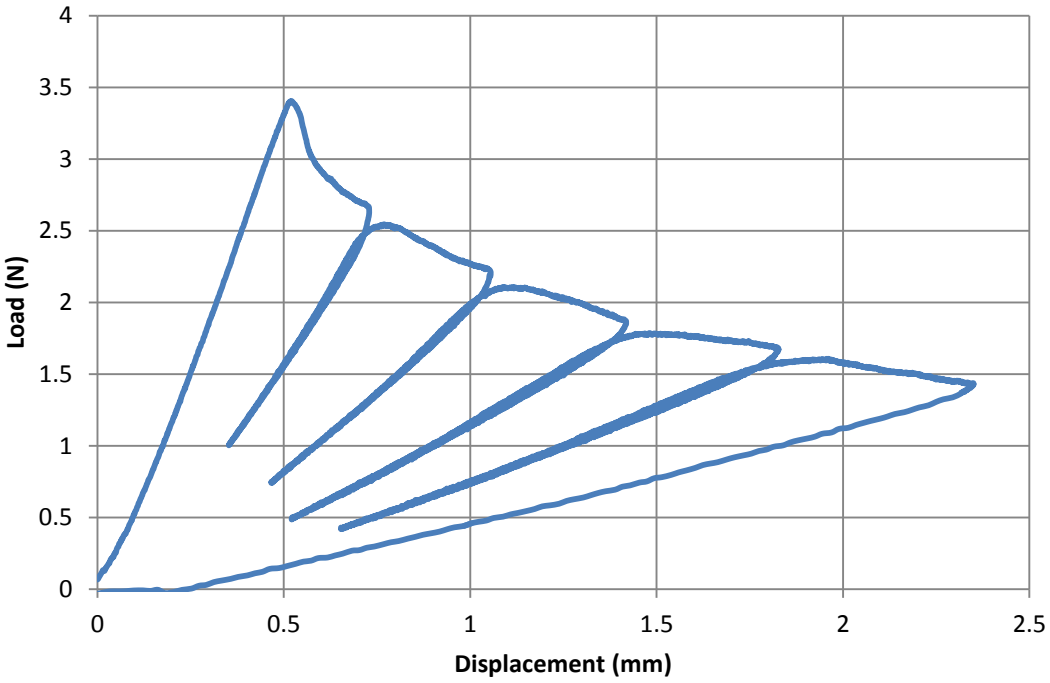

Figure A.13 - Experimental load vs. displacement data for EMC/copper sample conditioned at 60%R.H. & 30°C for 192hrs, sample 2

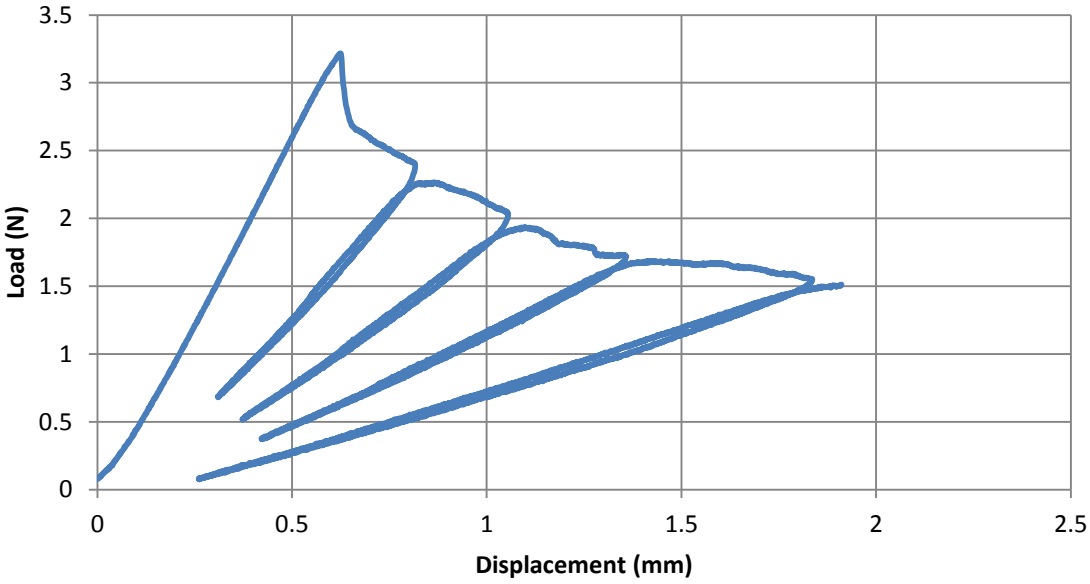

Figure A.14- Experimental load vs. displacement data for EMC/copper sample conditioned at 60%R.H. & 30°C for 192hrs, sample 3

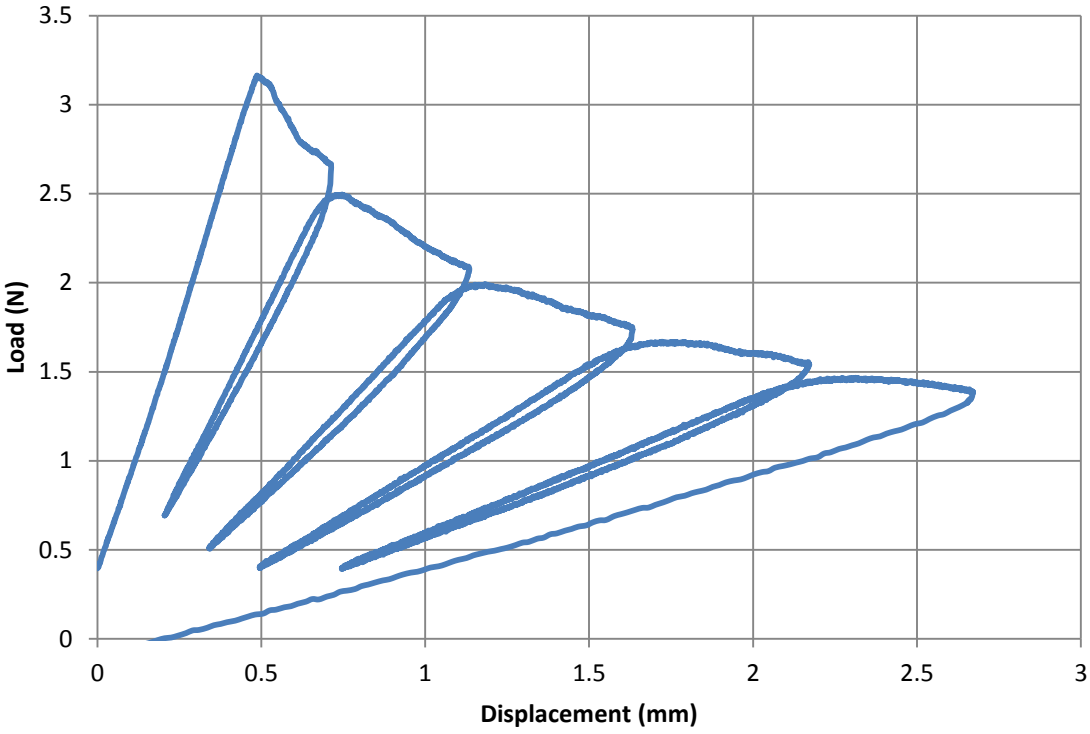

Figure A.15 - Experimental load vs. displacement data for EMC/copper sample conditioned at 60%R.H. & 30°C for 192hrs, sample 4

A.2.2 DCB data for EMC/Copper samples humidity conditioned at 85%R.H & 110°C for 264hrs

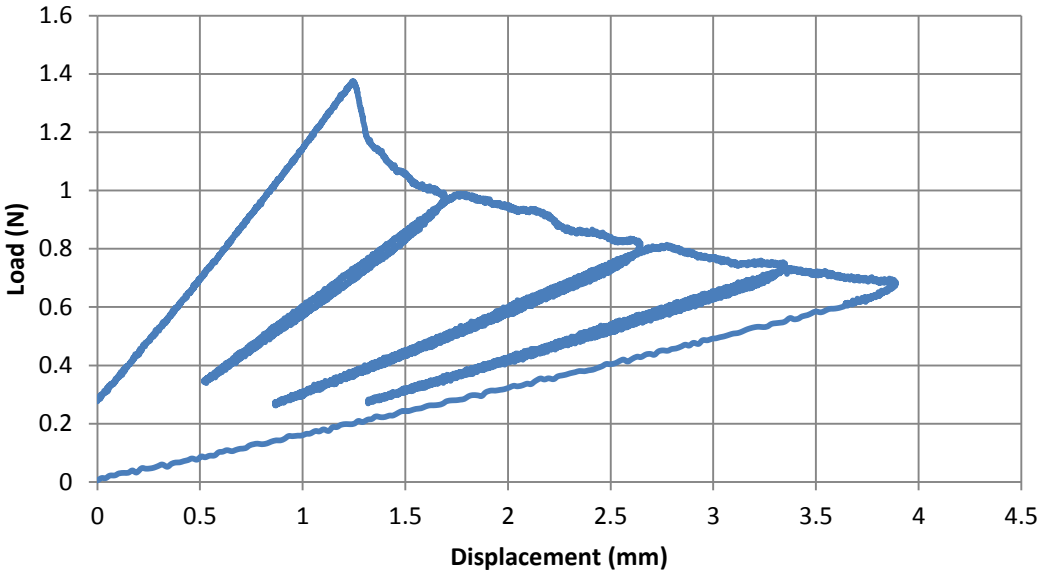

Figure A.16 - Experimental load vs. displacement data for EMC/copper sample conditioned at 85%R.H. & 110°C for 264hrs, sample 1

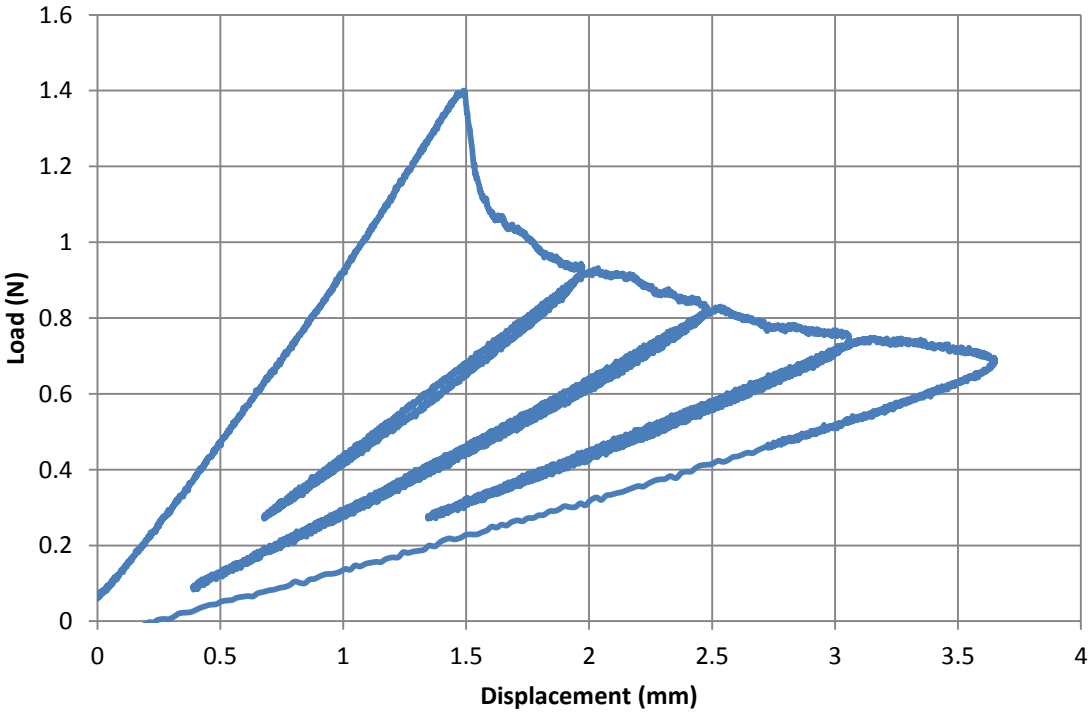

Figure A.17 - Experimental load vs. displacement data for EMC/copper sample conditioned at 85%R.H. & 110°C for 264hrs, sample 2

A.2.3 DCB data for EMC/Copper samples humidity conditioned at 85%R.H & 110°C for 528hrs

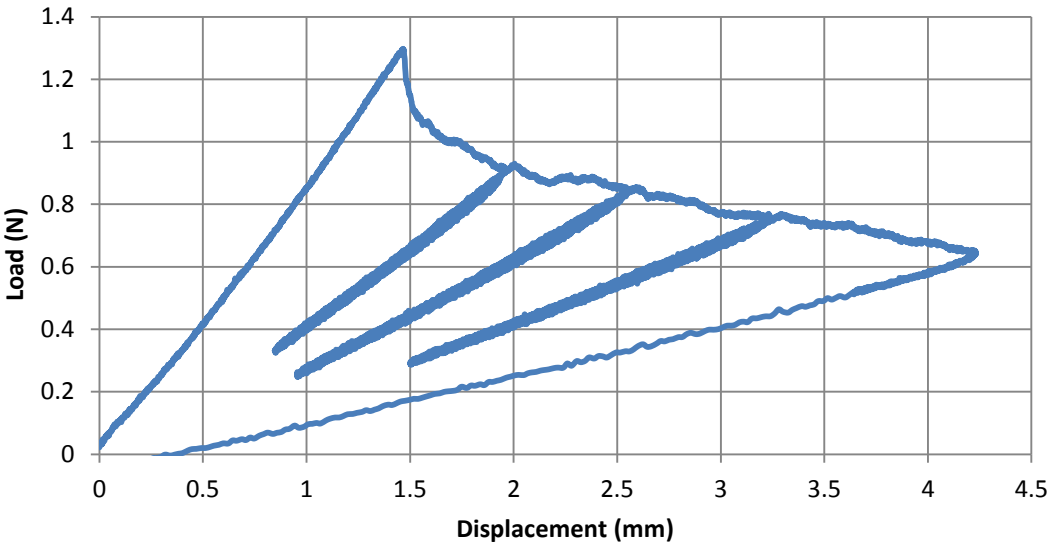

Figure A.18- Experimental load vs. displacement data for EMC/copper sample conditioned at 85%R.H. & 110°C for 528hrs, sample 1

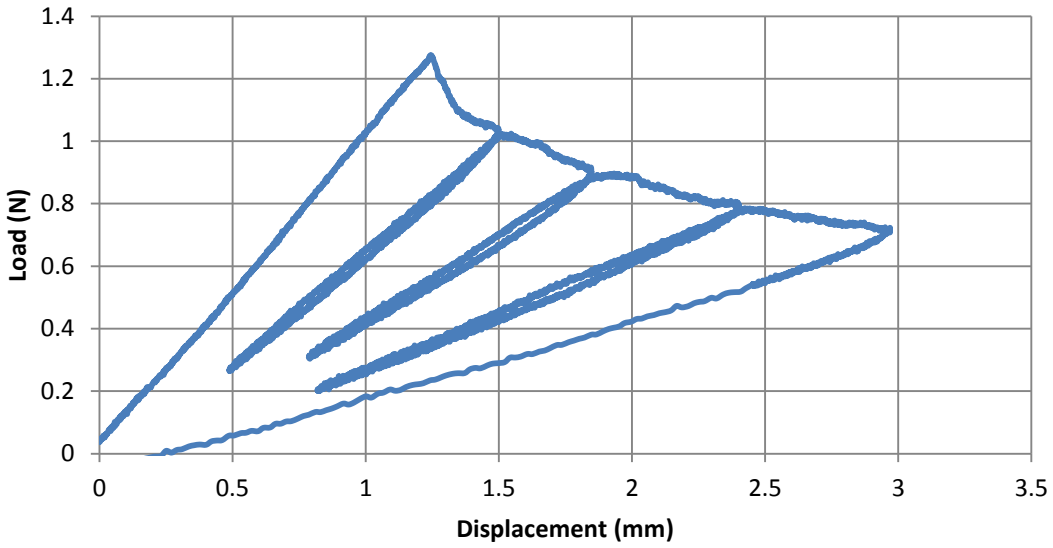

Figure A.19 - Experimental load vs. displacement data for EMC/copper sample conditioned at 85%R.H. & 110°C for 528hrs, sample 2

A.2.4 DCB data for EMC/Copper samples humidity conditioned at 85%R.H & 130°C for 96hrs

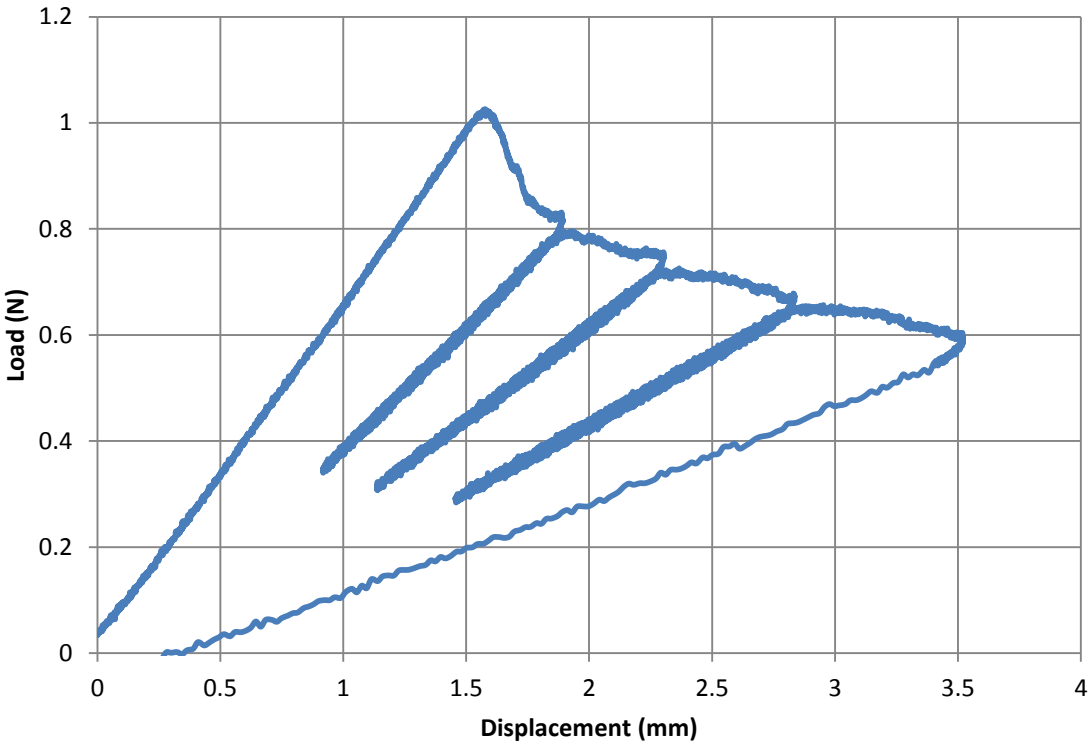

Figure A.20 - Experimental load vs. displacement data for EMC/copper sample conditioned at 85%R.H. & 130°C for 96hrs, sample 1

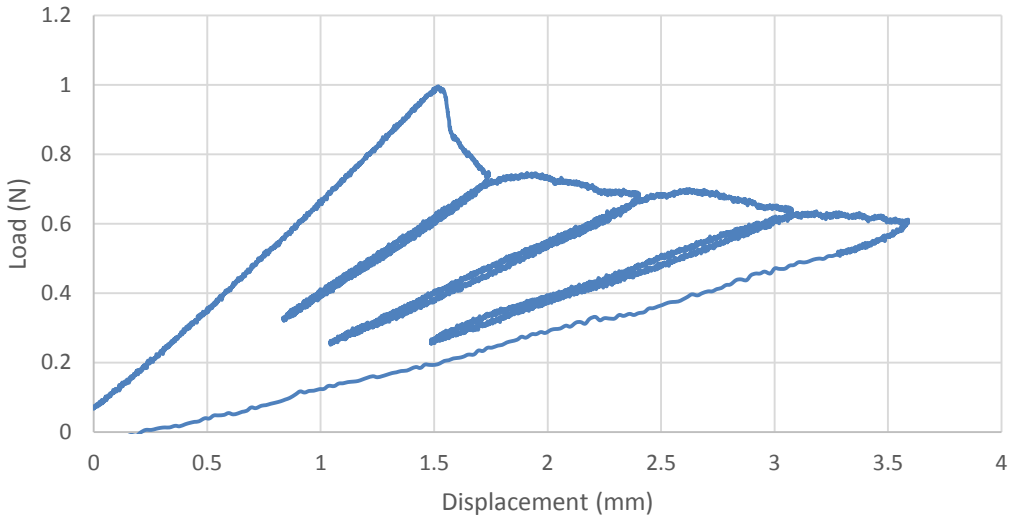

Figure A.21- Experimental load vs. displacement data for EMC/copper sample conditioned at 85%R.H. & 130°C for 96hrs, sample 2

A.2.5 DCB data for EMC/Copper samples humidity conditioned at 85%R.H & 130°C for 192hrs

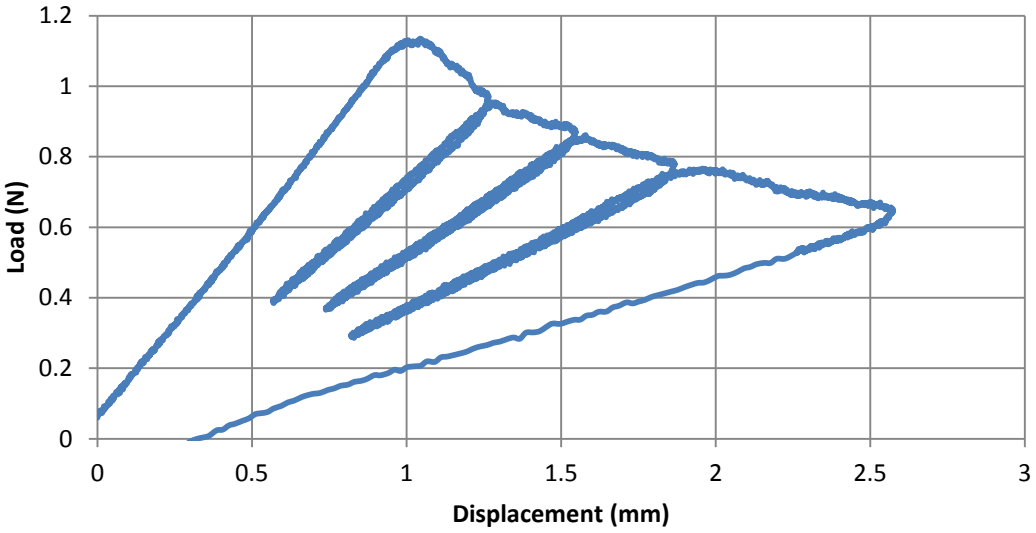

Figure A.22 - Experimental load vs. displacement data for EMC/copper sample conditioned at 85%R.H. & 130°C for 192hrs, sample 1

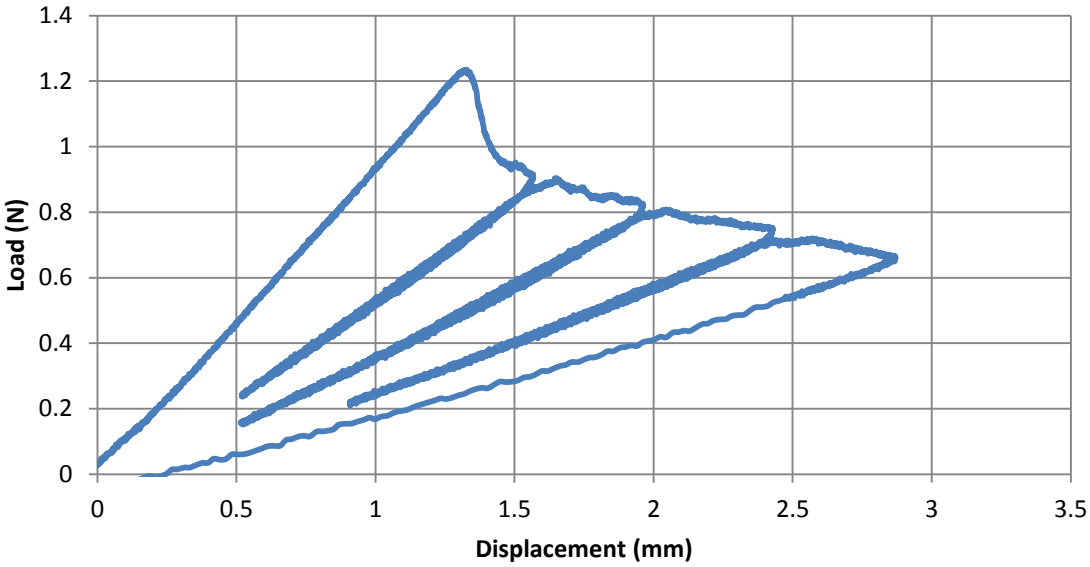

Figure A.23 - Experimental load vs. displacement data for EMC/copper sample conditioned at 85%R.H. & 130°C for 192hrs, sample 2

A.3 Thermally aged DCB data

The following figures illustrate the experimental load vs. displacement graphs obtained from DCB tests conducted on thermally aged EMC/Copper samples.

A.3.1 DCB data for EMC/Copper samples thermally aged at 150°C for 168hrs

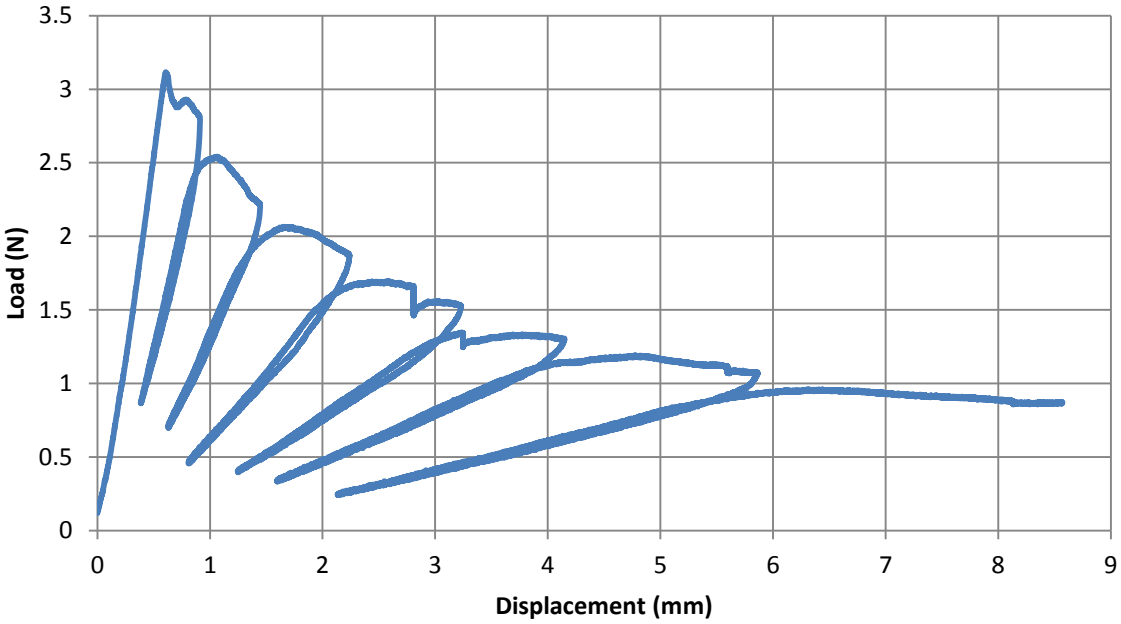

Figure A.24 - Experimental load vs. displacement data for EMC/copper sample thermally aged at 150°C for 168hrs, sample 1

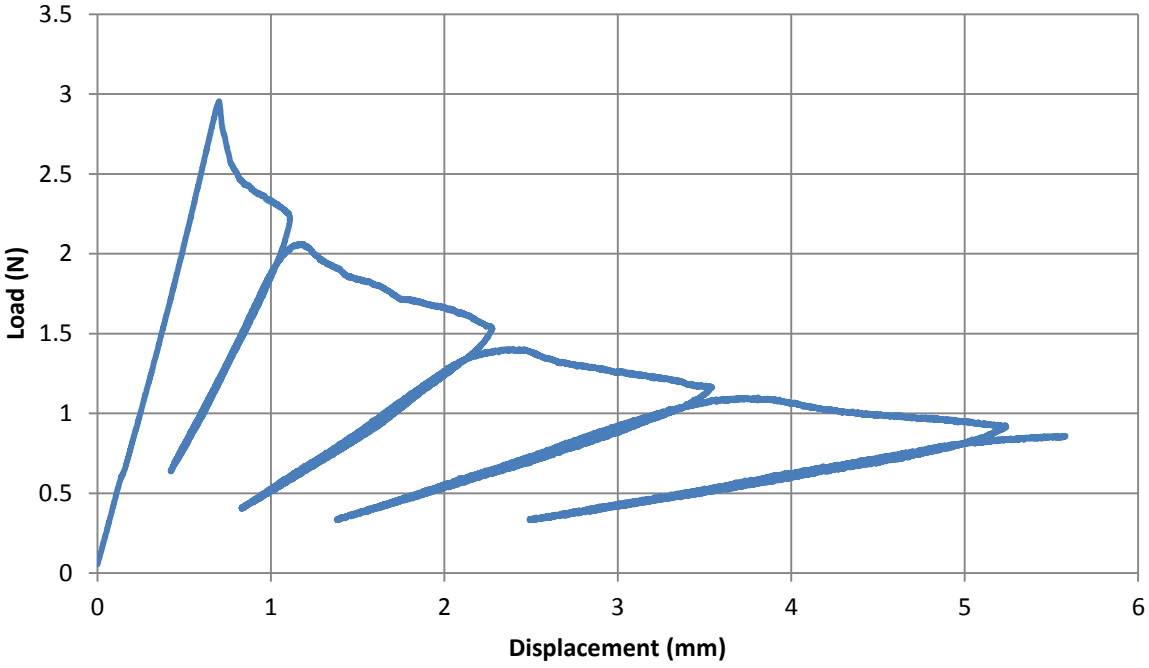

Figure A.25- Experimental load vs. displacement data for EMC/copper sample thermally aged at 150°C for 168hrs, sample 2

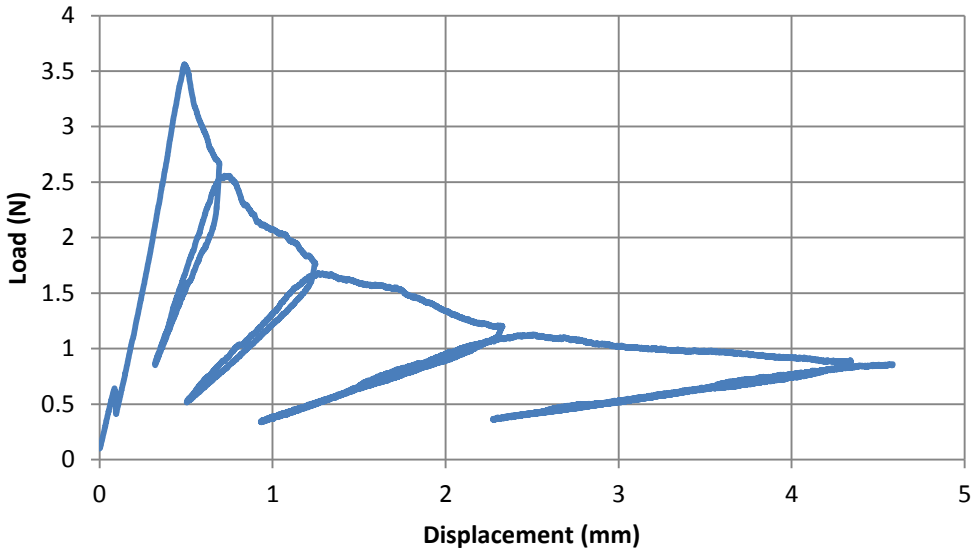

Figure A.26- Experimental load vs. displacement data for EMC/copper sample thermally aged at 150°C for 168hrs, sample 3

A.3.2 DCB data for EMC/Copper samples thermally aged at 150°C for 504hrs

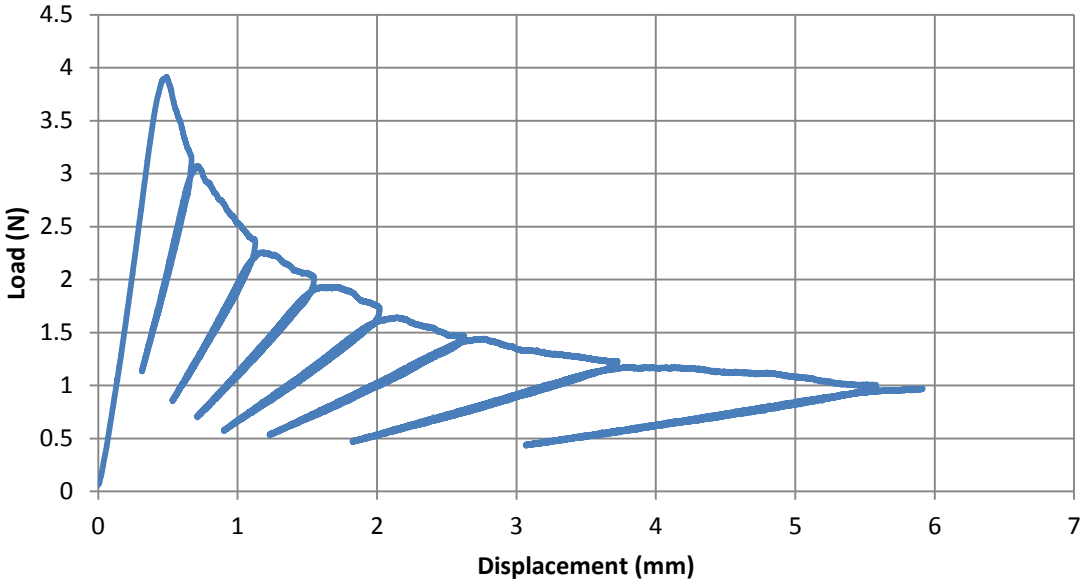

Figure A.27- Experimental load vs. displacement data for EMC/copper sample thermally aged at 150°C for 504hrs, sample 1

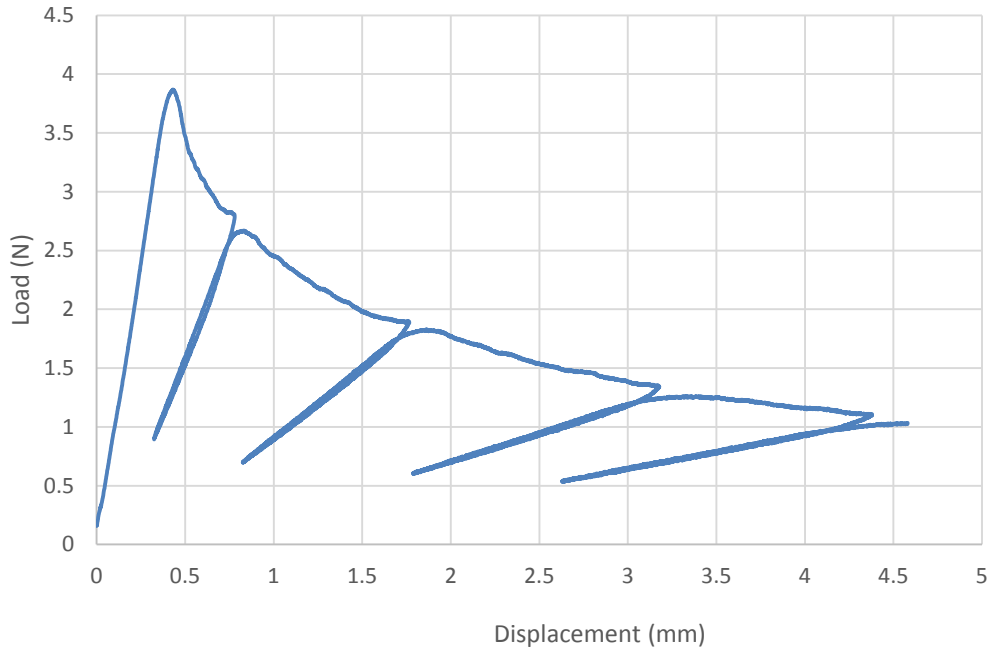

Figure A.28- Experimental load vs. displacement data for EMC/copper sample thermally aged at 150°C for 504hrs, sample 2

A.3.3 DCB data for EMC/Copper samples thermally aged at 150°C for 1000hrs

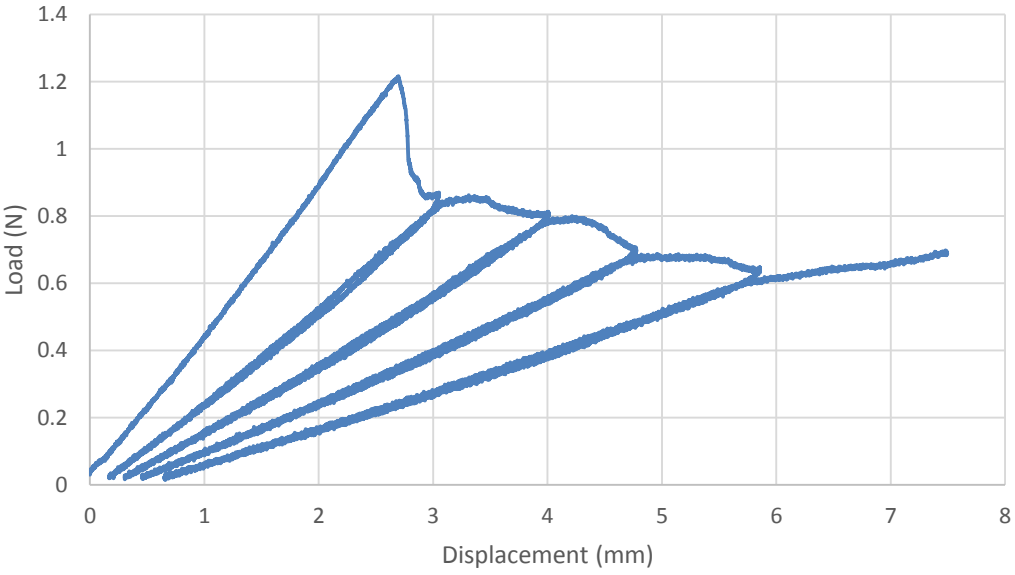

Figure A.29 - Experimental load vs. displacement data for EMC/copper sample thermally aged at 150°C for 1000hrs, sample 1

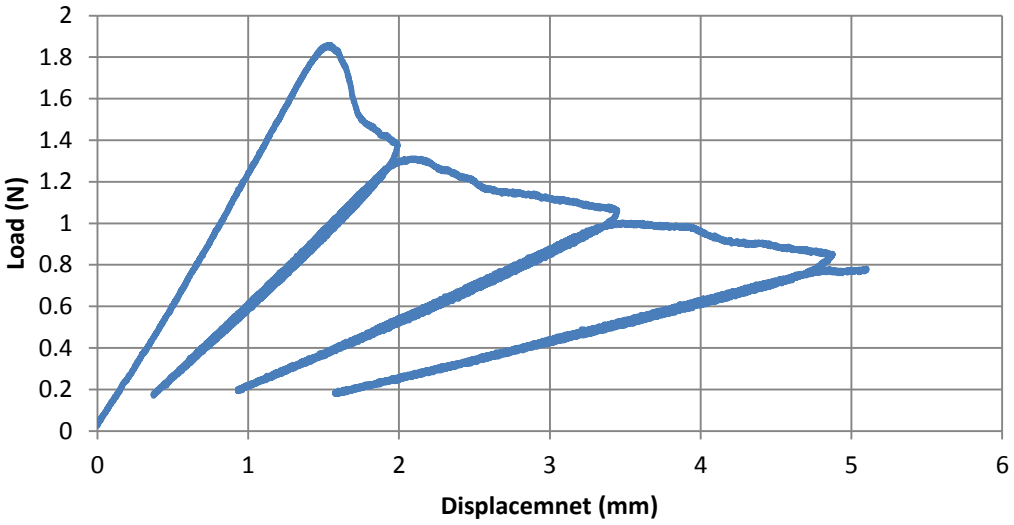

Figure A.30 - Experimental load vs. displacement data for EMC/copper sample thermally aged at 150°C for 1000hrs, sample 2

A.3.4 DCB data for EMC/Copper samples thermally aged at 175°C for 168hrs

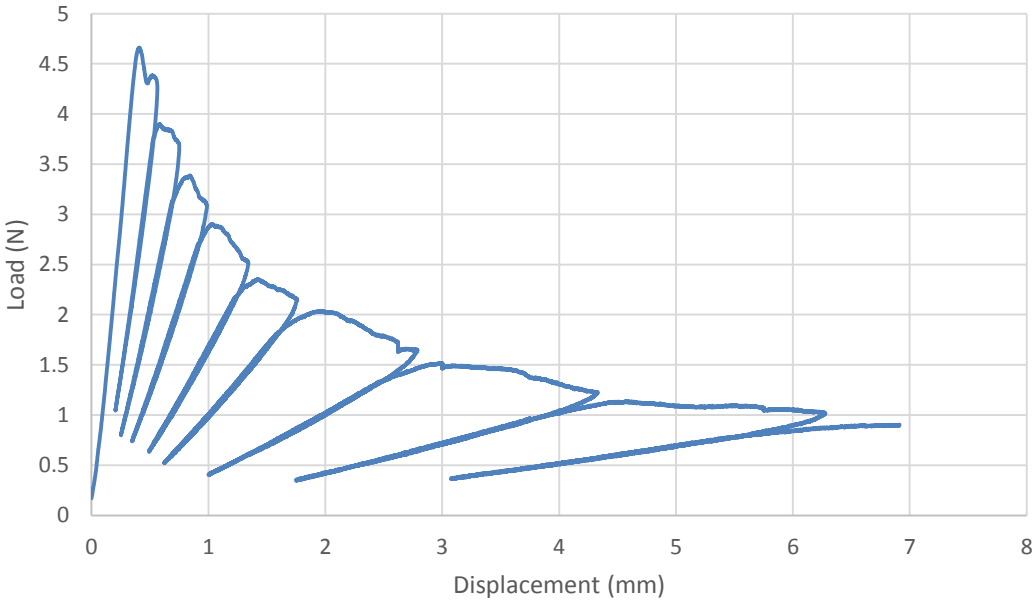

Figure A.31- Experimental load vs. displacement data for EMC/copper sample thermally aged at 175°C for 168hrs, sample 1

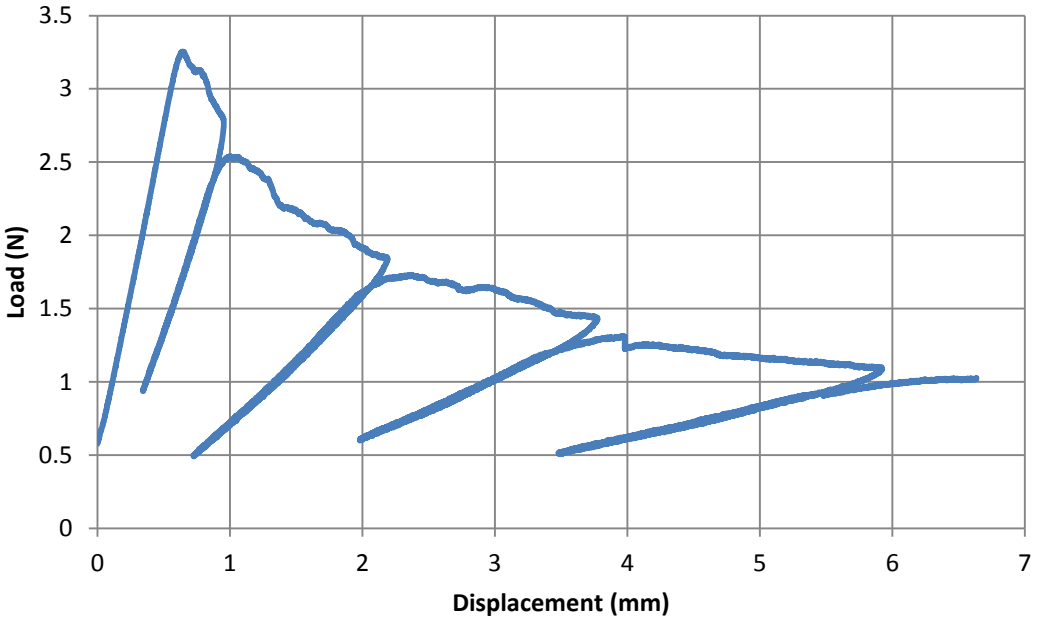

Figure A.32- Experimental load vs. displacement data for EMC/copper sample thermally aged at 175°C for 168hrs, sample 2

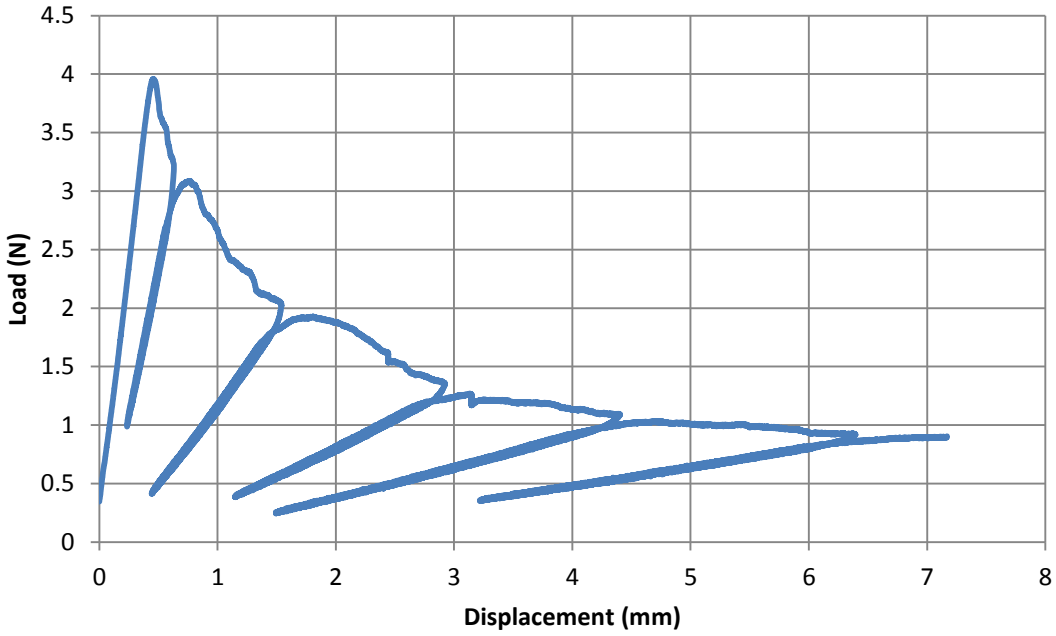

Figure A.33- Experimental load vs. displacement data for EMC/copper sample thermally aged at 175°C for 168hrs, sample 3

A.3.5 DCB data for EMC/Copper samples thermally aged at 175°C for 504hrs

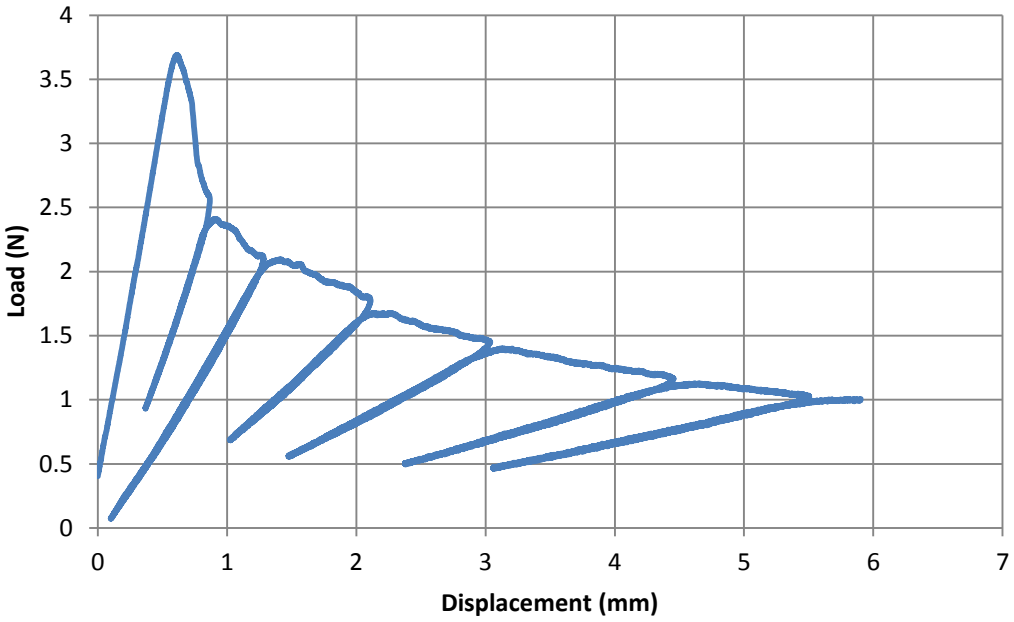

Figure A.34 - Experimental load vs. displacement data for EMC/copper sample thermally aged at 175°C for 504hrs, sample 1

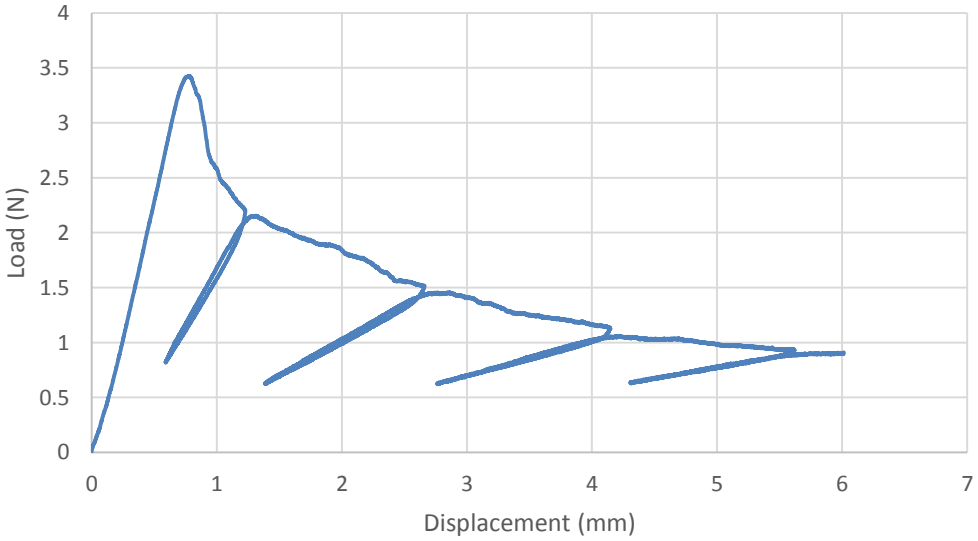

Figure A.35- Experimental load vs. displacement data for EMC/copper sample thermally aged at 175°C for 504hrs, sample 2

A.3.6 DCB data for EMC/Copper samples thermally aged at 175°C for 1000hrs

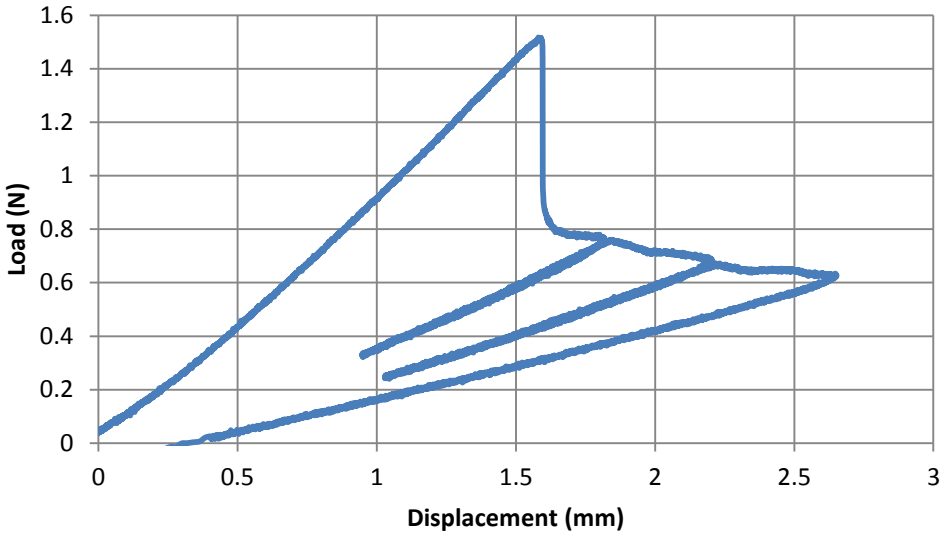

Figure A.36 - Experimental load vs. displacement data for EMC/copper sample thermally aged at 175°C for 1000hrs, sample 1

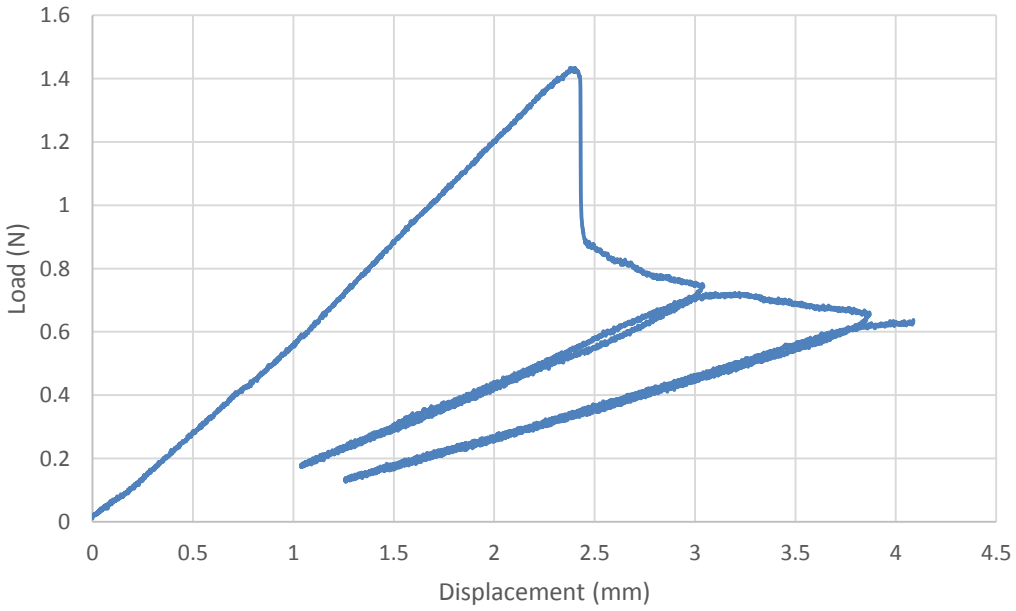

Figure A.37- Experimental load vs. displacement data for EMC/copper sample thermally aged at 175°C for 1000hrs, sample 2

APPENDIX B. EXPERIMENTAL LOAD VS. DISPLACEMENT DATA OBTAINED FOR AS-RECEIVED, THERMALY AGED AND HUMIDITY CONDITIONED EMC/COPPER SAMPLES

This appendix shows the experimental data obtained for DCB tests conducted on as-received, thermally aged and humidity conditioned EMC/Copper samples.

B.1 As-Received DCB data

Table B.1 – As Received EMC/Copper samples experimental data

Sample Number	Compliance	Crack Length (mm)	$P_{critical}$(N)	G_c (J/m^2) [VCCT]
1	0.268	9.30	2.59	47.0
1	0.435	11.0	2.17	45.6
1	0.810	13.6	1.80	47.5
1	1.141	15.2	1.67	51.3
2	0.131	7.25	3.27	46.3
2	0.223	8.73	2.70	45.2
2	0.367	10.4	2.24	43.3
2	0.546	11.9	1.96	43.2
3	0.391	10.6	2.31	48.1
3	0.682	12.8	1.92	48.1
3	0.972	14.4	1.71	48.3
3	1.417	16.4	1.45	44.7
4	0.253	9.12	2.54	43.6
4	0.383	10.5	2.12	39.9
4	0.558	11.9	1.88	40.4
4	0.792	13.5	1.70	41.7
5	0.414	10.8	2.29	49.0
5	0.792	13.5	1.81	47.2
5	1.423	16.4	1.46	45.4
5	2.328	19.4	1.21	43.3

5	3.517	22.3	1.05	42.9
6	0.612	12.3	1.87	42.5
6	1.072	14.9	1.58	44.1
7	0.329	9.97	2.38	45.5
7	0.538	11.8	2.05	46.8
8	0.306	9.73	2.37	43.0
8	0.638	12.5	1.84	42.3
9	0.409	10.7	2.26	47.4
9	0.643	12.5	1.92	46.3
10	0.420	10.8	2.13	42.9
10	0.607	12.3	1.92	44.6

B.2 Humidity Conditioned DCB data

The following tables show the experimental data obtained from DCB tests conducted on humidity conditioned EMC/Copper samples.

B.2.1 DCB data for EMC/Copper samples humidity conditioned at 60% R.H. and 30°C for 192hrs

Table B.2- DCB data for EMC/Copper sample humidity conditioned at *60% R.H. and 30°C for 192hrs*

Sample Number	Compliance	Crack Length (mm)	$P_{critical}$(N)	G_c (J/m^2) [VCCT]
1	0.279	9.42	2.47	44.0
1	0.484	11.38	2.05	43.5
1	0.786	13.42	1.75	43.7
1	1.25	15.72	1.50	44.2
2	0.256	9.15	2.54	44.0
2	0.452	11.11	2.11	44.1
2	0.722	13.03	1.79	43.3
2	1.03	14.72	1.61	44.5
3	0.317	9.85	2.27	40.3
3	0.506	11.55	1.94	40.2

3	0.753	13.22	1.69	39.7
3	1.17	15.37	1.51	42.9
4	0.293	9.59	2.50	46.3
4	0.560	11.96	1.99	45.4
4	0.957	14.35	1.67	45.6
4	1.42	16.41	1.47	45.8

B.2.2 DCB data for EMC/Copper samples humidity conditioned at 85% R.H. and 110°C for 264hrs

Table B.3 - DCB data for EMC/Copper sample humidity conditioned at *85% R.H. and 110°C for 264hrs*

Sample Number	Compliance	Crack Length (mm)	$P_{critical}$(N)	G_c (J/m^2) [VCCT]
1	1.96	18.3	0.989	25.8
1	3.58	22.4	0.814	26.1
2	2.07	18.6	0.932	23.8
2	3.08	21.3	0.830	24.6

B.2.3 DCB data for EMC/Copper samples humidity conditioned at 85% R.H. and 110°C for 528hrs

Table B.4 - DCB data for EMC/Copper sample humidity conditioned at *85% R.H. and 110°C for 528hrs*

Sample Number	Compliance	Crack Length (mm)	$P_{critical}$(N)	G_c (J/m^2) [VCCT]
1	2.04	18.5	0.930	23.4
1	2.93	21.0	0.855	25.2
2	1.41	16.4	1.02	22.2
2	2.00	18.4	0.897	21.5
2	2.91	20.9	0.786	21.2

B.2.4 DCB data for EMC/Copper samples humidity conditioned at 85% R.H. and 130°C for 96hrs

Table B.5 - DCB data for EMC/Copper sample humidity conditioned at *85% R.H. and 130°C for 96hrs*

Sample Number	Compliance	Crack Length (mm)	$P_{critical}$(N)	G_c (J/m^2) [VCCT]
1	1.32	16.0	0.954	18.5
1	1.76	17.6	0.861	18.2
1	2.37	19.5	0.767	17.6
2	1.66	17.3	0.904	19.0
2	2.38	19.5	0.808	19.3
2	3.17	21.5	0.720	18.5

B.2.5 DCB data for EMC/Copper samples humidity conditioned at 85% R.H. and 130°C for 192hrs

Table B.6- DCB data for EMC/Copper sample humidity conditioned at *85% R.H. and 130°C for 192hrs*

Sample Number	Compliance	Crack Length (mm)	$P_{critical}$(N)	G_c (J/m^2) [VCCT]
1	1.96	18.3	0.989	25.8
1	3.58	22.4	0.814	26.1
2	2.07	18.6	0.932	23.8
2	3.08	21.3	0.830	24.6

B.3 Thermally Aged DCB data

The following tables show the experimental data obtained from DCB tests conducted on thermally aged EMC/Copper samples

B.3.1 DCB data for EMC/Copper samples humidity conditioned at 150°C for 168hrs

Table B.7- DCB data for EMC/Copper sample thermally aged at *150°C for 168hrs*

Sample Number	Compliance	Crack Length (mm)	$P_{critical}$(N)	G_c (J/m^2) [VCCT]

1	0.598	12.2	2.01	48.3
1	1.176	15.4	1.70	54.2
1	2.046	18.6	1.35	49.5
1	3.066	21.3	1.19	50.4
1	5.258	25.5	0.960	47.0
2	0.472	11.3	2.06	43.4
2	1.387	16.3	1.40	41.1
2	2.956	21.0	1.11	42.7
2	5.486	25.9	0.860	38.8
3	0.274	9.4	2.56	46.5
3	0.688	12.8	1.68	37.1
3	1.895	18.0	1.13	32.7
3	4.544	24.3	0.86	34.2

B.3.2 DCB data for EMC/Copper samples humidity conditioned at 150°C for 504hrs

Table B.8- DCB data for EMC/Copper sample thermally aged at *150°C for 504hrs*

Sample Number	Compliance	Crack Length (mm)	$P_{critical}$(N)	G_c (J/m^2) [VCCT]
1	0.197	8.37	3.07	53.9
1	0.440	11.0	2.26	49.8
1	0.723	13.0	1.93	50.6
1	1.12	15.1	1.64	48.9
1	1.66	17.3	1.44	49.0
1	2.76	20.5	1.18	46.2
1	5.06	25.2	0.97	46.8
2	0.259	9.18	2.67	48.8
2	0.848	13.8	1.83	50.6
2	2.12	18.8	1.26	44.2
2	3.60	22.5	1.03	42.4

B.3.3 DCB data for EMC/Copper samples humidity conditioned at 150°C for 1000hrs

Table B.9- DCB data for EMC/Copper sample thermally aged at *150°C for 1000hrs*

Sample Number	Compliance	Crack Length (mm)	$P_{critical}$(N)	G_c (J/m^2) [VCCT]
1	3.60	22.5	0.862	29.4
2	2.28	19.3	0.843	20.8
3	1.45	16.5	1.31	37.1
3	3.14	21.5	1.01	36.9

B.3.4 DCB data for EMC/Copper samples humidity conditioned at 175°C for 168hrs

Table B.10- DCB data for EMC/Copper sample thermally aged at *175°C for 168hrs*

Sample Number	Compliance	Crack Length (mm)	$P_{critical}$(N)	G_c (J/m^2) [VCCT]
1	0.297	9.62	2.90	63.0
1	0.490	11.4	2.35	57.8
1	0.763	13.3	2.04	58.5
1	1.56	16.9	1.52	52.3
1	3.23	21.7	1.14	47.8
2	0.379	10.5	2.54	56.9
2	1.16	15.3	1.73	55.8
2	2.45	19.7	1.31	52.6
3	0.207	8.50	3.09	56.2
3	0.742	13.2	1.93	51.5
3	2.05	18.6	1.27	43.9

B.3.5 DCB data for EMC/Copper samples humidity conditioned at 175°C for 504hrs

Table B.11- DCB data for EMC/Copper sample thermally aged at *175°C for 504hrs*

Sample Number	Compliance	Crack Length (mm)	$P_{critical}$(N)	G_c (J/m^2) [VCCT]
1	0.331	10.0	2.41	46.8
1	0.628	12.4	2.10	54.5
1	1.12	15.1	1.68	51.1
1	1.94	18.2	1.40	51.4
1	3.50	22.3	1.13	49.7

2	0.513	11.6	2.16	50.4
2	1.64	17.2	1.46	49.9
2	3.390	22.0	1.06	42.7

B.3.5 DCB data for EMC/Copper samples humidity conditioned at 175°C for 1000hrs

Table B.12- DCB data for EMC/Copper sample thermally aged at *175°C for 1000hrs*

Sample Number	Compliance	Crack Length (mm)	$P_{critical}$(N)	G_c (J/m^2) [VCCT]
1	2.1158	18.77	0.761	16.08
1	3.0837	21.32	0.672	16.12
2	3.7614	22.8	0.724	21

REFERENCES

1. D.R.Frear, *Materials Issues in Area-Array Microelectronic Packaging* JOM, 1999. **51**: p. 22-27.

2. Y.Liu, S.I., M. Rioux, A. J. Schoenberg, D.Chong *Die Attach Delamination Characterization Modeling for SOIC Package* IEEE, 2002 p. 839-846.

3. W.E.R.Krieger, S.R., S.K.Sitaraman *Experiments for Obtaining Cohesive-Zone Parameters for Copper-Mold Compound Interfacial Delamination* IEEE 2016. **6**(9): p. 1389-1398.

4. C.J. Zhai, S., R.C.Blish II, R.N.Master *Investigation and Minimization of Underfill Delamination in Flip Chip Packages* IEEE, 2004 **1530**: p. 86-91

5. W. Xie, H.H., S.K. Sitaraman *Role of Base Substrate Material on Dielectric and Copper Interlayer Separation* International Microelectronics and Packaging Society 2001. **25**: p. 160-177.

6. J.Zheng, V.J., J.Wakil, J.Coffin, S.Iruvanti, R.Langlois, E.Yarmchuk, M.Gaynes, H.Liu, K.Sikka, P.Brofman *Delamination Mechanisms of Thermal Interface Materials in Organic Packages during Reflow and Moisture Soaking* IEEE 2009. **978**: p. 469 - 474

7. N.J.Chhanda, J.C.S., P.Lall, *Effect of Moisture Exposure on the Mechanical Behavior of Flip Chip Underfills in Microelectronic Packaging* IEEE 2014 **978**: p. 333-346.

8. T.Ferguson, J.Q., *Effect of Moisture on the Interfacial Adhesion of the Underfill/Solder Mask Interface* ASME 2002 **124**: p. 106-110

9. T.Ferguson, J.Q., *Moisture and Temperature Effects on the Reliability of Interfacial Adhesion of a Polymer/Metal Interface* IEEE, 2004: p. 1752-1758.

10. Tummala, R.R., *Fundamentals of Microsytems Packaging*. 1997, New York McGraw-Hill.

11. Tummala, R.R. and M. Swaminathan, *System on Package: Miniaturization of the Entire System* 2008, New York McGraw-Hill.

12. Liu, S., Y. Mei, and T. Y. Wu, *Bimaterial Interfacial Crack Growth as a Function of Mode Mixity* IEEE 1995. **18**: p. 618-626.

13. Nishimura, A., I. Hirose, and N. Tanaka, *A New Method for Measuring Adhesion Strength of IC Molding Compounds* ASME, 1992. **114**: p. 407-412.

14. Liechti, K.M. and Y.-S. Chai, *Biaxial Loading Experiments for Determining Interfacial Fracture Toughness.* ASME, 1991. **58**: p. 680-687.

15. O'Dowd, N.P., C.F. Shih, and M.G. Stout, *Test Geometries for Measuring Interfacial Fracture Toughness.* International Journal of Solids and Structures, 1991. **29**(5): p. 571-589.

16. Anderson, T.L., *Fracture Mechanics: Fundamentals and Applications, Third Edition: Taylor & Francis, 2005.* .

17. Harries, R.J. and S.K. Sitaraman, *Numerical Modeling of Interfacial Delamination Propogation in a Novel Peripheral Array Package* IEEE, 2001. **24**(2): p. 256-264.

18. Liu, X., et al., *Failure analysis of through-silicon vias in free-standing wafer under thermal-shock test* Microelectronics Reliability, 2013. **53**: p. 70-78.

19. Sundararaman, V. and S.K. Sitaraman, *Interfacial Fracture Toughness for Delamination Growth Prediction in a Novel Peripheral Array Package* IEEE, 2001. **24**(2): p. 265-270.

20. Xie, W. and S.K. Sitaraman, *Investigation of Interfacial Delamination of a Copper-Epoxy Interface Under Monotonic and Cyclic Loading: Modeling and Evaluation* IEEE, 2003. **26**(4): p. 441-446.

21. Van Driel, W.D., et al., *Prediction of Delamination Related IC & Packaging Reliability Problems.* Microelectronics Reliability 2005. **45**: p. 1633-1638.

22. Xia, G., F. Qin, and W. Zhu, *Interfacial delamination and reliability design of exposed pad packages* IEEE, 2012.

23. Kanninen, E.F.R.a.M.F., *A Finite Element Calculation of Stress Intensity Factors by a Modified Crack Closure Integral* Engineering Fracture Mechanics, 1977. **9**: p. 931-938.

24. Krueger, R., *Virtual crack closure technique: History, approach, and applications* Applied Mechanics 2004 **57**(2): p. 109-143.

25. Williams, M.L., *The Stresses Around a Fault or Crack in Dissimilar Media* Bulletin of the Seismological Society of America 1959 **49**(2): p. 199-204.

26. G.C.Sih, J.R.R., *Plane Problems of Cracks in Dissimilar Media* Applied Mechanics 1965. **32**(2): p. 418-423.

27. Z.Suo, J.W.H.a., *Mixed Mode Cracking in Layered Materials.* Advances in applied mechanics 1992. **29**: p. 63-191.

28. P.P.L Matos, R.M.M., P.G. Charalambides and M.D. Drory *A method for calculating stress intensities in bimaterial fracture* International Journal of Fracture 1988. **40**: p. 235-254.

29. J.F. Yau, S.S.W., H.T.Corten *A Mixed-Mode Crack Analysis of Isotropic Solids using Conservation Laws of Elasticity* Applied Mechanics 1980. **47**(2): p. 335-341.

30. S.Raghavan, I.S., G.Leal, S.K.Sitaraman *Framework to Extract Cohesive Zone Parameters Using Double Cantilever Beam and Four-Point Bend Fracture Tests.* IEEE, 2014. **978**(1): p. 1-5.

31. H.Mei, S.G., K.M.Liechti, R.Huang *Initiation and Propagation of Interfacial Delamination in Integrated Thin-Film Structures* 978, 2010. **1**: p. 4244-5343.

32. S.Li, M.D.T., A.M. Waas, J.A. Schroeder, P.D. Zavattieri *Mixed-mode cohesive-zone models for fracture of an adhesively bonded polymer-matrix composite* Engineering Fracture Mechanics 2006. **73**: p. 64-78.

33. P.R.Kumar, A.J., S.J.Bennison, S.Saigal and S.Muralidhar *Polymer Interfacial Fracture Simulations using cohesive elements* Acta Materialia 1999. **47**(15): p. 4161-4169.

34. R.L. Fernandes, R.D.S.G.C., *Numerical evaluation of dissimilar cohesive zone models to predict the behavior of Double-Cantilever Beam specimens.* Structural Integrity, 2016. **1**: p. 42-49.

35. G.Alfano, M.A.C., *Finite Element Interface models for the Delamination Analysis of Laminated Composites: Mechanical and Computational Issues* International Journal for Numerical Methods in Engineering 2001. **50**: p. 1701-1736.

36. M.H. Shirangi, X.J.F., B.Michael *Mechanism of Moisture Diffusion, Hygroscopic Swelling and Adhesion Degradation in Epoxy Molding Compounds* IMAPS, 2008: p. 1082-1089.

37. E.Suhir, X.F., *Moisture Sensitivity of Plastic Packages of IC Devices* Technology and Engineering 2010: Springer Science & Business Media 558

38. Tran, H.T., et al., *Temperature, moisture and mode-mixity effects on copper leadframe/EMC interfacial fracture toughness.* International Journal of Fracture, 2014. **185**(1-2): p. 115-127.

39. M.H.Shirangi, *Simulation-based Investigation of Interface Delamination in Plastic IC Packages under Temperature and Moisture Loading* in *Faculty V*

Mechanical Engineering and Transport Systems 2010, Technical University of Berlin Berlin. p. 187.

40. M.H. Shirangi, B.W., O. Wittler, H. Walter, B. Michel *Modeling Cure Shrinkage and Viscoelasticity to Enhance the Numerical Methods for Predicting Delamination in Semiconductor Packages* IEEE, 2009. **978**(1): p. 4244-4161.

41. F.Xiao, C.Y.H., E.J. Kramer *Analysis of a mixed mode fracture specimen: the asymmetric double cantilever beam* Journal of Materials Science 1993. **28**: p. 5620-5629.

42. V.Sundararaman, B.D.D., *A single leg bending test for interfacial fracture toughness determination* International Journal of Fracture, 1996. **78**: p. 193-210.

43. W.O. Soboyejo, G.Y.L., S.Chengalva, J.Zhang, V.Kenner, *A modified mixed-mode bending specimen for the interfacial fracture testing of dissimilar materials.* Fatigue & Fracture of Engineering Materials & Structures 1999. **22**(9): p. 799-810.

44. P.G. Charalambides, J.L., A.G. Evans, R.M. McMeeking *A Test Specimen for Determining the Fracture Resistance of Bimaterial Interfaces* Journal of Applied Mechanics 1989. **56**: p. 77-82.

45. *Failure Mechanism Based Stress Test Qualification For Integrated Circuits* A.E. Council, Editor 2014.